Linear MMSE Receivers for Interference Suppression & Multipath Diversity Combining in Long-code DS-CDMA Systems

by

Arash Mirbagheri

A thesis

presented to the University of Waterloo

in fulfilment of the

thesis requirement for the degree of

Doctor of Philosophy

in

Electrical and Computer Engineering

Waterloo, Ontario, Canada, 2003

I hereby declare that I am the sole author of this thesis. This is a true copy of the thesis, including any required final revisions, as accepted by my examiners.

I understand that my thesis may be made electronically available to the public.

Abstract

This thesis studies the design and implementation of a linear minimum mean-square error (LMMSE) receiver in asynchronous bandlimited direct-sequence code-division multiple-access (DS-CDMA) systems that employ long-code pseudo-noise (PN) sequences and operate in multipath environments. The receiver is shown to be capable of multiple-access interference (MAI) suppression and multipath diversity combining without the knowledge of other users' signature sequences. It outperforms any other linear receiver by maximizing output signal-to-noise ratio (SNR) with the aid of a new chip filter which exploits the cyclostationarity of the received signal and combines all paths of the desired user that fall within its supported time span.

This work is motivated by the shortcomings of existing LMMSE receivers which are either incompatible with long-code CDMA or constrained by limitations in the system model. The design methodology is based on the concept of linear/conjugate linear (LCL) filtering and satisfying the orthogonality conditions to achieve the LMMSE filter response. Moreover, the proposed LMMSE receiver addresses two drawbacks of the coherent Rake receiver, the industry's current solution for multipath reception. First, unlike the Rake receiver which uses the chip-matched filter (CMF) and treats interference as additive white Gaussian noise (AWGN), the LMMSE receiver suppresses interference by replacing the CMF with a new chip pulse filter. Second, in contrast to the Rake receiver which only processes a subset of strongest paths of the desired user, the LMMSE receiver harnesses the energy of all paths of the desired user that fall within its time support, at no additional complexity.

The performance of the proposed LMMSE receiver is analyzed and compared with that of the coherent Rake receiver with probability of bit error, P_e, as the figure of merit. The analysis is based on the accurate improved Gaussian approximation (IGA) technique. Closed form conditional P_e expressions for both the LMMSE and Rake receivers are derived. Furthermore, it is shown that if quadriphase random spreading, moderate to large spreading factors, and pulses with small excess bandwidth are used, the widely-used standard Gaussian Approximation (SGA) technique becomes accurate even for low regions of P_e. Under the examined scenarios tailored towards current narrowband system settings, the LMMSE receiver achieves 60% gain in capacity (1.8 dB in output SNR) over the selective Rake receiver. A third of the gain is due to interference suppression capability of the receiver while the rest is credited to its ability to collect the energy of the desired user diversified to many paths. Future wideband systems will yield an ever larger gain.

Adaptive implementations of the LMMSE receiver are proposed to rid the receiver from dependence on the knowledge of multipath parameters. The adaptive receiver is based on a fractionally-spaced equalizer (FSE) whose taps are updated by an adaptive algorithm. Training-based, pilot-channel-aided (PCA), and blind algorithms are developed to make the receiver applicable to both forward and reverse links, with or without the presence of pilot signals. The blind algorithms are modified versions of the constant modulus algorithm (CMA) which has not been previously studied for long-code CDMA systems. Extensive simulation results are presented to illustrate the convergence behavior of the proposed algorithms and quantify their performance loss under various levels of MAI. Computational com-

plexities of the algorithms are also discussed. These three criteria (performance loss, convergence rate, and computational complexity) determine the proper choice of an adaptive algorithm with respect to the requirements of the specific application in mind.

Acknowledgements

Although only one name appears on the cover, this thesis would not have come to existence if it were not for the support of many individuals and organizations. I would like to sincerely thank my supervisor Dr. Young C. Yoon for his supervision and support during the program. I will never forget those lengthy meetings and phone conversations. I would also like to express my deep gratitude to Professor Amir K. Khandani for his co-supervision and efforts in the absence of Dr. Yoon. I would like to extend my grateful acknowledgement to Professor Pas S. Pasupathy for his efforts and time to appraise this work. I gratefully acknowledge other members of the Ph.D. thesis examination committee: Professors En-hui Yang, George Freeman, and Brendan Frey.

Acknowledgement is due to the following organizations which supported my work over the last three years through scholarships: Natural Sciences and Engineering Research Council of Canada, Canadian Wireless Telecommunications Association, Ontario Graduate Scholarship Program for Science and Technology, Institute for Computer Research at University of Waterloo, and Department of Electrical and Computer Engineering, University of Waterloo.

My special thanks to the administrative staff of the department, particularly, Wendy Boles and Wendy Gauthier for their support, help, and patience. Many thanks to Professor John Thistle, Associate Chair of Graduate Studies, for his efforts to make the last months of my program smooth.

I am most grateful to all members of my family, specially my wife, Rana, and my parents who were always behind me with full emotional support in this endurance

game. I owe it all to them.

Last but not least, my sincere and humble gratitude to the guy upstairs who has always watched over me. Thank you, God. Amazingly, I still deeply believe in you.

August 2003

To Rana

for her infinite love, support, and patience.

"One never notices what has been done;
but can only see what remains to be done."

- Marie Curie

Contents

List of Tables

List of Figures

Abbreviations

1xEV-DO	Single-carrier EVolution- Data Optimized
ARake	All Rake
AWGN	Additive White Gaussian Noise
BPSK	Binary Phase-Shift Keying
BW	BandWidth
CDMA	Code-Division Multiple-Access
CLT	Central Limit Theorem
CM	Constant Modulus
CMA	Constant Modulus Algorithm
CMF	Chip-Matched Filter
CLMF	Chip-delayed Locked Matched Filter
CS	CycloStationarity
CSD	Cross Spectral Density
DD	Decision-Directed
DFE	Decision-Feedback Equalizer
DS	Direct-Sequence

FIR	Finite Impulse Response
FSE	Fractionally-Spaced Equalizer
G	Generation
HSR	Harmonic Series Representation
HYB	Hybrid
i.i.d.	independent and identically distributed
IC	Interference Cancellation
ICI	Inter-Chip Interference
IGA	Improved Gaussian Approximation
IPI	Inter-Path Interference
IS	Interim Standard
ISI	Inter-Symbol Interference
LCL	Linear/Conjugate-Linear
LCMA	Leaky Constant Modulus Algorithm
LMMSE	Linear Minimum Mean-Square Error
LMS	Least-Mean-Square
MAI	Multiple-Access Interference
MOE	Minimum output energy
MRC	Maximal-Ratio-Combining
NLMS	Normalized Least-Mean-Square
NWMF	Noise-Whitening Matched Filter
PCA	Pilot-Channel-Aided
PG	Processing Gain

PN	Pseudo-Noise
PRake	Partial Rake
PSA	Pilot-Symbol-Aided
PSD	Power Spectral Density
QAM	Qaudrature Amplitude Modulation
QoS	Quality of Service
QPSK	Quadrature Phase-Shift Keying
RCMA	Recursive Constant Modulus Algorithm
RLS	Recursive Least-Squares
RV	Random Variable
SGA	Standard Gaussian Approximation
SNR	Signal-to-Noise Ratio
Sqrt-RC	Square-root Raised-Cosine
SRake	Selective Rake
WCDMA	Wideband CDMA
WSCS	Wide-Sense CycloStationary
WSS	Wide-Sense Stationary

Nomenclature

$a_i^{(\mathcal{B},k)}$	ith chip of the PN sequence of user k on the $\mathcal{B}$ phase
$a_n^{(\mathcal{B},k)}(t)$	Spreading waveform for the nth bit of user k on the $\mathcal{B}$ phase
$\boldsymbol{a}_n^{(\mathcal{B},k)}$	Spreading sequence for the nth bit of user k on the $\mathcal{B}$ phase
$\mathcal{A}_n^{(\mathcal{B},0)}$	Z-transform of the desired user's PN sequence $\boldsymbol{a}_n^{(\mathcal{B},0)}$
$b_n^{(k)}$	nth bit of user k
$\hat{b}_n^{(0)}$	Estimated nth bit of user 0
$B_l(f)$	Fourier transform of $\rho_l^2(t)$ scaled by $1/T_c$
$\boldsymbol{c}^{(k,P)}$	Walsh code of the pilot channel associated with user k
$\boldsymbol{c}^{(k,T)}$	Walsh code of the traffic channel associated with user k
$c_l^{(k)}(t), C_l^{(k)}(f)$	Impulse response of the channel corresponding to the lth path of user k
$c^{(k)}(t), C^{(k)}(f)$	Impulse response of the multipath channel for user k
$\boldsymbol{C}^{(0)}(f)$	Matrix holding the HSR elements of $C^{(0)}(f)$
$d_n^{(\mathcal{B},k,l)}$	nth bit of the lth path of user k on the $\mathcal{B}$ phase scrambled with corresponding PN sequence
$\tilde{d}$	Estimated value of the pilot symbol: $+1$.
E_b	Bit energy for user 0

$g_l(t), G_l(f)$	Sub filter of the LMMSE receiver corresponding to the lth path of user 0
$g(t), G(f)$	The LMMSE filter
$\boldsymbol{I}_{M\times M}$	The $M \times M$ identity matrix
$\mathcal{I}$	Contribution of IPI to bit decision statistic
$\boldsymbol{k}_P$	The $M \times 1$ complex gain vector of the pilot channel in recursive algorithms
$\boldsymbol{k}_T$	The $M \times 1$ complex gain vector of the traffic channel in recursive algorithms
$J_l^{(k)}$	Bit delay of the lth path of the kth user
$\mathcal{J}_{CM}$	Constant modulus cost function
$\mathcal{J}_{MSE}$	Mean-square error cost function
$\mathcal{J}_L$	Complexity penalty term
$L^{(k)}$	Number of paths associated with user k
M	Number of FSE tap weights
$\mathcal{M}$	Contribution of MAI to bit decision statistic
$\mathcal{M}_k$	Contribution of user k to bit decision statistic
$n(t)$	Noise signal with respect to user 0
N_s	Sampling rate to chip rate ratio
$N^{(k)}$	Spreading factor of user k
$\mathcal{N}_0$	PSD of AWGN
P_e	Probability of bit error
P_k	Signal power of user k
$\boldsymbol{P}$	The $M \times M$ inverse correlation matrix of the recursive algorithms
$\mathcal{P}$	MAI power matrix
$q(t), Q(f)$	Chip pulse

$\mathcal{Q}(x)$	The error probability function
$r(t)$	Received signal
$\boldsymbol{R}(f)$	Cross spectral density matrix of the noise
R_p	Dispersion constant
$R_{xx^*}(t,u)$	Autocorrelation function of the complex random process $x(t)$
$R_{xx}(t,u)$	Complementary autocorrelation function of the complex random process $x(t)$
$\boldsymbol{R}$	Correlation matrix of the FSE input vector
$s^{(k)}(t)$	Transmit signal of user k
T_b	Bit period
T_c	Chip period
T_{s_1}	FSE sampling period
$T_l^{(k)}$	Chip delay of the lth path of the user k
$\boldsymbol{T}$	The set containing $\boldsymbol{T}^{(k)}$ for all k
$\boldsymbol{T}^{(k)}$	The $1 \times L^{(k)}$ vector containing the chip delays of user k
$x_{\mathcal{B}}^{(k)}$	Signal component in the $\mathcal{B}$ branch of of user k
$\boldsymbol{x}$	The $M \times 1$ FSE input vector
$\boldsymbol{x}_P$	Time-averaged FSE input vector with respect to the pilot channel
$\boldsymbol{x}_T$	Time-averaged FSE input vector with respect to the traffic channel
$X_i^{\mathcal{I}}$	The statistic of the ith despread chip due to IPI
$X_i^{\mathcal{M}}$	The statistic of the ith despread chip due to MAI
$\boldsymbol{w}$	The $M \times 1$ FSE tap weight vector
α	Chip pulse excess BW
$\alpha_l^{(k)}$	Attenuation factor of the lth path of the kth user

β_k	Percentage of the total signal power of user k allocated to its pilot channel
γ	Normalized strength of the desired signal at the LMMSE output
δ_{mn}	Kronecker delta, equal to 1 if $m = n$ and zero elsewhere
$\varepsilon(n)$	Error in the estimated nth bit
$\varepsilon_{CM}(n)$	Constant modulus error of the nth iteration
$\varepsilon_P(n)$	Error of the pilot channel in the nth iteration
$\varepsilon_T(n)$	Error of the traffic channel in the nth iteration
ζ_k	Scaled square-root of relative power of user k to user 0: $\frac{1}{2}\sqrt{\frac{P_k}{P_0}}$
$\eta(t)$	AWGN
$\theta_l^{(k)}$	Phase-shift of the lth path of user k
$\mathbf{\Theta}$	The set containing $\mathbf{\Theta}^{(k)}$ for all k
$\mathbf{\Theta}^{(k)}$	The $1 \times L^{(k)}$ vector containing the phase offsets of user k
κ	Virtual number of interfering users contributing to MAI
κ_0	Virtual number of interfering paths contributing to IPI
λ	Regularization (or hybrid) parameter
μ	Step size in the LMS and LCMA algorithms
ν	Forgetting factor in the RLS and RCMA algorithms
$\rho_l(t)$	Inverse Fourier transform of $(1/T_c)Q(f)G_l(f)$
$\rho'_l(t)$	Inverse Fourier transform of $(1/T_c)G_l(f)G_l(f)$
$\sigma^2_{\mathcal{I}}$	Variance of IPI
$\sigma^2_{\mathcal{M}}$	Variance of MAI
$\tau_l^{(k)}$	Arrival delay of the lth path of user k

Chapter 1

Introduction

Wireless communications has experienced a tremendous evolution over the last few decades. From analog voice services of first generation (1G) systems in early 1980s to digital voice services of 2G in late 1980s to high speed packet data calls of 3G currently in roll-out, the industry has witnessed a pace of roughly a generation per decade [1]. Broadband next-generation systems are presently being developed which offer always-on access to information anywhere whether moving or stationary.

Since its commercial introduction by the IS-95 system [2], direct-sequence code-division multiple-access (DS-CDMA) has turned into a dominant wireless technology among others. DS-CDMA is a spread spectrum technique where the transmitted signal energy occupies a bandwidth often much larger than, and approximately independent of, the information bit rate [3]. Bandwidth spreading is accomplished by direct modulation of a data-modulated carrier via a wideband pseudo-noise (PN) spreading code. Demodulation can be partly performed by correlating the received signal with a replica of the PN code used to spread the information signal. Anti-

interference, multiple user random access communications with selective addressing capability [4], soft hand-off [5], higher capacity [6], lower power consumption, electromagnetic compatibility, and multipath rejection [7] are among the many benefits that DS-CDMA offers. One of its drawbacks is poor spectrum efficiency (in terms of bits per second/Hz) in isolated single cell scenarios or microwave point-to-point applications such as satellite-based systems [8]. Another disadvantage of DS-CDMA is the hardware complexity of code synchronization and power control systems [3]. Nonetheless, the attractive features of DS-CDMA has resulted in contending standards (e.g., cdma2000 [9], WCDMA [10], and 1xEV-DO [11]) that follow the wireless industry trends.

Like all real-world communication systems, those based on CDMA are prone to adverse effects of many types of interference and signal distortion. Major sources of performance degradation in CDMA systems are: *i)* multiple-access interference (MAI), *ii)* multipath channel conditions, *iii)* inter-symbol interference (ISI), and *iv)* inter-chip interference (ICI). Their strength are not necessarily in the above order.

MAI occurs when a number of users share a common channel simultaneously. In this context, signals from other users appear as interference from the perspective of the desired user. Multipath channel conditions appear in environments where, due to the reflection, refraction, and scattering of radio waves by buildings and other man-made obstacles, the transmitted signal most often reaches the receiver via more than one path [12]. ISI (or ICI) occurs since, in bandwidth-efficient systems, the effect of each symbol (or chip) transmitted over a time-dispersive channel extends

beyond the time interval used to represent that symbol (or chip). The distortion caused by the resulting overlap of received symbols (or chips) is called ISI (or ICI) [13].

The performance of CDMA systems is well known to be limited by interference, whether MAI, ISI, or ICI. Therefore, suppressing interference directly translates into an increase in system capacity [6]. Interference suppression has been the focus of many research efforts. The overwhelming complexity of the optimum multiuser detector articulated in [14] has motivated the search for sub-optimum receivers with less computational complexity. Sub-optimum receivers can be categorized in two groups: linear and non-linear. Non-linear techniques are primarily based on the principle of decision feedback. The common structure in this class belongs to those which perform interference cancellation (IC). They estimate the dominant interfering terms from the perspective of a desired user and subtract these estimates from the statistics of the user of interest. The use of decision feedback method necessitates the knowledge of at least the estimates of users' parameters. An in-depth treatment of these receivers along with an extensive list of references can be found in [15]. Linear techniques, however, exploit the dimensional separation of the users obtained by assigning the users unique PN spreading codes. They are simpler to implement and can be made adaptive thus avoiding the need for the knowledge of users' parameters. The linear minimum mean-square error (LMMSE) receiver is a widely-used example of this class and has been studied in the context of suppressing MAI in CDMA systems (e.g., [16]-[18]), combating ISI in wired communication systems (e.g., [13] and references therein), and countering ICI in

high data rate CDMA systems (e.g., [19, 20]). The LMMSE technique has also been effectively applied to perform multipath diversity combining [21, 22].

Hence, in mitigating the diverse deleterious effects of a typical CDMA system noted above, the LMMSE technique recurs in mind as an efficient method. That is why the topic of this dissertation has been chosen so. A LMMSE receiver is proposed which is capable of performing both interference suppression and multipath diversity combining. The thesis elaborates on the theory, design, and implementation of the proposed receiver. A distinguishing aspect of this work is its focus on long-code DS-CDMA systems. Long-code CDMA refers to systems which use PN sequences with very large periods (e.g., IS-95 and cdma2000) such that the spreading sequence effectively changes with each bit [23, 24]. Such systems (also referred to as Random-CDMA in [25]) are argued to have lower performance variability among users ([25]-[27]). Yet, the majority of prior art on LMMSE receivers and their adaptive implementations has been limited to CDMA systems in which each bit of a user is spread by the same short pseudo-noise (PN) sequence assigned to that user (e.g., [16, 17, 28, 29]). Although LMMSE receivers for short-code CDMA demonstrate excellent near-far resistance and low computational complexity, they cannot be directly applied to long-code CDMA [25]. Discussions on long-code vs. short-code CDMA can be found in [25] and [27].

The next chapter identifies the specific problems that have motivated this work, surveys the literature, and ends with the thesis statement.

Chapter 2

Problem Identification

This chapter elaborates on the motivation behind this work. The shortcomings of the existing linear receivers are identified and supported by an extensive literature survey. The thesis statement is presented in the end.

2.1 Motivation

Acknowledging their efficiency in suppressing MAI and simple implementations through adaptive architectures, the author in [26] argues that LMMSE receivers suffer from the disadvantage of requiring the use of short spreading sequences. This is so since the statistics of MAI should be periodic (i.e., MAI must be cyclostationary) in order for the adaptive algorithms to function. However, MAI in long-code CDMA systems remains to be a wide-sense cyclostationary (WSCS) process with its period reduced from one bit interval to one chip interval [18, 30]. The LMMSE receiver and its adaptive implementations are, therefore, feasible even in long-code

CDMA as evident in [18, 21] [31]-[33] although they do not demonstrate the excellent near-far resistance and low computational complexity of their counterparts in short-code systems.

The focus of all existing works on LMMSE receivers, except [21], is on MAI suppression under the additive white Gaussian noise (AWGN) channel. Multipath channel conditions are investigated in [21] but with chip waveforms time-limited to one chip period. With bandwidth-efficient chip pulses in mind, the intent of this thesis is to generalize the design of the LMMSE receiver for long-code CDMA to multipath channels and examine its adaptive implementations. Emphasis will be on performing interference suppression and multipath diversity combining simultaneously. In doing so, two major drawbacks of the standard coherent selective Rake receiver[1] are also addressed.

The coherent Rake [34], a linear receiver, is the current industry solution for multipath reception [7]. The receiver processes a subset of the strongest resolvable paths of the desired user by assigning a finger to each path in the subset. The collective contribution of processed paths improves the signal-to-noise ratio (SNR). The conventional Rake receiver employs a common chip-matched filter (CMF) for all its fingers. The CMF is the optimum filter only in AWGN channels [35]. It not only maximizes output SNR in such channels but also provides *sufficient statistics*, i.e., the CMF output delivers all the necessary information required to detect the transmitted signal waveforms. However, in CDMA systems, where the predominant source of interference, often MAI, is neither white nor Gaussian [14], the CMF does

[1]For a brief overview of the coherent Rake receiver, refer to Appendix A.

not maximize output SNR and is no longer guaranteed to provide sufficient statistics. An alternative solution must be considered to improve performance. The LMMSE filter is a viable alternative. The second shortcoming of the Rake receiver arises from its selective nature and limited number of fingers. The number of fingers in the Rake architecture is constrained by limits on power consumption and structural complexity [36]. In sparse multipath channels where multipath components are low in number and apart by a few chip periods, the selective Rake receiver performs well. Future wideband systems, however, bring along dense multipath environments with a large number of resolvable multipath components which cause substantial performance degradation in a Rake receiver with fixed complexity [37]. The LMMSE receiver will be shown to be capable of processing all the desired paths that fall within its time support, no matter how many, at no additional complexity.

Applications of the proposed LMMSE receiver will be in future wideband CDMA systems which not only require the existence of a receiver with ARake[2] feature as the authors in [38] have argued, but also demand an efficient solution to suppress interference, specially ISI and ICI as they can become predominant in high data rate services [19, 20].

The following lists the next logical steps in addressing the shortcomings of prior art and sets the pathway of this thesis.

1. The design of the LMMSE receiver is generalized to multipath channel conditions under a realistic system model. Bandlimited chip waveforms and quadriphase random spreading are two important features of such models often

[2]ARake is the terminology used in [36] for referring to a Rake receiver that has as many fingers as the number of resolvable paths associated with the desired user. Refer to Appendix A.

neglected in previous works.

2. An accurate performance analysis, with probability of bit error (P_e) as the figure of merit, is conducted to quantify the performance improvement.

3. Adaptive and blind adaptive implementations of the LMMSE receiver, which either rely on training through pilot symbols or have a self-organized learning process, are developed to rid the receiver from dependence on the knowledge of a majority of parameters associated with active users. The performance and complexity of the adaptive implementations are also investigated to set guidelines for the proper choice of algorithm with respect to different applications.

2.2 Literature Survey

This section surveys the literature according to the general road map outlined previously. While acknowledging the contributions of existing works, the survey identifies the specific areas in which the thesis makes original contributions.

2.2.1 Design of the LMMSE Receiver

Previous work on LMMSE receivers for one-shot bit symbol detection in asynchronous Random-CDMA can be found in [18, 21, 31, 32]. The work in [21] investigates multipath channel conditions but with chip waveforms time-limited to one chip period. In [18, 31, 32], on the other hand, focus is on bandlimited chip waveforms under the AWGN channel. [18] presents a discrete-time correlator, which

approximates the continuous-time correlator of the LMMSE receiver in [31, 32]. In contrast, the work of [31, 32] derives accurate and explicit formulation of the frequency response of the LMMSE receiver. The quartet of [18, 21, 31, 32] are the most relevant papers to the first part of the thesis. Here, the intent is to generalize the work of [31, 32], which originally considered the AWGN channel, to multipath channels. It will be shown that the LMMSE receiver, a single-user detector, simultaneously performs multipath diversity combining and interference suppression.

Model-specific works on LMMSE receivers for long-code CDMA can also be found in the literature. Examples include, but are not limited to, [39]-[42]. They are aimed at the forward link where orthogonal short codes are scrambled again with cell-specific long codes and transmitted synchronously to different users. The intent is to restore the orthogonality of the codes, lost due to the presence of multipath channels, at the receiver side by employing the MMSE technique. The work of this thesis assumes a more general case. It is not limited to the forward or reverse link and can be applied to both. The PN codes are not necessarily orthogonal and the signals are asynchronous in general. In limiting conditions, however, this thesis verifies some of the end results of [39]-[42].

It is acknowledged again that techniques other than LMMSE filtering have been investigated for long-code CDMA systems. In [43], for instance, adaptive procedures based on the least-squares and serial interference cancellation (SIC) approaches are developed for multiuser detection and channel estimation. The resulting receivers, however, are usually more complex than the LMMSE receiver [25]. As another example, [44] investigates the application of Kalman filters to linear re-

ceivers for suppressing MAI. In order to make their proposed method applicable to multipath channels, the authors use a pre-detection Rake receiver. Hence, the problems of multipath diversity combining and interference suppression are treated separately. Moreover, the proposed receiver of [44] is still prone to one of the shortcomings of the Rake receiver in dense multipath channels: insufficient number of fingers. In contrast, this work does not separate the two tasks of diversity combining and interference suppression. The LMMSE receiver is explicitly solved for the case when both MAI and multipath conditions are present.

The drawbacks of the coherent selective Rake receiver, described in the previous section, have also been addressed with a different approach. In [45, 46], a generalized Rake receiver for the downlink is proposed. The work in [46] models interference as colored Gaussian noise and benefits from the orthogonality of the spreading codes. It employs a maximum likelihood formulation for the finger weights and delivers significant gains by increasing the number of fingers beyond the number of multipath components. The extra fingers are responsible for suppressing interference. The work in [45] is similar to that of [46] except that MAI is modelled as a wide sense stationary process. In fact, both [45, 46] improve the Rake receiver by optimizing the number of fingers, their delays and weights. However, they restrict the solution to a finite impulse response (FIR) filter with a number of taps comparable to the Rake receiver. The LMMSE receiver of this work, on the other hand, is not restricted to the Rake structure. The presented solution is exact and explicit.

Fig. 2.1 illustrates the roadmap of DS-CDMA receivers and shows the area

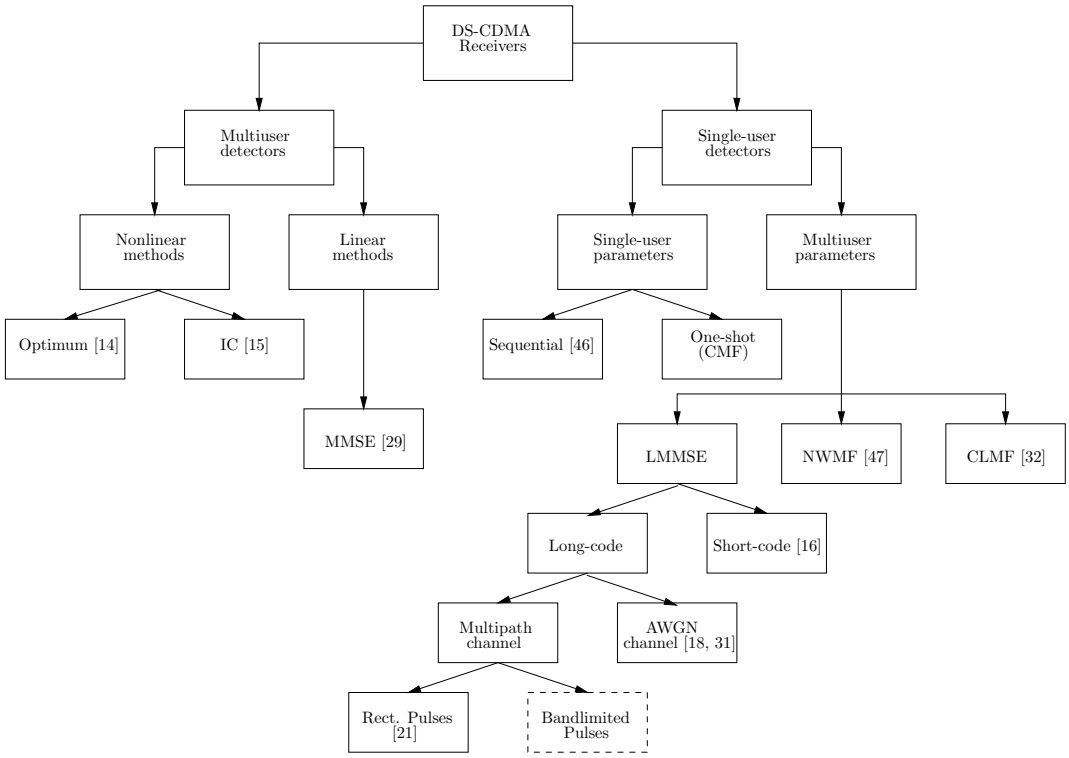

Figure 2.1: Roadmap of DS-CDMA receivers. The area that this thesis covers is shown with a dashed block.

where the thesis covers. It is emphasized that the intent of Fig. 2.1 is to visually demonstrate where the thesis contributes, not to present a complete classification of DS-CDMA receivers.

2.2.2 Performance Analysis of the LMMSE Receiver

The thesis analyzes the performance of the LMMSE receiver and compares it with that of the coherent selective Rake receiver based on probability of bit error (P_e). Although SNR is the most common figure of merit in performance analysis, the contribution of the thesis is in the P_e analysis which plays a crucial role in many

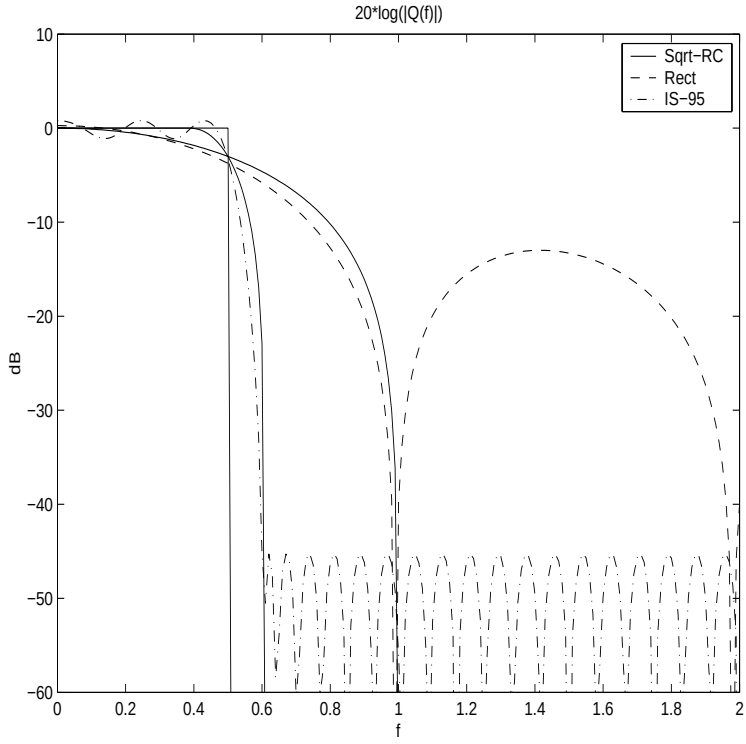

Figure 2.2: The normalized energy density spectrum of $|Q(f)|^2$ (in dB) of several pulse shaping filters: the square-root raised-cosine pulse with excess bandwidths $\alpha = \{0, 0.22, 1.0\}$, the rectangular pulse, and the IS-95 pulse.

areas of DS-CDMA systems such as capacity estimation and receiver design.

Two general focal points distinguish this part from existing analyses. The first is its focus on chip pulse shaping as in the design of the LMMSE receiver. Regardless of the receiver under study, most existing performance analyses neglect the effect of pulse shaping and consider time-limited rectangular chip pulses (e.g., [48]-[51] on the chip-matched filter receiver, [52] on the Rake receiver, and [21, 39] on the LMMSE receiver). To highlight the different behaviors of pulse filters commonly used in the literature, Fig. 2.2 plots the energy density spectrums of bandwidth-

efficient pulse filters (the square-root raised-cosine pulse and the IS-95 pulse) and compares it with that of the rectangular pulse.

The second point is the accuracy of P_e analysis for both the LMMSE and Rake receivers. A vast majority of existing works invoke the standard Gaussian approximation (SGA) for P_e performance analysis without investigating its accuracy. The SGA is known to return increasingly over-optimistic results as P_e decreases [50, 51]. This drawback is countered here. The presented P_e analysis is based on the improved Gaussian approximation (IGA) and extends a recent result [53, 54] which studies, in detail, the P_e performance of CDMA systems with random quadriphase spreading in AWGN channels. The work in [53, 54] shows that the IGA reduces to the SGA for pulse shapes of zero excess bandwidth (BW). Moreover, it is shown that the SGA is an accurate approximation for spreading factors of moderate to large values and chip pulses of small excess BW. The presented analysis has two important distinctions from those of [53, 54]: *i)* it is extended to multipath channels in contrast to those in [53, 54] which are limited to AWGN channels, and *ii)* it is extended to general filters in the receiver side in contrast to those in [53, 54] which are limited to the CMF receiver. Monte Carlo simulations are also included to verify the accuracy of the analysis.

It is acknowledged that, in an independent work parallel to this work, the authors in [55] also present an accurate P_e analysis for bandlimited quadriphase Random-CDMA systems. In [55], accurate average P_e expressions based on conditional Gaussian approximation are derived that do not require numerical integration. However, the analysis in [55] is limited to AWGN channels. The intention

of this work is to present a general P_e analysis for multipath channels that can be applied to systems with identical or different transmit and receive filters (e.g., the coherent Rake and LMMSE receivers, respectively).

Contributions on performance analysis of LMMSE receivers for long-code CDMA systems include, but are not limited to, [18, 21, 31, 32, 39, 56, 57]. As noted earlier, in [21, 39], pulse shaping is neglected and rectangular chip pulses are assumed. However, in [18, 31, 32], pulse shaping is brought to attention but the receiver design is limited to AWGN channels. Moreover, the figure of merit in the performance analyses of [18, 21, 31, 32, 39] is not P_e. Also in [56], P_e performance of a related adaptive chip equalizer is only evaluated via simulations and no analysis is presented. In contrast, [57] investigates the P_e performance. However, a fundamental difference exists between the work of [57] and this work. The LMMSE receiver considered in [57] was originally designed for short-code CDMA systems and is the same as that of [16]. Long spreading codes are considered only in performance analysis where output SNR is determined and the SGA is applied to derive the bit error probability. Here, the performance of the LMMSE receiver specifically designed for long-code CDMA is studied. The effect of chip pulse shaping, quadriphase spreading and the accuracy of the SGA, neglected in [57], are of special interest in this work.

Performance analysis of the Rake receiver has also been the subject of many papers (e.g., [36, 52][58]-[60]). In [58, 59], the effect of orthogonality of the spreading sequences on the SNR performance of the Rake receiver is studied. In [36, 60], the impact of spreading bandwidth and the number of Rake fingers on the SNR

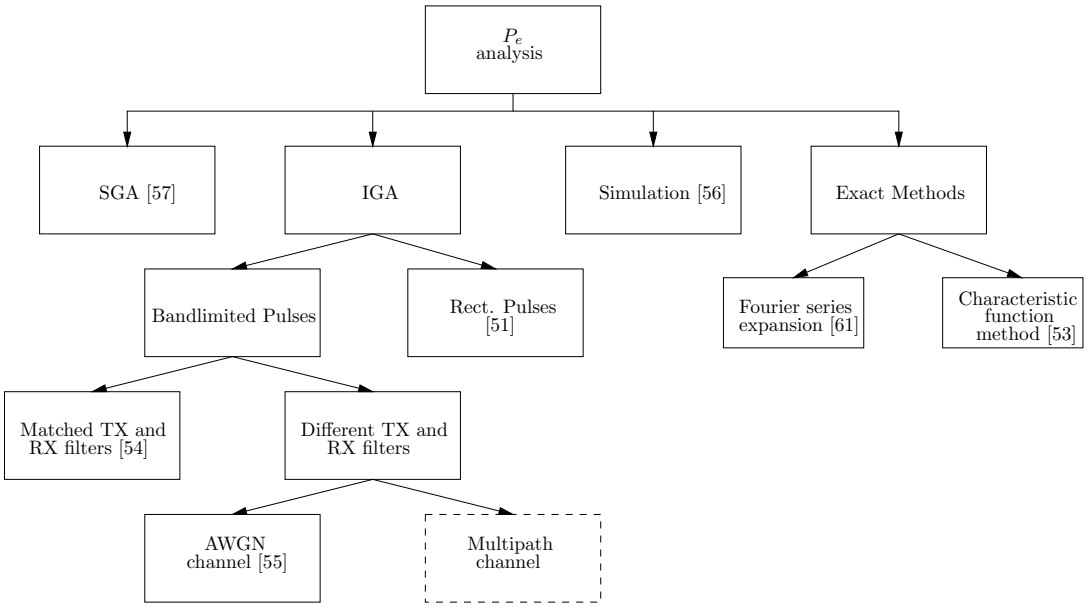

Figure 2.3: Roadmap of methods of P_e analysis. The area that this thesis covers is shown with a dashed block.

performance is investigated. In [52], on the other hand, the P_e performance of the Rake receiver is analyzed. However, rectangular chip pulses are again assumed in the system model.

Fig. 2.3 illustrates the roadmap of methods of P_e analysis and shows the area where the thesis covers. It is emphasized that the intent of Fig. 2.3 is to visually demonstrate where the thesis contributes, not to present a complete classification of methods of P_e analysis.

2.2.3 Adaptive Implementations of the LMMSE Receiver

The LMMSE receiver will be shown to be dependent on the knowledge of multipath parameters of the desired and interfering users, which are normally not available in

the receiver side. Whether such information is accessible or not, it is advantageous to rid the receiver from depending on it in order to reduce complexity. Hence, adaptive realizations appear as the practical way of implementation.

Adaptive algorithms are furnished by training sequences, known to the receiver, to converge to a desired solution. Training sequences are provided to the receiver prior to data transmission. When the adaptive receiver converges to the desired solution (or when the output SNR is high enough to make the outputs of the decision device reliable), training is ceased and data transmission starts. Pilot signals can also be used as training sequences. Pilot signals can be present in current CDMA systems in two forms: they are either time-multiplexed or code-multiplexed with the information symbols. In the former, referred to as the pilot-symbol-aided (PSA) method, pilot signals are inserted periodically in between the information symbols. In the latter, however, the pilot sequence is constantly transmitted on a separate code-multiplexed channel, usually orthogonal to the traffic channel. This method is referred to as the pilot-channel-aided (PCA). Pilot channels, which already exist in the forward link, has recently been incorporated in the reverse link of CDMA systems to make coherent reception feasible [9, 10, 62].

Both training-based and PCA methods are investigated in this thesis. Previous works on training-based adaptive LMMSE receivers for long-code CDMA include [18, 21, 33] which have already been reviewed in the previous sections. In addition to the distinguishing features between [18, 21, 33] and this work noted earlier, another important difference appears in the architecture of the proposed receiver: despreading is performed after equalization in contrast to [18, 21, 33]

which do it prior to equalization. One implication of such rearrangement is savings in complexity which will be explained later in further detail.

PCA methods in Random-CDMA have been examined in [63]-[66]. In [63]-[65], non-linear interference cancellation schemes, as opposed to the linear MMSE method, are studied. In contrast, the figure of merit in [66] is MMSE. However, the proposed receiver has still a Rake architecture. The focus is on moving averages based on adaptable integration times in each finger to equalize the mutlipath channel. Moreover, [66] considers dynamic adjustment of the pilot channel power to improve performance. In this thesis, however, pilot power optimization is not investigated. The intent is to demonstrate how the proposed LMMSE receiver can be realized, with or without the presence of pilot signals.

In the absence of pilot signals, blind adaptive algorithms become appealing for their self-organized learning process. Among blind algorithms, the constant modulus algorithm (CMA) [67, 68] has attracted much attention due to its practicality and near-MMSE performance. In an effort to rid the adaptive receiver from dependence on pilot signals, constant modulus (CM) approaches are examined to develop blind receivers. The CMA has already been studied for short-code CDMA systems in the AWGN channel [69, 70] and multipath environments [71]. The work in [69, 70] is based on linear constraints that originate from short PN sequences assigned to the desired user. In [71], the work of [69, 70] is extended to multipath channels with the additional condition of knowing the arrival delays of all the desired paths, a condition rendered unnecessary in the proposed receiver of this work. To the best of the author's knowledge, the CMA has not been investigated

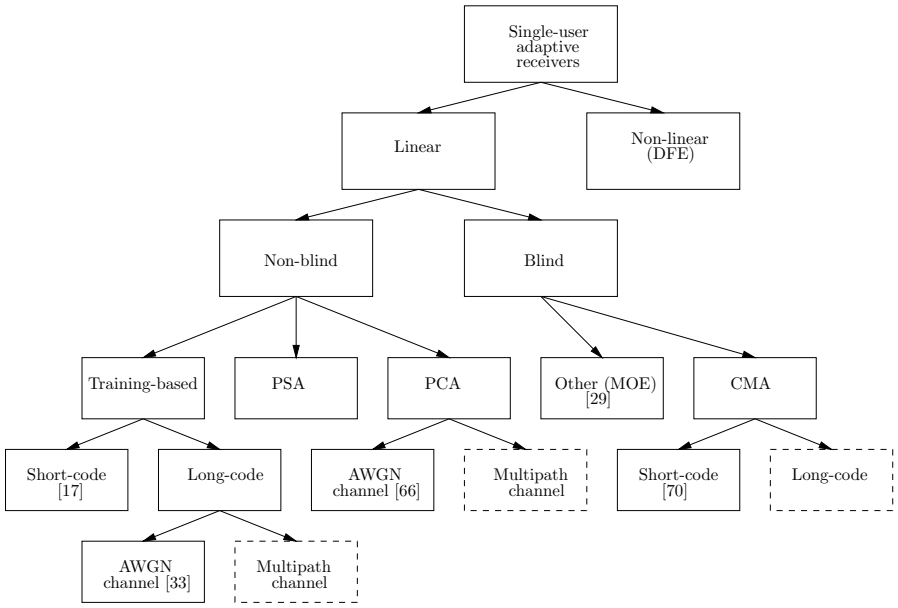

Figure 2.4: Roadmap of single-user adaptive CDMA receivers. The areas that this thesis covers are shown with a dashed block.

for long-code CDMA systems.

Finally, a novel set of algorithms are proposed to improve the power-efficiency of PCA schemes in the reverse link. The accuracy of channel estimation in the reverse link is strongly dependent on the pilot channel power, which often constitutes a small portion of the mobile user signal power. Higher levels of pilot power improve the performance in channel estimation but compromise the capacity of the traffic channel. To address this tradeoff and inspired by the CM-based approaches of the proposed blind algorithms, a new set of algorithms are examined that jointly utilize the pilot and traffic channel statistics to improve the performance while maintaining a low level of pilot power. This is in contrast to conventional PCA algorithms which only rely on the pilot channel statistics. The idea of jointly utilizing the pilot and

traffic channel statistics is not original and has appeared before in the literature (e.g., [63]). However, the proposed algorithms of this work build on blind CM algorithms noted earlier which have not been explored in CDMA systems with random aperiodic spreading sequences.

All the discussed algorithms are compared and contrasted with each other based on three criteria: *i)* their performance in terms of output SNR, *ii)* their rate of convergence, and *iii)* their computational complexity. The complexity analysis is straightforward. The number of summation, multiplication, division, and square root operations required per each update interval are calculated and compared. Analysis for SNR performance and convergence rate are based on extensive and quantitative simulations rather than detailed analyses. They are compared with the results of general analyses available in the literature. Studies on the performance of adaptive algorithms based on general adaptive filter theory can be found in [72, 73] and references therein. They are usually based on the assumptions of independence theory [72] to make them mathematically tractable. However, the independence theory, which assumes successive samples of the received signal are independent, does not always hold true for the CDMA system model. This has motivated model-specific works such as [74] for convergence rate analysis of short-code CDMA. Similar work is essential for long-code CDMA models in order to set guidelines for the selection of a suitable algorithm corresponding to a specific application. This issue is a topic for future study.

Fig. 2.4 illustrates the roadmap of single-user adaptive CDMA receivers and shows the areas where the thesis covers. It is emphasized that the intent of Fig. 2.4

is to visually demonstrate where the thesis contributes, not to present a complete classification of adaptive receivers.

2.3 Thesis Statement

Taking the preceding discussions and survey into consideration, the thesis statement can be summarized as follows:

> "The thesis studies the design and implementation of a LMMSE receiver for bandlimited DS-CDMA systems that employ quadriphase random spreading and operate in multipath environments. The receiver is shown to be capable of interference suppression and multipath diversity combining without the knowledge of other users' signature sequences. It maximizes output SNR and processes all paths of the desired user that fall within its time support. The impulse response of the receiver is explicitly derived. Its performance is accurately evaluated and compared with that of coherent selective Rake receiver. An adaptive architecture is proposed for the implementation of the receiver. Training-based, PCA, and blind algorithms are examined. Their performance loss and convergence rate are quantified via extensive simulations. Accompanied by a complexity analysis, these results set the guidelines for the proper choice of algorithms suitable for specific applications."

The remaining of the thesis is organized as follows. Chapter 3 discusses the design of the LMMSE receiver. The system model is described first. Next, the

impulse response of the LMMSE receiver is derived. Its structure is then discussed and compared with that of the coherent selective Rake receiver. Chapter 4 is on the performance analysis of the LMMSE receiver. Accurate P_e analysis is conducted. The performance of the LMMSE receiver is compared with that of the selective Rake receiver to quantify the achievable improvements. Chapter 5 proposes an adaptive architecture for realizing the LMMSE receiver and examines several adaptive algorithms. Simulation results are presented that quantify the performance of the proposed adaptive algorithms. A complexity analysis is also accompanied. Chapter 6 outlines topics for future study.

Chapter 3

Theory & Design

In this chapter, the theory and design of the LMMSE receiver are discussed. The contributions of this chapter are as follows:

- The LMMSE receiver for bandlimited CDMA with quadriphase spreading in the presence of multipath channels are derived. The filter frequency response is explicitly formulated and its shape is examined under limiting conditions of interest.

- For the ideal Nyquist chip pulse, the LMMSE receiver is shown to reduce to a maximal-ratio-combining (MRC) receiver that processes *all* paths of the desired user that fall within the time support of the new chip filter.

- When the excess bandwidth of the chip pulse is nonzero, the LMMSE receiver is shown to exploit the cyclostationarity of the received signal and suppress interference.

The system model is explained first. Based on the principle of LMMSE filtering, the receiver is then derived and formulated. Its structure is investigated next. The receiver is finally examined under some limiting conditions. The material of this chapter can also be found in [75, 76].

3.1 System Model

The reverse link of a quadrature phase-shift keying (QPSK) DS-CDMA system with $K+1$ asynchronous users in a multipath environment is under review. This section describes the modeling of the multipath channel and the received signal. An arbitrary user is designated as the desired user and indexed as user 0.

3.1.1 Multipath Channel

The conventional multipath model as described in [77] is considered with simplifications in the modeling of the parameters to ease system analysis. User k encounters a multipath channel with an impulse response of the form

$$c^{(k)}(t) = \sum_{l=1}^{L^{(k)}} e^{j\theta_l^{(k)}} \alpha_l^{(k)} \delta\left(t - \tau_l^{(k)}\right). \tag{3.1}$$

The transmitted signal from user k is received via $L^{(k)}$ paths. The lth path is characterized by three variables: its attenuation factor $\alpha_l^{(k)}$, its arrival delay $\tau_l^{(k)}$, and its carrier phase shift $\theta_l^{(k)}$. The forward link can also be accommodated in the above model as a special case where $c^{(0)}(t) = c^{(1)}(t) = \ldots = c^{(K)}(t)$ without any loss of generality.

The number of paths associated with user k, $L^{(k)}$, is considered to be a constant number as opposed to a random variable (RV). Attenuation factors, $\alpha_l^{(k)}$, are real and the multipath channel is assumed to be lossless[1] for all users in the sense that

$$\sum_{l=1}^{L^{(k)}} \left|\alpha_l^{(k)}\right|^2 = 1, \quad \forall k. \tag{3.2}$$

The parameters $\alpha_l^{(k)}$ and $\tau_l^{(k)}$ are independent RVs assumed to be known to the receiver. Their distributions can arbitrarily be any of those accepted in the literature for modelling them (e.g., Rayleigh distribution for $\alpha_l^{(k)}$ and exponential distribution for $\tau_l^{(k)}$ [78]).[2] Phase shifts, $\theta_l^{(k)} \in [0, 2\pi)$, are modeled as uniformly distributed RVs. Moreover, they are considered to be mutually independent across all l and k. Each user experiences a stable (time-invariant) multipath channel. Hence, the channel parameters are assumed to remain fixed during the course of transmission. Coherent reception is considered. Therefore, the phase shifts of all paths of the desired user, $\theta_l^{(0)}$, are assumed to be known to the receiver and remain constant.

Later on in Chapter 5, the above limiting assumptions will be relaxed to some extent. Specifically, it will be shown that none of the multipath parameters (except an estimate of $\tau_1^{(0)}$) need to be known for adaptive implementations. Also, the channel can vary as long as the variation rate is sufficiently below the convergence rate of the employed adaptive algorithm.

[1]Lossy channels can be modeled in a similar fashion by an extra path with an attenuation factor equal to the total channel loss.

[2]The distributions of $\alpha_l^{(k)}$ and $\tau_l^{(k)}$ do not affect the design of the receiver but they influence its performance.

3.1.2 Received Signal

The received signal can be written as

$$r(t) = \sum_{k=0}^{K} s^{(k)}(t) \otimes c^{(k)}(t) + \eta(t) \tag{3.3}$$

using the complex baseband representation of passband signals. The second term $\eta(t)$ is a complex, circularly symmetric, zero-mean AWGN process with a two-sided noise power spectral density (PSD) of $\mathcal{N}_0$ [79, pp. 311–316]. The first term represents the sum of the received signals from each user where $s^{(k)}(t)$ is the transmitted signal of user k and $\otimes$ represents the convolution operator. The baseband representation of the quadriphase DS-CDMA signal of user k can be expressed as

$$s^{(k)}(t) = \sqrt{\frac{P_k}{2}} \left[x_I^{(k)}(t) - j x_Q^{(k)}(t) \right] \tag{3.4}$$

where the in-phase (I) and quadrature-phase (Q) signal components are

$$x_{\mathcal{B}}^{(k)}(t) = \sum_{n=-\infty}^{\infty} b_n^{(k)} a_n^{(\mathcal{B},k)} (t - nT_b^{(k)}) \tag{3.5}$$

and $\mathcal{B} \in \{\mathrm{I}, \mathrm{Q}\}$. The bits $b_n^{(k)} \in \{\pm 1\}$ of user k are transmitted at a rate of $1/T_b^{(k)}$ over both the I and Q branches. The bits of each user are assumed to form an independent and identically distributed (i.i.d.) random sequence with equal probabilities and with independence between the bits of different users. The symbol P_k represents the signal power of user k. Code acquisition, carrier-phase and bit symbol timing synchronization for the earliest path of the desired user are

assumed such that $\tau_1^{(0)} = 0$ and $\theta_1^{(0)} = 0$.

The spreading waveforms $a_n^{(I,k)}(t)$ and $a_n^{(Q,k)}(t)$, used to spread $b_n^{(k)}$, are

$$a_n^{(\mathcal{B},k)}(t) = \sum_{i=0}^{N^{(k)}-1} a_{i+nN^{(k)}}^{(\mathcal{B},k)} q(t - iT_c) \tag{3.6}$$

where $a_i^{(\mathcal{B},k)} \in \{\pm 1\}$ represents the ith chip of the PN sequence corresponding to the $\mathcal{B}$ branch of user k generated at the rate of $1/T_c$ common to all users. The PN sequences are assumed to be equally likely i.i.d. random sequences with equal probabilities and with independence between the chips of different users. Mutual independence is also assumed among the PN sequences of the I and Q branches. The spreading sequences associated with $b_n^{(k)}$ are defined as

$$\boldsymbol{a}_n^{(\mathcal{B},k)} = [a_{nN^{(k)}}^{(\mathcal{B},k)}, a_{nN^{(k)}+1}^{(\mathcal{B},k)}, \ldots, a_{nN^{(k)}+N^{(k)}-1}^{(\mathcal{B},k)}]. \tag{3.7}$$

The ratio of the chip rate to the bit rate of each user, $N^{(k)}$, is referred to as the *spreading factor* of user k.

The chip pulse $q(t)$, assumed to be real, satisfies the following three constraints: *i)* it satisfies the energy constraint: $\int_{-\infty}^{\infty} |q(t)|^2 \, dt = T_c$; *ii)* it can be approximated as a time-limited pulse of duration $(2M-1)T_c$ such that $q(t) = 0$ if $t < (-M+1)T_c$ or $t > MT_c$ for an integer, M. For example, for the IS-95 chip pulse, $M = 12$; and *iii)* α represents the percentage of BW in excess of the minimum bandwidth $1/(2T_c)$ required for symbol transmission at the chip rate of $1/T_c$. Hence, the BW of the chip waveform is $(1+\alpha)/(2T_c)$. For instance, for the Wideband CDMA (WCDMA) chip pulse which is the square-root raised-cosine (Sqrt-RC) pulse, $\alpha = 22\%$ [23].

The *processing gain* (or BW expansion factor) of user k is $\mathrm{PG}^{(k)} = N^{(k)}(1+\alpha)$ [4].

The system model supports *multi-rate* CMDA since, in general, $N^{(k)} \neq N^{(k')}$ for $k \neq k'$ leading to multiple bit rates for different users. Moreover, if the baseband signal component defined in (3.5) experiences a delay of $\tau_l^{(k)}$, corresponding to the delay of the lth path of the kth user, it can alternatively be expressed as

$$x_{\mathcal{B}}^{(k)}(t-\tau_l^{(k)}) = \sum_{n=-\infty}^{\infty} d_n^{(\mathcal{B},k,l)} q(t - T_l^{(k)} - nT_c) \tag{3.8}$$

where

$$d_n^{(\mathcal{B},k,l)} = b^{(k)}_{\lfloor (n-J_l^{(k)})/N^{(k)} \rfloor} a^{(\mathcal{B},k)}_{n-J_l^{(k)}}, \tag{3.9}$$

$$J_l^{(k)} = \lfloor \tau_l^{(k)}/T_c \rfloor, \tag{3.10}$$

and,

$$T_l^{(k)} = \mathrm{mod}(\tau_l^{(k)}, T_c) \tag{3.11}$$

represent, respectively, the direct-sequence spread bits, the bit delay as an integer multiple of T_c and the bit delay *modulo* the chip period such that $J_l^{(k)} \in \{0, \ldots, N^{(k)}-1\}$, $T_l^{(k)} \in [0, T_c)$ and $\tau_l^{(k)} = J_l^{(k)} T_c + T_l^{(k)}$. The floor function $\lfloor x \rfloor$ returns the integer portion of a real number x. The term $T_l^{(k)}$ is referred to as the *chip delay* of the lth path of the kth user. With this reformulation of (3.8), from the perspective of the lth path of user 0, $d_n^{(\mathcal{B},k,l')} \in \{\pm 1\}$ (with $l' \neq l$ when $k = 0$) can be effectively modeled as equally likely i.i.d. random sequences. Thus, the effects of the interferer bits and integer bit delays disappear under the random spreading assumption.

3.2 Design

This section addresses the design of the linear MMSE receiver for user 0. The approach is similar to that of [31, 32] except for generalizing the AWGN channel to the multipath channel. It differs from the method of [18, 21] which approximates the continuous-time correlator of the LMMSE receiver based on observables that are output samples from the despreader; the PN sequence of the desired user modulated by the chip waveform. Here, the general frequency response of the LMMSE filter is accurately and explicitly derived by solving a *Fredholm integral equation of the first kind* [80, p. 224] based on an infinite observation interval.

Linear time-invariant filtering of a real signal is known to be equivalent to linear time-invariant filtering of its *analytical* signal (or its complex envelope). However, in general, linear time-variant filtering of a real signal is equivalent to distinct linear time-variant filtering of each of the complex envelope and its complex conjugate. Hence, if complex signals are to be used, as adopted in the system model, the problems of optimum and adaptive time-variant filtering must be approached as bivariate filtering problems, where a signal and its conjugate are jointly filtered and then added together [81, 82]. This is referred to as linear/conjugate linear (LCL) filtering. The receiver structure is depicted in Fig. 3.1 and consists of a pair of LCL filters [83, p. 259], $\phi_n(t)$ and $\psi_n(t)$, a complex conjugation operator, two summers and a bit-rate sampler. Let $N = N^{(0)}$, $T_b = T_b^{(0)}$, and $\mathrm{PG} = \mathrm{PG}^{(0)}$. The index n is used to denote the filter response associated with the detection of $b_n^{(0)}$. The estimate of $b_n^{(0)}$, sampled at $t = (n+1)T_b$ at the LCL filter output, determines the error between the transmitted and estimated nth bit: $\varepsilon(n) = b_n^{(0)} - \hat{b}_n^{(0)}$ where

$\hat{b}_n^{(0)}$ can be expressed as

$$\hat{b}_n^{(0)} = \int_{-\infty}^{\infty} r(u)\phi_n(T_b - u) + r^*(u)\psi_n(T_b - u)du. \tag{3.12}$$

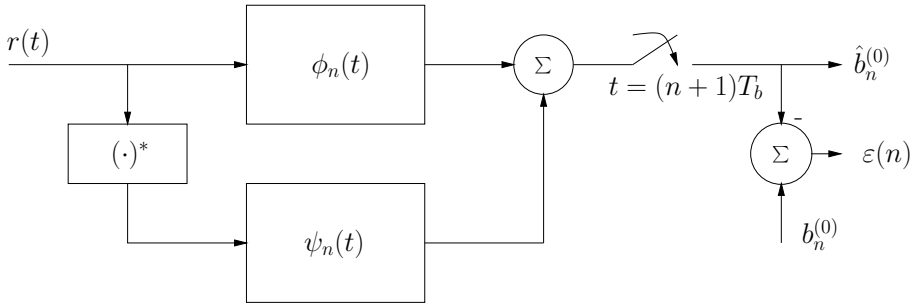

Figure 3.1: The linear/conjugate linear (LCL) filtering structure for user 0.

The two impulse responses, $\phi_n(t)$ and $\psi_n(t)$, are designed to minimize the MSE whose cost function can be written as:

$$\mathcal{J}_{MSE,n} = \mathrm{E}[|\varepsilon(n)|^2]. \tag{3.13}$$

The expectation operation is conditioned on $\boldsymbol{a}_n^{(0)}$, the path signal powers $P_k|\alpha_l^{(k)}|^2$, bit delays $\tau_l^{(k)}$ (for $1 \leq l \leq L^{(k)}$ and $0 \leq k \leq K$), and carrier phase shifts of the desired user $\theta_l^{(0)}$ for $1 \leq l \leq L^{(0)}$. The phase shifts of the interfering paths play no role in the integral equation as it will be clear shortly.

The filters $\phi_n(t)$ and $\psi_n(t)$ are determined using the two orthogonality conditions for complex envelopes [83]: $\mathrm{E}[\varepsilon(n)r(t)] = 0$ and $\mathrm{E}[\varepsilon(n)r^*(t)] = 0$. Substituting $\varepsilon(n)$

and $\hat{b}_n^{(0)}$ into the first orthogonality condition yields the linear integral equation:

$$\int_{-\infty}^{\infty} R_{rr}(t,u)\phi_n(T_b-u)+R_{rr^*}(t,u)\psi_n(T_b-u)du = \mathrm{E}[b_n^{(0)}r(t)],\ -\infty < t < \infty \quad (3.14)$$

where

$$R_{xx^*}(t,u) = E[x(t)x^*(u)] \quad (3.15)$$

and

$$R_{xx}(t,u) = E[x(t)x(u)] \quad (3.16)$$

denote, respectively, the autocorrelation function and complementary autocorrelation function of a complex random process $x(t)$ [79, p. 312]. The second orthogonality condition reveals that the impulse response of $\psi_n(t)$ satisfies $\psi_n(t) = \phi_n^*(t)$. The impulse response of $\phi_n(t)$ can be determined by replacing $r(t)$ in (3.14) with its equivalent from (3.3) and defining $\phi_n(t)$ as

$$\phi_n(t) = \beta_n h_n(t). \quad (3.17)$$

The solution for of $h_n(t)$ is presented next. The expression for the scalar β_n can be found in Appendix B.

The Fredholm integral equation in (3.14) simplifies to

$$\frac{1}{2}\int_{-\infty}^{\infty} R_{nn^*}(t,u)h_n^*(T_b-u)du = \sum_{l=1}^{L^{(0)}} e^{j\theta_l^{(0)}}\alpha_l^{(0)}\left[a_n^{(I,0)}(t-\tau_l^{(0)}) - ja_n^{(Q,0)}(t-\tau_l^{(0)})\right], \quad (3.18)$$

for $-\infty < t < \infty$, where $R_{nn^*}(t,u)$ represents the autocorrelation function of the

noise

$$n(t) = \sum_{k=1}^{K} s^{(k)}(t) + \eta(t). \tag{3.19}$$

The right hand side of (3.18) is the received signal associated with $b_n^{(0)}$. It is straightforward to show that $R_{nn}(t,u) = 0$ for quadriphase random spreading. It is also noted that the phase shifts of the interfering paths disappear from the integral equation of (3.18) in quadriphase CDMA systems regardless of their distributions or conditioning in the expectation operations. The expression for $R_{nn^*}(t,u)$ can also be shown to simplify to

$$R_{nn^*}(t,u) = \sum_{k=1}^{K} \sum_{l=1}^{L^{(k)}} P_k |\alpha_l^{(k)}|^2 \left(\sum_{n=-\infty}^{\infty} q(t - T_l^{(k)} - nT_c) q(u - T_l^{(k)} - nT_c) \right) + \mathcal{N}_0. \tag{3.20}$$

The noise taken into account in the design neglects ISI and ICI. This can be justified when the duration of the transmitted symbol is large compared with the duration of the multipath profile [77]. In DS-CDMA systems, this translates to large values for N. Moreover, as the number of interferers increase, the effects of ISI and ICI fade in significance substantially. On the other hand, they can turn to the dominant source of interference in high-data-rate applications of next-generation systems when the number of high-powered users is low and the spreading factor is small. In either case, whether they are negligible or not, adaptive implementations of the proposed receiver considers ISI and ICI and shapes its frequency response accordingly. In contrast, the Rake receiver ignores them.

The noise defined by (3.19) and (3.20) can be shown to be a wide-sense cyclostationary (WSCS) process [83] with a period of T_c [18, 30]. The method of solving

for $h_n(t)$ from the integral equation in (3.18) follows that of [31, 32]. The harmonic series representation (HSR) technique [83] is applied and the cyclostationarity of noise is used to solve for $h_n(t)$ explicitly. The expression for $h_n(t)$ is presented here in brief; details concerning its derivation can be found in [30]. The frequency response of $h_n(t)$ can be expressed as

$$H_n(f) = G(f)\left[\mathcal{A}_n^{(I,0)*}(e^{j2\pi fT_c}) + \mathcal{A}_n^{(Q,0)*}(e^{j2\pi fT_c})\right] e^{-j2\pi fT_b} \tag{3.21}$$

where

$$\mathcal{A}_n^{(\mathcal{B},0)}(z) = \sum_{l=0}^{N-1} a_{l+nN}^{(\mathcal{B},0)} z^{-l} \tag{3.22}$$

is the Z-transform of the desired user's spreading sequence $\boldsymbol{a}_n^{(\mathcal{B},0)}$. The filter $G(f)$, whose frequency response is summarized in Appendix C, represents a new chip pulse filter replacing the CMF, $Q^*(f)$, where $Q(f)$ is the Fourier transform of $q(t)$. The proposed receiver minimizes MSE which is given by $\mathcal{J}_{MSE,n}^{\min} = (1 + \mathrm{SNR}_{\max,n})^{-1}$. The expression for the $\mathrm{SNR}_{\max,n}$ can be found in Appendix B.

3.3 Structure

The resulting LMMSE receiver structure is depicted in Fig. 3.2 in the form of a coherent correlator. The new chip pulse filter $G(f)$ replaces $Q^*(f)$ and the factor β_n scales the bit-decision statistics. The remaining components are identical to those of the CMF receiver.

The $G(f)$ filter can be broken to $L^{(0)}$ branches, as shown in Fig. 3.3, where each branch functions as a finger of the Rake receiver and processes one path of the

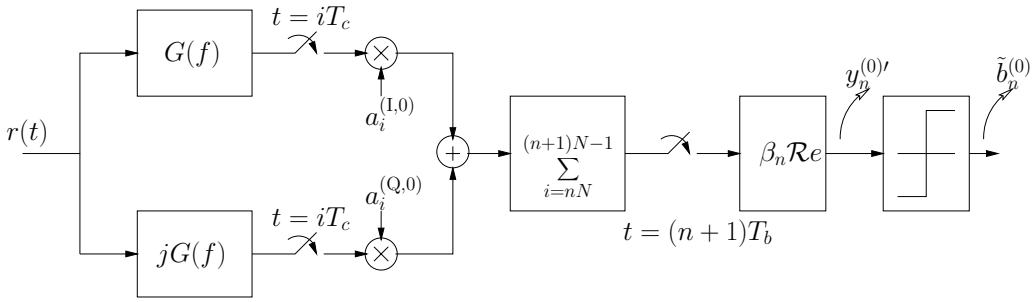

Figure 3.2: Linear MMSE receiver structure for user 0.

desired user. More specifically,

$$G(f) = \sum_{l=1}^{L^{(0)}} C_l^{*(0)}(f) G_l(f) \tag{3.23}$$

where $G_l(f)$ is the new chip filter corresponding to the lth path formulated in Appendix C and $C_l^{(0)}(f)$ is the Fourier transform of the lth path channel response. The desired user's channel impulse response can be written as:

$$C^{(0)}(f) = \sum_{l=1}^{L^{(0)}} C_l^{(0)}(f) \tag{3.24}$$

$$C_l^{(0)}(f) = \alpha_l^{(0)} e^{j\theta_l^{(0)}} e^{-j2\pi f \tau_l^{(0)}}. \tag{3.25}$$

The structure of the $G(f)$ filter can be compared and contrasted with that of the coherent Rake receiver explained in Appendix A. In each branch, the $G_l(f)$ replaces the CMF, $Q^*(f)$. As in the Rake receiver, the frequency response $C_l^{*(0)}$ can be interpreted as a filter matched to the lth path of the desired user. The exponential term in (3.25), $e^{j2\pi f \tau_l^{(0)}}$, aligns the lth finger to the lth path. The weighting

coefficient, $\alpha_l^{(0)} e^{j\theta_l^{(0)}}$, realizes the MRC scheme. The $G_l(f)$ filter distinguishes itself from CMF as α increases from zero and MAI dominates AWGN. The shape of its frequency response is discussed next with the aid of a simple example.

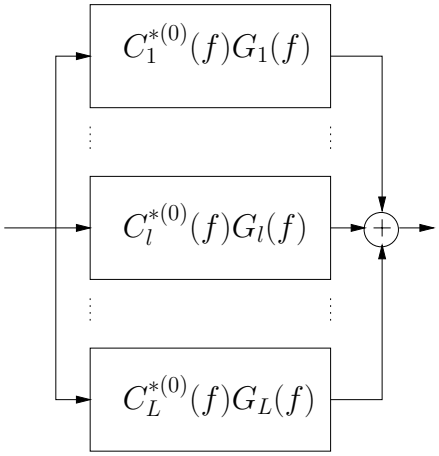

Figure 3.3: The structure of the $G(f)$ filter where $L^{(0)} = L$.

Fig. 3.4 illustrates an example of the normalized frequency response of $G_l(f)$ for the Sqrt-RC chip pulse with $\alpha = 0.22$ excess BW in the reverse link of a DS-CDMA system with two active users. This example will be referred to again later in the next chapter. The signal of each user is received via two paths $L^{(0)} = L^{(1)} = 2$ and both users are equally powered. The effect of AWGN is ignored by setting $\mathcal{N}_0 = 0$. Also, $T_c = 1$. Attenuation factors, chip delays, and phase shifts of all paths are indicated in $\boldsymbol{A}$, $\boldsymbol{T}$, and $\boldsymbol{\Theta}$ matrices [3], respectively, where $[\boldsymbol{A}]_{k,l} = \alpha_l^{(k-1)}$, $[\boldsymbol{T}]_{k,l} = T_l^{(k-1)}$, and $[\boldsymbol{\Theta}]_{k,l} = \theta_l^{(k-1)}$.

[3]

$$\boldsymbol{A} = \begin{bmatrix} 0.60 & 0.80 \\ 0.71 & 0.71 \end{bmatrix} \quad \boldsymbol{T} = \begin{bmatrix} 0.0 & 0.6 \\ 0.8 & 0.3 \end{bmatrix} \quad \boldsymbol{\Theta} = \begin{bmatrix} 0 & \frac{2\pi}{3} \\ \pi & \frac{\pi}{2} \end{bmatrix}$$

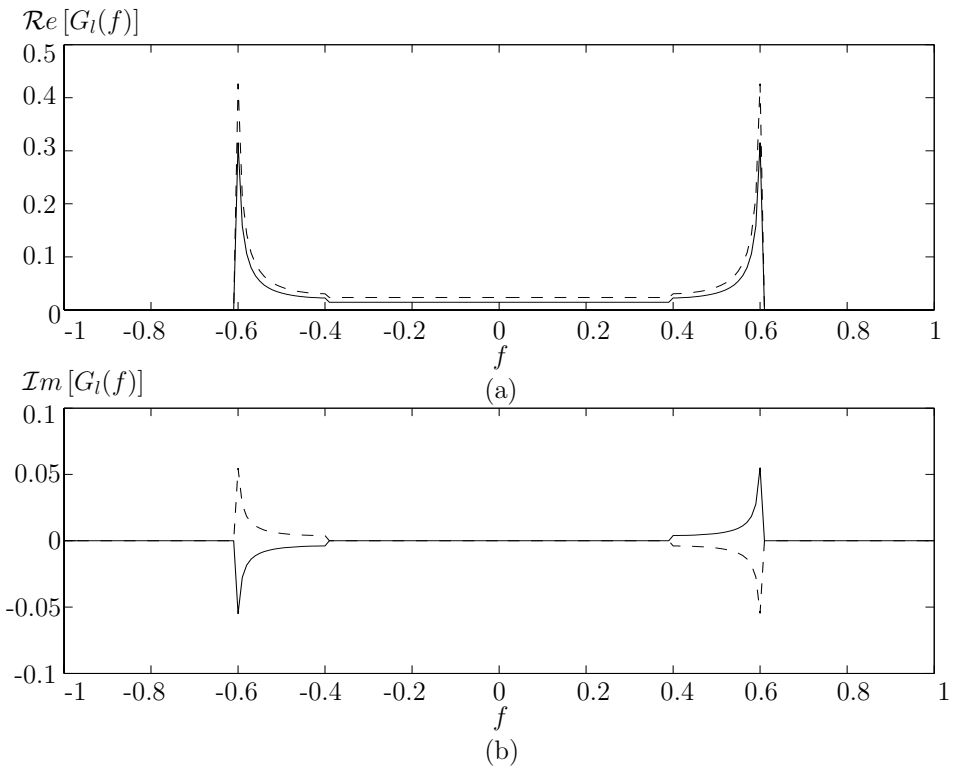

Figure 3.4: The normalized frequency responses of the $G_l(f)$ filters for a system with two active users equally powered, $L^{(0)} = L^{(1)} = 2$, $\mathcal{N}_0 = 0$, and $T_c = 1$. The chip pulse is the Sqrt-RC pulse with $\alpha = 22\%$. The solid and dashed lines represent, respectively, the frequency responses of $G_1(f)$ and $G_2(f)$ with the real and imaginary parts illustrated in (a) and (b).

The new filter exploits the CS property of MAI through the excess BW of the chip pulse shape. As the power of MAI increases, the frequency responses of the $G_l(f)$ filter converges to that of the noise-whitening matched-filter (NWMF) [47] under uniform power conditions and in multipath environments. As seen in Fig. 3.4, the two filters, $G_1(f)$ and $G_2(f)$, amplify the spectral components of the received signal where the power of noise is negligible (i.e., $1/(2T_c) \leq |f| \leq (1+\alpha)/(2T_c)$) but suppress the spectral components corresponding to large noise PSD (i.e., $|f| \leq$

$1/(2T_c)$). In contrast to the CMF that is designed to maximize SNR when AWGN is the main source of interference, $G(f)$ is balanced to suppress both interference and AWGN.

3.4 Limiting Conditions

The impulse response of the $G(f)$ filter is now examined in four limiting conditions: *i)* chip pulses with zero excess BW, *ii)* AWGN-limited channels, *iii)* asynchronous MAI-limited channels, and *iv)* synchronous CDMA.

3.4.1 Chip Pulses with Zero Excess BW

When $\alpha = 0$, the matrices in the frequency response of $G(f)$ in Appendix C become scalars. Moreover,

$$G_l(f) = \frac{Q^*(f)}{\frac{\mathcal{N}_0}{2} + \frac{1}{2T_c}|Q(f)|^2 \left(\sum_{k=1}^{K} P_k + P_0 \sum_{l'=1}^{L^{(0)}} |\alpha_{l'}^{(0)}|^2 \right)}. \tag{3.26}$$

where $l' \neq l$.

It follows immediately that for the ideal Nyquist pulse, the frequency response of $G_l(f)$ becomes equal to $Q^*(f)$ except for a scaling factor γ where

$$\gamma = \frac{\mathcal{N}_0}{2} + \frac{1}{2T_c} \sum_{k=1}^{K} P_k + \frac{P_0}{2T_c} \sum_{l'=1}^{L^{(0)}} |\alpha_{l'}^{(0)}|^2. \tag{3.27}$$

If the interpath interference (IPI), the last term, can be ignored with respect to the

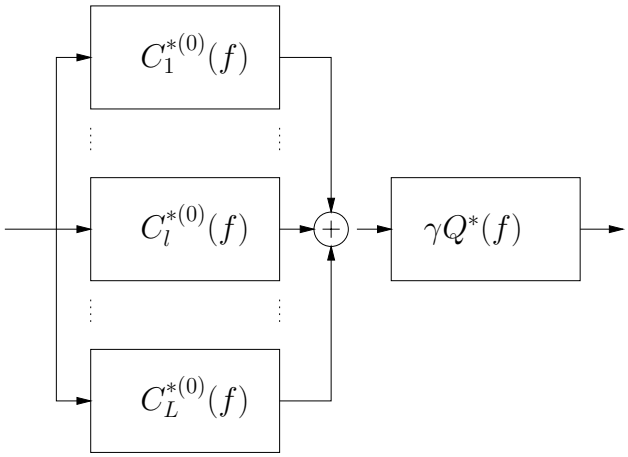

Figure 3.5: The structure of the $G(f)$ filter with $L = L^{(0)}$ for $\alpha = 0$.

other terms, then

$$\gamma \approx \frac{\mathcal{N}_0}{2} + \frac{1}{2T_c}\sum_{k=1}^{K} P_k. \tag{3.28}$$

Thus, the $G(f)$ filter in Fig. 3.3 reduces to the ARake receiver of Fig. 3.5 with $L^{(0)}$ fingers that employ a common CMF.

3.4.2 AWGN-Limited Channels

When AWGN is the predominant source of noise, the cross spectral density (CSD) matrix of (C.4) reduces to

$$\boldsymbol{R}(f) \approx \frac{\mathcal{N}_0}{2}\boldsymbol{I}_{L_H}. \tag{3.29}$$

Consequently, the LMMSE receiver reduces to the ARake receiver again as shown in Fig. 3.5 with $\gamma = \frac{\mathcal{N}_0}{2}$. This has also been reported in [21].

3.4.3 Asynchronous MAI-Limited Channels

As the power of MAI grows, the CSD matrix of (C.4) approaches

$$\boldsymbol{R}(f) \approx \frac{1}{2T_c}\boldsymbol{Q}^H(f)\mathcal{P}\boldsymbol{Q}(f) \tag{3.30}$$

and the LMMSE receiver converges to the NWMF [47] under uniform power conditions. This can also be seen in the expression for $G(f)$ filter in (3.26). Needless to say, for the case of $\alpha = 0$, the CMF and the NWMF are equivalent. As α increases from zero, the LMMSE receiver distinguishes itself from the CMF by approaching the NWMF solution as seen in Fig. 3.4.

3.4.4 Synchronous CDMA

The power matrix, defined by the expression (C.6) of Appendix C, indicates that the chip delays of interfering users, $T_l^{(k)}$, play a vital role in shaping the impulse response of the LMMSE receiver. In synchronous CDMA ($T_l^{(k)} = 0$), the $G_l(f)$ filters reduce to the CMF and will have no interference suppression ability [18]. However, the LMMSE receiver still has an ARake structure and is capable of multipath diversity combining [21].

3.5 Discussion

The LMMSE receiver maximizes output SNR. It is shown in [84, pp. 252–261] and [30, Appendix A] that for linear time-invariant (LTI) filters, the LMMSE filter is equivalent to the SNR maximizing filter. Hence, the derived receiver performs

better than (or at least equal to) *any* other linear receiver (e.g., the coherent Rake receiver) in terms of the output-SNR criterion and under the adopted system model.

Two sources of performance improvement will be discussed next. One is the fact that the LMMSE receiver harnesses the energy of the received signal from all paths of the desired user provided that the time-support of the filter $G(f)$ is large enough to span the desired user's multipath profile. This is in contrast to an L-finger Rake (where often $L \leq L^{(0)}$) which only considers the L strongest resolvable paths. Two or more paths with arrival delays less than T_c apart cannot be distinguished from one another in CDMA systems. In the Rake architecture, they are perceived as one path and combined with a single imperfect weight. However, the LMMSE receiver, as it will be shown in Chapter 5, can be implemented with a fractionally-spaced equalizer (FSE). Hence, it can assign more than one tap weight to a T_c-second interval yielding improved diversity combining. Moreover, in the Rake receiver, the detection of signals in each path depends on the success of the code acquisition system (also called *searcher*) [7]. Weak paths can remain undetected or unused even if the Rake has a sufficient number of fingers. In dense multipath environments where signals arrive from many distinct paths (e.g., future wideband CDMA systems), the energy per path decreases and the channel estimate in each finger of the Rake worsens. Consequently, the achieved SNR gain of the LMMSE receiver over the Rake receiver grows substantially.

The other source of performance improvement is the MAI suppression capability of the LMMSE receiver. The difference between the frequency response of $G(f)$ and that of the CMF becomes more apparent in multipath channels as α increases and

MAI dominates AWGN. The new filter exploits the CS property of MAI through the excess bandwidth of the chip pulse shape. As the power of MAI increases, the frequency response of the $G(f)$ filter converges to that of the chip delay locked matched filter in AWGN channels and under uniform power conditions [32]. Under multipath conditions and uniform power distributions, the frequency response of the $G(f)$ filter converges to that of NWMF. It amplifies the spectral components of the received signal where the power of noise is negligible but suppresses the spectral components corresponding to large noise PSD. Similarly, in the generalized Rake receiver of [46], extra fingers are responsible for interference suppression by approximating an inverse channel filter and undoing the noise correlation. In contrast to the CMF that is designed to maximize SNR when AWGN is the main source of interference, $G(f)$ is balanced to suppress both MAI and AWGN.

3.6 Summary of the Required Parameters

The following list summarizes the required parameters to construct the $G(f)$ filter for the detection of $b_n^{(0)}$:

1. *Multipath profile of the desired user:* This includes the desired user's power, the attenuation factor, arrival delay, and phase shift of each its paths. Namely, these are, respectively, P_0, $\alpha_l^{(0)}$, $\tau_l^{(0)}$, and $\theta_l^{(0)}$.

2. *Desired user's signature sequences:* These are the PN sequences of the I and Q phases used to spread $b_n^{(0)}$: $\boldsymbol{a}_n^{(I,0)}$ and $\boldsymbol{a}_n^{(Q,0)}$.

3. *Multipath profiles of the interfering users:* These include the power of each

interfering user, the attenuation factor, and chip delay of each interfering path. Namely, these are, respectively, P_k, $\alpha_l^{(k)}$, and $T_l^{(k)}$ for $k > 0$.

4. *Chip pulse shape:* $Q(f)$.

5. *Chip rate:* $1/T_c$.

6. *AWGN PSD:* $\mathcal{N}_0$.

Later in Chapter 5, adaptive implementations of the LMMSE receiver will be examined that do not require a majority of the above parameters.

3.7 Concluding Remarks

This chapter investigated the theory and design of the LMMSE receiver. The system model was first explained in detail. The impulse response of the LMMSE receiver was then derived based on the orthogonality principles. Closed form expression of its frequency response were presented. It was shown that the LMMSE receiver is capable of MAI suppression and multipath diversity combining simultaneously. For zero excess BW chip pulses, the LMMSE receiver reduces to the ARake receiver which processes all paths of the desired user as long as the time-span of the new filter, $G(f)$, supports the desired user's multipath profile. As excess BW of the chip pulse increases, the LMMSE receiver exploits the CS property of MAI and suppresses it. This can be intuitively explained through the concept of frequency-shift filtering discussed in the cyclic Wiener filtering theory [82] where spectral coherence is exploited for signal detection by adding up properly weighted

frequency shifted versions of the signal. It has been established that a signal can exhibit spectral coherence if and only if it is cyclostationary [82]. In such cases, the input signal is subjected to a number of frequency-shifting operations, each followed by a linear time-invariant filtering operation, and the results are added together. This is exactly what the HSR technique yields in the $G(f)$ filter responses of Appendix C. Frequency shifting is thus an effective use of the spectral redundancy inherent in the excess BW to improve performance.

In MAI-limited channel conditions, the LMMSE receiver converges to the NWMF receiver under uniform power conditions. The chip delays of the interfering paths was shown to be vital in shaping the impulse response of the new filter. In synchronous CDMA systems where the chip delays are zero, the LMMSE receiver is unable to suppress MAI but can still process the desired paths as the ARake receiver does. For the brute-force implementation of the receiver, many parameters of the desired and interfering multipath channels are needed, a list of which was presented in the end of the chapter.

The next chapter analyzes the performance of the LMMSE receiver and compares it with that of the Rake receiver.

Chapter 4

Performance Analysis

This chapter is mainly focused on the bit error rate, P_e, analysis of the proposed LMMSE receiver and comparison of its performance with that of the coherent Rake receiver. The contributions of this chapter are as follows:

- An accurate study of P_e analysis for the LMMSE and Rake receivers is presented. The analysis is based on the IGA technique of [53, 54] but with two important distinctions: *i)* the presented analysis is extended to multipath channels in contrast to those in [53, 54] which are limited to AWGN channels, and *ii)* the presented analysis is extended to general filters in the receiver in contrast to those in [53, 54] which are limited to the CMF. Based on a common framework, closed form conditional P_e expressions for both the LMMSE and Rake receivers are derived. An accurate P_e analysis of the LMMSE receiver under the multipath channel, does not exist elsewhere to the best of the author's knowledge. Regarding the Rake receiver, accurate P_e analyses do exist but with limitations in the system model. The presented analysis,

however, is not restricted to such limitations.

- Three conditions in the system model are derived which, upon satisfaction, reduce the IGA to the SGA. It will be shown that these conditions make the SGA an accurate approximation even when the number of active users in the system is small.

- The performance improvement achieved by the LMMSE receiver over the coherent Rake receiver are investigated and quantified. Moreover, the effects of chip pulse excess BW, density of multipath channels, and non-uniform power distribution of users on the performance of both receivers are examined.

The chapter begins with the presentation of bit decision statistics. The contributions of MAI and IPI are derived . Their distributions are then investigated. As the chapter proceeds with the formulation of P_e expressions, the conditions for the accuracy of the SGA are derived. Monte Carlo simulations are provided to verify the accuracy of analytical results. Finally, numerical results are presented to quantify the performance improvements achieved by the LMMSE receiver over the Rake receiver. A brief discussion on the near-far resistance of the LMMSE receiver is also included. The material in this chapter can also be found in [85, 86].

4.1 Bit Decision Statistics

The analysis is based on the receiver structure of Figs. 3.2 and 3.3. Although the two figures depict the structure of the LMMSE receiver, they can be easily transformed to that of the coherent Rake receiver by simply setting $G_l(f) = Q^*(f)$

for all l. However, by focusing on the $G_l(f)$ filters, the analysis is extended to multipath channel conditions with more general filters in the receiver side than the CMF.

The received signal of (3.3) is passed through the $G_l(f)$ filters in the I and Q branches to form the contribution of baseband signals of each path. It is next sampled at the chip rate and direct-sequence despread. The outputs of the two branches are added to make a chip estimate. A summation device adds N chip estimates to generate the bit decision statistic

$$y_m^{(0)'} = \mathcal{R}e\left\{\sum_{i=mN}^{(m+1)N-1}\sum_{l=1}^{L^{(0)}}\alpha_l^{(0)}e^{-j\theta_l^{(0)}}\left[a_i^{(\mathrm{I},0)}\int_{-\infty}^{\infty}r(iT_c-u)g_l(T_l^{(0)}+u)du + ja_i^{(\mathrm{Q},0)}\int_{-\infty}^{\infty}r(iT_c-u)g_l(T_l^{(0)}+u)du\right]\right\} \quad (4.1)$$

where $g_l(t) = \mathcal{F}^{-1}\left[G_l(f)\right]$ is the inverse Fourier transform of $G_l(f)$. This statistic is fed to a hard decision device to produce the bit decision $\tilde{b}_m^{(0)} = \mathrm{sgn}\left(y_m^{(0)'}\right)$ where $\mathrm{sgn}(\cdot)$ is the *signum* function. Without loss of generality, the bit decision statistic $y_0^{(0)'}$ for bit 0 of user 0, $b_0^{(0)}$, is considered. For simplicity, $y_0^{(0)'}$ is re-scaled and expressed as

$$y_0^{(0)} = b_0^{(0)} + \mathcal{M} + \mathcal{I} + \eta \quad (4.2)$$

where $y_0^{(0)} = y_0^{(0)'}/\left(\sqrt{2P_0}NT_c\gamma\right)$. The parameter γ is defined as

$$\gamma = \sum_{l=1}^{L^{(0)}}\left|\alpha_l^{(0)}\right|^2\rho_l(0) \quad (4.3)$$

where

$$\rho_l(t) = \mathcal{F}^{-1}\left[\frac{Q(f)G_l(f)}{T_c}\right]. \tag{4.4}$$

The parameter γ can be physically interpreted as the normalized strength of the desired signal at the output of the LMMSE filter. It can be shown that

$$\eta \sim \mathcal{N}\left[0, \frac{\mathcal{N}_0\gamma'}{2E_b\gamma^2}\right] \tag{4.5}$$

where $E_b = P_0(NT_c)$ is the bit energy for user 0, the parameter γ' is defined as $\gamma' = \sum_{l=1}^{L^{(0)}} |\alpha_l^{(0)}|^2 \rho_l'(0)$ with $\rho_l'(t) = \mathcal{F}^{-1}\left[\frac{G_l(f)G_l(f)}{T_c}\right]$, and $X \sim \mathcal{N}[\mu_X, \sigma_X^2]$ denotes "X is a Gaussian RV with a mean of μ_X and variance of σ_X^2". It can be shown that for the AWGN channel ($L^{(0)} = 1$) and CMF, $\gamma = \gamma' = 1$ and hence, $\eta \sim \mathcal{N}[0, \frac{\mathcal{N}_0}{2E_b}]$. This is consistent with the result in [53, 54].

The contribution of MAI can be expressed as $\mathcal{M} = \sum_{k=1}^{K} \mathcal{M}_k$ where

$$\begin{aligned}\mathcal{M}_k = \sum_{l=1}^{L^{(0)}} \sum_{l'=1}^{L^{(k)}} \zeta_k \frac{\alpha_l^{(0)}\alpha_{l'}^{(k)}}{N\gamma} \\ \Big[\cos(\theta_{l'}^{(k)} - \theta_l^{(0)}) Z(a^{I,l}, d^{(I,k,l')}) - \sin(\theta_{l'}^{(k)} - \theta_l^{(0)}) Z(a^{Q,l}, d^{(I,k,l')}) \\ +\sin(\theta_{l'}^{(k)} - \theta_l^{(0)}) Z(a^{I,l}, d^{(Q,k,l')}) + \cos(\theta_{l'}^{(k)} - \theta_l^{(0)}) Z(a^{Q,l}, d^{(Q,k,l')})\Big],\end{aligned} \tag{4.6}$$

$\zeta_k = \frac{1}{2}\sqrt{\frac{P_k}{P_0}}$ and

$$Z(a^{\mathcal{B}_1,l}, d^{(\mathcal{B}_2,k,l')}) = \sum_{i=0}^{N-1} \sum_{n=-\infty}^{\infty} a_i^{(\mathcal{B}_1,0)} d_n^{(\mathcal{B}_2,k,l')} \rho_l\left((i-n)T_c - T_{l'}^{(k)} + T_l^{(0)}\right) \tag{4.7}$$

with $\mathcal{B}_1, \mathcal{B}_2 \in \{\mathrm{I}, \mathrm{Q}\}$. The contribution of interpath interference (IPI) can be ex-

pressed similarly as

$$\mathcal{I} = \sum_{l=1}^{L^{(0)}} \sum_{\substack{l'=1 \\ l' \neq l}}^{L^{(0)}} \zeta_0 \frac{\alpha_l^{(0)} \alpha_{l'}^{(0)}}{N\gamma} \tag{4.8}$$
$$\Big[\cos(\theta_{l'}^{(0)} - \theta_l^{(0)}) Z(a^{I,l}, d^{(I,0,l')}) - \sin(\theta_{l'}^{(0)} - \theta_l^{(0)}) Z(a^{Q,l}, d^{(I,0,l')})$$
$$+\sin(\theta_{l'}^{(0)} - \theta_l^{(0)}) Z(a^{I,l}, d^{(Q,0,l')}) + \cos(\theta_{l'}^{(0)} - \theta_l^{(0)}) Z(a^{Q,l}, d^{(Q,0,l')})\Big]$$

For bandlimited chip pulses, the function $\rho_l(t)$ has an infinite time support. However, such pulses can be approximated with arbitrary accuracy by a truncated version. For instance, $q(t)$ can be considered to have a time support of $t \in [-MT_c, MT_c]$ where M can be selected to ensure that 99% or more of its energy is contained in the truncated pulse. A truncated version of the ideal Nyquist pulse with $M = 20$ carries 99% of its energy. Consequently, the second summation in (4.7) can be expressed as a summation over the integer index of $n \in [-M, N + M - 1]$.

4.2 Distribution of MAI and IPI

The expressions in (4.6) and (4.8) can be re-arranged to make a normalized summation of N chip statistics. Assume that $\boldsymbol{T}^{(k)} = [T_1^{(k)}, \ldots, T_{L^{(k)}}^{(k)}]$ and $\boldsymbol{\Theta}^{(k)} = [\theta_1^{(k)}, \ldots, \theta_{L^{(k)}}^{(k)}]$ are $1 \times L^{(k)}$ vectors containing the chip delays and phase shifts of the paths of user k. Letting $m = i - n$ and noting that $n \in [-M, N + M - 1]$, the chip statistics generated solely by MAI (conditioned on $\boldsymbol{T} = \{\boldsymbol{T}^{(1)}, \ldots, \boldsymbol{T}^{(K)}\}$ and

$\boldsymbol{\Theta} = \{\boldsymbol{\Theta}^{(1)}, \ldots, \boldsymbol{\Theta}^{(K)}\}$) can be expressed as[1]

$$\mathcal{M}_{|\boldsymbol{T},\boldsymbol{\Theta}} = \frac{1}{N}\sum_{i=0}^{N-1} X_i^{\prime\mathcal{M}} \tag{4.9}$$

where the chip statistic $X_i^{\prime\mathcal{M}}$ is

$$\begin{aligned} X_i^{\prime\mathcal{M}} = a_i^{(I,0)} \Bigg\{ & \sum_{l=1}^{L^{(0)}} \sum_{k=1}^{K} \sum_{l'=1}^{L^{(k)}} \zeta_k \frac{\alpha_l^{(0)} \alpha_{l'}^{(k)}}{\gamma} \sum_{m=-(M-1)}^{M} \rho_l(mT_c - T_{l'}^{(k)} + T_l^{(0)}) \\ & \left[d_{i-m}^{(I,k,l')} \cos(\theta_{l'}^{(k)} - \theta_l^{(0)}) + d_{i-m}^{(Q,k,l')} \sin(\theta_{l'}^{(k)} - \theta_l^{(0)}) \right] \Bigg\} + \\ a_i^{(Q,0)} \Bigg\{ & \sum_{l=1}^{L^{(0)}} \sum_{k=1}^{K} \sum_{l'=1}^{L^{(k)}} \zeta_k \frac{\alpha_l^{(0)} \alpha_{l'}^{(k)}}{\gamma} \sum_{m=-(M-1)}^{M} \rho_l(mT_c - T_{l'}^{(k)} + T_l^{(0)}) \\ & \left[-d_{i-m}^{(I,k,l')} \sin(\theta_{l'}^{(k)} - \theta_l^{(0)}) + d_{i-m}^{(Q,k,l')} \cos(\theta_{l'}^{(k)} - \theta_l^{(0)}) \right] \Bigg\}. \end{aligned} \tag{4.10}$$

In a similar fashion, the contribution of IPI can be expressed as

$$\mathcal{I}_{|\boldsymbol{T}^{(0)},\boldsymbol{\Theta}^{(0)}} = \frac{1}{N}\sum_{i=0}^{N-1} X_i^{\prime\mathcal{I}} \tag{4.11}$$

where the chip statistic $X_i^{\prime\mathcal{I}}$ is

$$\begin{aligned} X_i^{\prime\mathcal{I}} = a_i^{(I,0)} \Bigg\{ & \sum_{l=1}^{L^{(0)}} \sum_{\substack{l'=1 \\ l' \neq l}}^{L^{(0)}} \zeta_0 \frac{\alpha_l^{(0)} \alpha_{l'}^{(0)}}{\gamma} \sum_{m=-(M-1)}^{M} \rho_l(mT_c - T_{l'}^{(0)} + T_l^{(0)}) \\ & \left[d_{i-m}^{(I,0,l')} \cos(\theta_{l'}^{(0)} - \theta_l^{(0)}) + d_{i-m}^{(Q,0,l')} \sin(\theta_{l'}^{(0)} - \theta_l^{(0)}) \right] \Bigg\} + \end{aligned} \tag{4.12}$$

[1]More generally, the statistics of MAI and IPI are also conditioned on the attenuation factors $\alpha_l^{(k)}$. However, for the sake of notational brevity, they are assumed known similar to signal powers P_k.

$$a_i^{(\mathrm{Q},0)} \left\{ \sum_{l=1}^{L^{(0)}} \sum_{\substack{l'=1 \\ l' \neq l}}^{L^{(0)}} \zeta_0 \frac{\alpha_l^{(0)} \alpha_{l'}^{(0)}}{\gamma} \sum_{m=-(M-1)}^{M} \rho_l(mT_c - T_{l'}^{(0)} + T_l^{(0)}) \right.$$
$$\left. \left[-d_{i-m}^{(I,0,l')} \sin(\theta_{l'}^{(0)} - \theta_l^{(0)}) + d_{i-m}^{(Q,0,l')} \cos(\theta_{l'}^{(0)} - \theta_l^{(0)}) \right] \right\}.$$

As discussed in [87], three impediments exist that prevent the application of central limit theorems (CLTs) [88] to the sums of RVs in the expressions of (4.9) and (4.11). These impediments and approaches to circumvent them are explained in Appendix D.

First, $X_i^{\mathcal{M}}$ is defined in (D.5) as a new form of MAI chip statistic. Then, based on the theorem of Appendix D and (D.7)-(D.9), for large but finite N where $\lambda = \kappa/N$ is constant, the MAI contribution to bit decision statistic can be approximated as

$$\mathcal{M}_{|\boldsymbol{T},\boldsymbol{\Theta}} \sim \mathcal{N}[0, \sigma^2_{\mathcal{M}|\boldsymbol{T},\boldsymbol{\Theta}}] \tag{4.13}$$

where

$$\sigma^2_{\mathcal{M}|\boldsymbol{T},\boldsymbol{\Theta}} = \lambda \mathrm{Var}(X_0^{\mathcal{M}}) \tag{4.14}$$

and κ is the virtual number of users contributing to MAI defined in Appendix D. In a similar fashion, for large but finite N and constant $\lambda_0 = \kappa_0/N$, the distribution of IPI component can be approximated as

$$\mathcal{I}_{|T^{(0)},\Theta^{(0)}} \sim \mathcal{N}[0, \sigma^2_{\mathcal{I}|T^{(0)},\Theta^{(0)}}] \tag{4.15}$$

where

$$\sigma^2_{\mathcal{I}|T^{(0)},\Theta^{(0)}} = \lambda_0 \mathrm{Var}(X_0^{\mathcal{I}}) \tag{4.16}$$

Prior to formulating $\mathrm{Var}(X_0^{\mathcal{M}})$ and $\mathrm{Var}(X_0^{\mathcal{I}})$, the first condition necessary for the accuracy of the SGA method is presented.

Condition 1: The SGA assumes that the MAI and IPI components, like AWGN, can be approximated by normal distributions as expressed in (4.13) and (4.15). For large but finite values of N, the MAI and IPI components tend to normal distributions.

The results of Monte Carlo simulations presented later in the chapter will demonstrate that even moderate values of N (as low as $N = 32$) satisfies the first condition. The expressions for the variances of MAI and IPI are presented next. Details concerning the derivations of $\mathrm{Var}(X_0^{\mathcal{M}})$ and $\mathrm{Var}(X_0^{\mathcal{I}})$ can be found in Appendix E.

The variance (or power) of MAI and IPI can be expressed as

$$\sigma^2_{\mathcal{M}|\boldsymbol{T}} = \lambda \mathrm{Var}(X_0^{\mathcal{M}}) = \frac{2}{N} \sum_{l=1}^{L^{(0)}} \frac{|\alpha_l^{(0)}|^2}{\gamma^2} \sum_{k=1}^{K} \sum_{l'=1}^{L^{(k)}} \zeta_k^2 |\alpha_{l''}^{(k)}|^2 \Omega_{l,l}^{(k,l')} \tag{4.17}$$

$$\sigma^2_{\mathcal{I}|T^{(0)}} = \lambda_0 \mathrm{Var}(X_0^{\mathcal{I}}) = \frac{2}{N} \sum_{l=1}^{L^{(0)}} \frac{|\alpha_l^{(0)}|^2}{\gamma^2} \sum_{\substack{l'=1 \\ l' \neq l}}^{L^{(0)}} \zeta_0^2 |\alpha_{l'}^{(0)}|^2 \Omega_{l,l}^{(0,l')} \tag{4.18}$$

where $\Omega_{l,l}^{(k,l')}$, more generally defined in (E.3), can be simplified to

$$\Omega_{l,l}^{(k,l')} = \sum_{m=-(M-1)}^{M} \rho_l^2 (mT_c - T_{l'}^{(k)} + T_l^{(0)}). \tag{4.19}$$

It is noted that the variances of MAI and IPI, expressed in (4.17) and (4.18), is no longer conditioned on $\boldsymbol{\Theta}$ and $\boldsymbol{\Theta}^{(0)}$, respectively. As proven in Appendix E, the phase offsets of the interfering users, $\boldsymbol{\Theta}$, disappear from MAI component if

random quadriphase spreading is employed. This is due to the fact that DS-QPSK modulation makes the MAI process circularly symmetric[2] as also shown in Section 3.2. Also, the average effect of the phase offsets of the desired paths, $\mathbf{\Theta}^{(0)}$, on the MAI and IPI is zero as shown in Appendix E. This leads to the second condition necessary for the accuracy of the SGA method.

Condition 2: The SGA implicitly assumes that the MAI and IPI, like AWGN, are circularly symmetric processes and independent of the interfering phase offsets. Quadriphase random spreading in the system model satisfies such assumption.

The stage is now set for applying the IGA method and deriving the closed form P_e expressions of the LMMSE and Rake receivers. However, in anticipation of the third condition for the accuracy of the SGA method which deals with the effect of pulse shaping, an alternative expression for $\Omega_{l,l}^{(k,l')}$ in the frequency domain is presented first. It is in contrast to (4.19) which is in the time domain. As shown in Appendix F,

$$\Omega_{l,l}^{(k,l')} = B_l(0) + \sum_{\substack{m=-1-\lfloor\alpha\rfloor \\ m\neq 0}}^{1+\lfloor\alpha\rfloor} \exp\left[j\frac{2\pi m(T_{l'}^{(k)} - T_l^{(0)})}{T_c}\right] B_l(-\frac{m}{T_c}) \tag{4.20}$$

where $B_l(f) = (1/T_c)\mathcal{F}[\rho_l^2(t)]$ is the Fourier transform of $\rho_l^2(t)$ defined in (4.4).

[2]A *circularly symmetric (or proper) process* is a complex process whose complementary autocorrelation function (or pseudo autocorrelation function) is zero [79, p. 313]

4.3 P_e of the LMMSE and Rake Receivers

The variances of AWGN, MAI, and IPI were previously derived in (4.5), (4.17), and (4.18), respectively. It is easy to show that these three components are uncorrelated random processes. By applying the IGA method, the conditional P_e expression can be written as

$$P_{e\ |\boldsymbol{T}^{(0)},\boldsymbol{T}}^{\text{LMMSE}} = \mathcal{Q}\left(\left[\sigma_\eta^2 + \sigma_{\mathcal{M}|\boldsymbol{T}}^2 + \sigma_{\mathcal{I}|\boldsymbol{T}^{(0)}}^2\right]^{-\frac{1}{2}}\right) \tag{4.21}$$

where $\mathcal{Q}(x)$ is defined as

$$\mathcal{Q}(x) = \frac{1}{\sqrt{2\pi}} \int_x^\infty e^{-t^2/2} dt, \quad x \geq 0. \tag{4.22}$$

The unconditional (or average) probability of error is obtained by taking the expectation of (4.21) with respect to chip delays $T^{(0)}$ and $\boldsymbol{T}$. More precisely,

$$P_e^{\text{LMMSE}} = E\left[P_{e\ |\boldsymbol{T}^{(0)},\boldsymbol{T}}^{\text{LMMSE}}\right] \tag{4.23}$$

The P_e analysis of the Rake receiver is a special case of the one presented for the LMMSE receiver which was developed for general receiver filters. By simply setting $G_l(f) = Q^*(f)$, the analysis can be readily applied to the coherent Rake receiver. If the attenuation factors of the desired user, $\alpha_l^{(0)}$, are indexed from strongest to weakest, then a coherent Rake receiver with $L \leq L^{(0)}$ fingers processes the first L paths. Hence, $\rho_l(t) = \rho(t) = \mathcal{F}^{-1}[|Q(f)|^2/T_c]$ and $\gamma' = \gamma = \sum_{l=1}^{L} |\alpha_l^{(0)}|^2$.

Consequently, the conditional P_e expression follows as

$$P_{e\ |\boldsymbol{T}^{(0)},\boldsymbol{T}}^{\text{RAKE}} = \mathcal{Q}\left(\left[\sigma_\eta^2 + \sigma_{\mathcal{M}|\boldsymbol{T}}^2 + \sigma_{\mathcal{I}|\boldsymbol{T}^{(0)}}^2\right]^{-\frac{1}{2}}\right) \tag{4.24}$$

where

$$\sigma_\eta^2 = \frac{\mathcal{N}_0}{2\gamma E_b} \tag{4.25}$$

$$\sigma_{\mathcal{M}|\boldsymbol{T}}^2 = \frac{2}{N}\sum_{l=1}^{L}\frac{|\alpha_l^{(0)}|^2}{\gamma^2}\sum_{k=1}^{K}\sum_{l'=1}^{L^{(k)}}\zeta_k^2|\alpha_{l''}^{(k)}|^2\Omega_{l,l}^{(k,l')} \tag{4.26}$$

$$\sigma_{\mathcal{I}|\boldsymbol{T}^{(0)}}^2 = \frac{2}{N}\sum_{l=1}^{L}\frac{|\alpha_l^{(0)}|^2}{\gamma^2}\sum_{\substack{l'=1\\l'\neq l}}^{L^{(0)}}\zeta_0^2|\alpha_{l'}^{(0)}|^2\Omega_{l,l}^{(0,l')} \tag{4.27}$$

The average probability of error is then obtained by

$$P_e^{\text{RAKE}} = E\left[P_{e\ |\boldsymbol{T}^{(0)},\boldsymbol{T}}^{\text{RAKE}}\right] \tag{4.28}$$

For chip pulses with zero excess BW, the P_e expressions in (4.21) and (4.24) can be further simplified. In Section 3.4.1, it was shown that, for $\alpha = 0$, the $G_l(f)$ filter reduces to the CMF except for a scalar. It can also be readily shown that if $\alpha = 0$, then $B_l(f) = 0$ for $f \geq 1/T_c$. Therefore, the second term in (4.20) vanishes for $\alpha = 0$. Moreover, $B_l(0) = B(0) = (1/T_c)\mathcal{F}[\rho^2(t)]$ for all l. Consequently, the variances of MAI and IPI will no longer be conditioned on $\boldsymbol{T}$ and $\boldsymbol{T}^{(0)}$ and the IGA method reduces to the SGA method. The P_e expression of the Rake receiver simplifies to

$$P_e^{\text{SGA}} = \mathcal{Q}\left(\left[\sigma_\eta^2 + \sigma_{\mathcal{M}}^2 + \sigma_{\mathcal{I}}^2\right]^{-\frac{1}{2}}\right) \tag{4.29}$$

where

$$\sigma^2_{\mathcal{M}} = \frac{B(0)}{2N\gamma^2}\sum_{k=1}^{K}\frac{P_k}{P_0} \tag{4.30}$$

$$\sigma^2_{\mathcal{I}} = \frac{B(0)}{2N\gamma^2}\sum_{l=1}^{L}|\alpha_l^{(0)}|^2\left(1-|\alpha_l^{(0)}|^2\right) \tag{4.31}$$

and the expression for σ^2_η remains as that in (4.25). As proved in Section 3.4.1, the LMMSE receiver reduces to the ARake receiver for $\alpha = 0$. Hence, the P_e expression in (4.29) can be used for the LMMSE receiver as well by setting $L = L^{(0)}$. This result is consistent with that reported in [54]. The third condition for the accuracy of the SGA method can now be described.

Condition 3: The SGA implicitly assumes that MAI and IPI, like AWGN, are wide-sense stationary (WSS) random processes. However, MAI and IPI are wide-sense cyclostationary (WSCS) random process for $\alpha > 0$. As $\alpha \to 0$, MAI and IPI become WSS and the SGA becomes an accurate approximation.

Appendix G presents an alternative proof by examining the autocorrelation function of noise, $R_{nn^*}(t,u)$, as $\alpha \to 0$.

4.4 Discussion

The three conditions that make the SGA an accurate approximation are as follows: *i)* moderate to large spreading factors, N, to make the CLT applicable to bit decision statistic, *ii)* quadriphase random spreading to make the interference circularly symmetric and rid the bit decision statistic from dependence on the phase offsets

$\boldsymbol{\Theta}$, and *iii)* zero to small chip pulse excess BW to make the interference WSS and independent from the chip delays $\boldsymbol{T}$.

The IGA is based on the premise that MAI and IPI converge to Gaussian random processes as N becomes large for *any* K when the chip delays and phase offsets are fixed [89]. As the system model satisfies the above conditions, the IGA reduces to SGA. Hence, the SGA inherits its independence of K from the IGA.

As a result of the above conditions, from the perspective of the $G_l(f)$ filter, all interfering paths ($1 \leq l' \leq L^{(k)}$ for $0 \leq k \leq K$ with $l' \neq l$ if $k = 0$) described in the system model can be considered as chip- and phase-synchronous signals without loss of generality. Under such circumstances, an interfering path contributing to MAI or IPI can be sufficiently modeled with only one parameter: its received power.

4.5 SNR Analysis

The presented P_e analysis can be readily modified to obtain the SNR expressions of the LMMSE and Rake receivers. The SNR before the decision device for both of the receivers can be expressed as

$$\mathrm{SNR}_{\max} = \frac{1}{\sigma_\eta^2 + \sigma_{\mathcal{M}|\boldsymbol{T}}^2 + \sigma_{\mathcal{I}|\boldsymbol{T}^{(0)}}^2} \tag{4.32}$$

where the variances of AWGN, MAI, and IPI for both of the receivers have been previously formulated. An alternative expression for $\mathrm{SNR}_{\max}$ of the LMMSE receiver in the frequency domain can be derived in terms of the matrices of Appendix C.

Replacing the HSR of (3.6) and (3.21) in (B.2) leads to

$$\mathrm{SNR}_{\max,n} = \frac{P_0}{2}\mathcal{R}e\left[\int_{-1(1/2T_c)}^{1/2T_c}\left(\left|\mathcal{A}_n^{(I,0)}(e^{j2\pi fT_c})\right|^2 + \left|\mathcal{A}_n^{(Q,0)}(e^{j2\pi fT_c})\right|^2\right) \right. \\ \left. .\boldsymbol{u}\boldsymbol{Q}(f)\boldsymbol{C}^{(0)}(f)\boldsymbol{R}^{-1}(f)\boldsymbol{C}^{(0)H}(f)\boldsymbol{Q}^H(f)\boldsymbol{u}^H df\right]. \tag{4.33}$$

The numerical results of this chapter, however, will be based on P_e. Performance comparisons of the two receivers based on $\mathrm{SNR}_{\max}$ can be found in [76].

4.6 Near-Far Resistance

It is well known that LMMSE receivers for short-code CDMA have superior near-far resistance over LMMSE receivers for long-code CDMA [25]. In [18, 30], it is shown that as long as the number of high-powered interferers satisfy $K \leq 1+\alpha$, the LMMSE receiver shows near-far resistance in AWGN channels and can effectively tune out the strong interferers. For instance, if the chip pulse is the Sqrt-RC pulse with $\alpha = 22\%$, then the receiver can suppress one high-powered interferer. However, this property does not necessarily hold true in multipath channels since the strong interferer's signal may be received via more than one high-powered path, making it appear to the receiver as more than one strong interferer. The effect of non-uniform power distribution and the presence of high-powered users on the receiver performance will be examined in the numerical results.

4.7 Numerical Results

This section presents the numerical results in two parts. First, the *Monte Carlo* simulation results are presented that verify the theoretical analysis of this chapter. The results demonstrate the accuracy of the derived P_e expressions for the LMMSE and Rake receivers based on the IGA method. Next, the P_e performance of the LMMSE receiver is compared with that of the coherent Rake receiver. The performance comparisons quantify the shares of capacity improvement achieved by two features of the LMMSE receiver: *i)* interference suppression ability, and *ii)* ARake capability. The numerical results examine both uniform and non-uniform power distributions. The effect of AWGN is ignored by setting $\mathcal{N}_0 = 0$. The LMMSE receiver is also assumed to span the multipath profile of the desired user.

4.7.1 Monte Carlo Simulations

Monte Carlo simulations were carried out to validate the analytical P_e expressions of the LMMSE and Rake receiver in (4.21) and (4.24). Fig. 4.1 illustrates the results for the two cases: (a) the SRake receiver, and (b) the LMMSE receiver. The signal of each user is assumed to arrive via $L^{(k)} = 5$ equally strong paths. The chip pulse is the Sqrt-RC pulse with $\alpha = \{22\%, 100\%\}$. The spreading factor is $N = \{32, 64\}$. The SRake receiver is also assumed to have $L = 3$ fingers. The simulations were conducted for a single set of $\boldsymbol{T}^{(0)}$, $\boldsymbol{T}$, $\boldsymbol{\Theta}^{(0)}$, and $\boldsymbol{\Theta}$ randomly selected from uniform distributions over $[0, T_c)$ and $[0, 2\pi)$, respectively. The simulation results are marked by 'x' and were obtained by runs of $100 - 1000$ times the inverse of estimated P_e.

Fig. 4.1-(a) shows that the analytical expression of (4.24) accurately predicts the

simulation results. The maximum prediction error is about 25% for low P_e values. For instance, with $K = 2$, $N = 32$ and $\alpha = 100\%$, the expression of (4.24) returns $P_e = 7.5 \times 10^{-6}$ whereas the simulation shows $P_e = 6 \times 10^{-6}$. It is noted that the simulation results of [54] for the SGA method in low regions of P_e return values which are two orders of magnitude off. Therefore, the accuracy of the presented analysis is remarkably improved. As K increases, the prediction error decreases.

Fig. 4.1-(b) verifies the analytical expression of (4.21) for the P_e performance of the LMMSE receiver. The prediction error shows the same type of behavior as that in Fig. 4.1-(a). For example, with $K = 4$, $N = 32$, and $\alpha = 22\%$, the expression of (4.21) returns $P_e = 2.3 \times 10^{-5}$ whereas the simulation shows $P_e = 1.8 \times 10^{-5}$. With such verifications, the numerical results of the next sections rely on the theoretical analysis to compare the performance of both receivers.

4.7.2 Performance Comparison

The performance comparison is based on the P_e expressions in (4.23) and (4.28). They are evaluated by calculating the conditional P_e expressions in (4.21) and (4.24) for a large number of multipath profiles and then averaging the results. For each examined scenario, the 99.9% *confidence interval* of P_e is computed according to the procedure outlined in [88, Chap. 9]. The upper and lower bounds of P_e for the LMMSE and Rake receivers are obtained by evaluating (4.21) and (4.24) for 10^4 multipath profiles. In most cases, the bounds are indistinguishable. Chip delays and attenuation factors are chosen from, respectively, a uniform distribution over $[0, T_c)$ and a Rayleigh distribution with mean $E[\alpha_l^{(k)}] = -80$ dBm [12] and

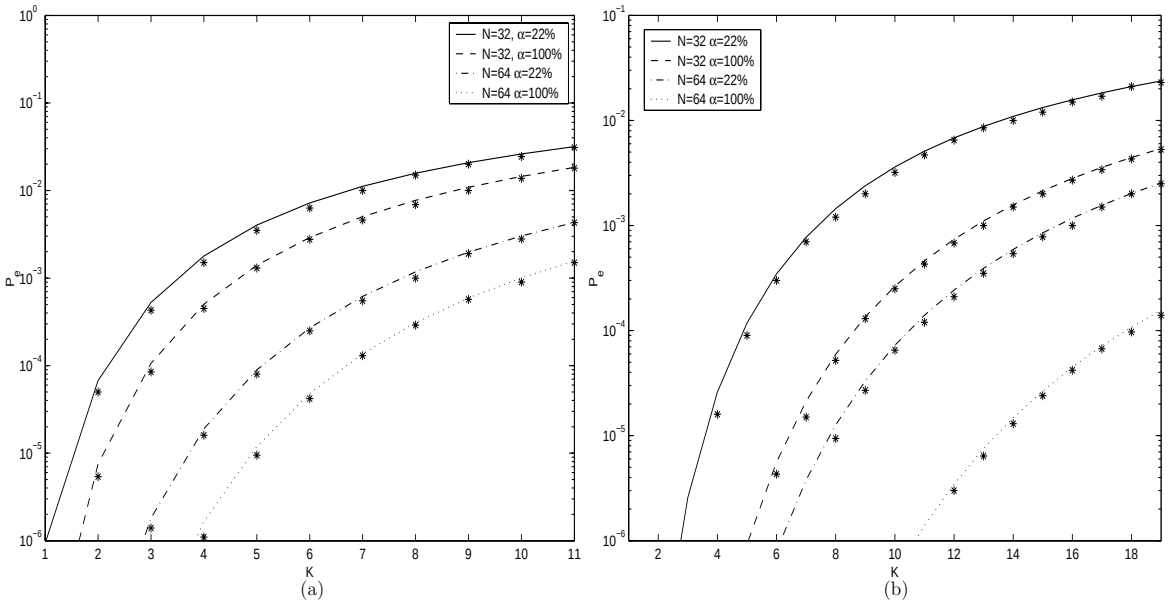

Figure 4.1: *Monte Carlo* simulation results P_e vs. K for a single multipath profile with $L^{(k)} = 5$, $N = \{32, 64\}$, and $\alpha = \{22\%, 100\%\}$ in two cases: (a) SRake receiver with $L = 3$, and (b) LMMSE receiver. The simulation results are marked by 'x'.

normalized according to (3.2). For both receivers, perfect code acquisition, tracking, channel estimation, and bit timing acquisition are assumed to be accomplished in each processed path. The effect of chip pulse shaping and the impact of multipath density and non-uniform power distributions on the performance of the LMMSE and Rake receivers are examined.

The Effect of Pulse Shaping

Fig. 4.2 plots the bounds of P_e vs. K for the LMMSE and Rake receivers when the chip pulse is the Sqrt-RC pulse with $\alpha = \{0, 0.22, 1\}$ for two cases: (a) $N = 32$, and (b) $N = 64$. The solid and dotted curves correspond to P_e of the LMMSE and

Rake receiver, respectively. The signal of each user is received via $L^{(k)} = 3$ paths and the coherent RAKE receiver has $L = 3$ fingers (i.e., it is the ARake receiver.). Therefore, both receivers can process all the desired paths. However, in contrast to the ARake receiver which treats MAI as AWGN, the LMMSE receiver suppresses MAI as α increases. Hence, it performs better than the ARake receiver. For $\alpha = 0$, the two receivers are identical and the corresponding curves are indistinguishable as expected. For $\alpha = 22\%$ and the desired quality of service (QoS) of digital voice transmission ($P_e = 10^{-3}$), the LMMSE receiver results in more than 20% capacity improvement for both cases due to pulse shaping. This improvement grows to more than 50% if $\alpha = 100\%$. Table 4.1 summarizes the results of Fig. 4.2 for $P_e = 10^{-3}$. It is noted that although Fig. 4.2 presents P_e curves for $N = \{32, 64\}$, similar results are obtained for larger spreading factors. Moreover, the capacity improvements are independent of N as expected from the performance analysis and the P_e expressions of (4.21) and (4.24). As N varies, the power level of interference changes equally for both the LMMSE and Rake receivers and interference remains Gaussian.

Scenario: $L^{(0)} = L = 3$	$K+1$ for ARake	$K+1$ for LMMSE	Capacity Improvement
$N = 32$, $\alpha = 22\%$	7	9	28%
$N = 64$, $\alpha = 22\%$	14	17	21%
$N = 32$, $\alpha = 100\%$	9	14	55%
$N = 64$, $\alpha = 100\%$	18	27	50%

Table 4.1: Capacity improvments of the LMMSE receiver over the ARake receiver for the scenarios of Fig. 4.2 with the QoS of $P_e = 10^{-3}$.

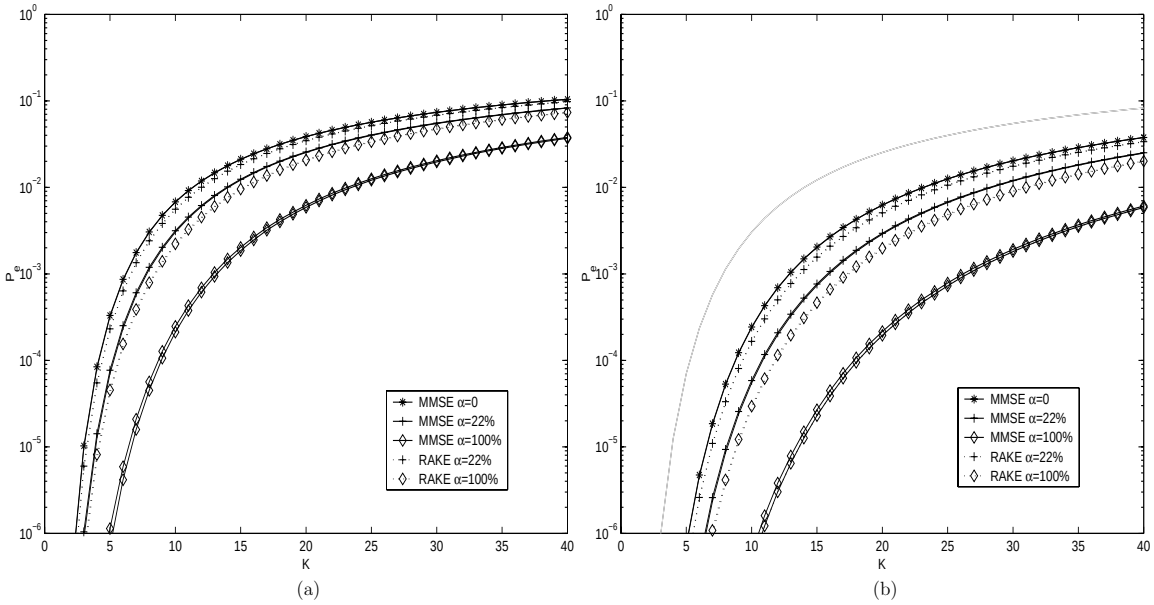

Figure 4.2: P_e vs. K for the LMMSE and coherent ARake receiver when $L^{(0)} = L = 3$. The chip pulse is the Sqrt-RC pulse with $\alpha = \{0, 0.22, 1\}$ excess BW. Solid and dotted curves represent, respectively, P_e for the LMMSE and Rake receivers in two cases: (a) $N = 32$, and (b) $N = 64$.

The Effect of Multipath Density

Reported field experiments indicate that the multipath density is usually high in heavily built-up urban areas [12, 37, 60]. For instance, a chip rate of 1.2288 MHz yields $L^{(0)} = 7$ paths in a channel spreading 6 μs [12, 60]. However, in the downlink of the IS-95 system, a coherent RAKE receiver with three fingers is employed [78]. Clearly, more resolvable paths will be available as the chip rate goes higher in next generation systems. The next set of examples illustrate the impact of multipath density on the performance of both receivers.

Fig. 4.3 plots the bounds of P_e vs. K for the LMMSE and Rake receivers when

the chip pulse is the ideal Nyquist pulse (the Sqrt-RC pulse with $\alpha = 0$) for two cases: (a) $N = 32$, and (b) $N = 64$. The solid and dotted lines represent the P_e of the LMMSE and Rake receiver, respectively. The intent of this figure is to examine the impact of multipath density (i.e., the number of resolvable paths in the time spread of the multipath channel) on the performance of the SRake receiver with a fixed number of fingers and compare it with that of the LMMSE receiver. Since $\alpha = 0$, the $G(f)$ filter in the LMMSE receiver reduces to the CMF. Consequently, the LMMSE receiver reduces to the ARake receiver. Hence, the only difference between the two receivers is in the number of paths they can process. The SRake receiver is assumed to have $L = 3$ fingers at all times while the number of resolvable paths increases from $L^{(0)} = 3$ to $L^{(0)} = 5$ and $L^{(0)} = 7$. Fig. 4.3 shows that the LMMSE receiver performs equally when the number of paths increases. It can also be observed that as $L^{(0)}$ increases, the power of IPI still remains insignificant compared to the strength of MAI. In contrast, the SRake receiver suffers from performance degradation as $L^{(0)}$ grows. At $P_e = 10^{-3}$, the LMMSE receiver yields about 17% improvement in system capacity for $L^{(0)} = 5$ while for $L^{(0)} = 7$, the capacity improvement grows to 40%. Table 4.2 summarizes the results of Fig. 4.3 for $P_e = 10^{-3}$. The results approximately match those reported in [36] which were obtained with SNR as the figure of merit and with no quadriphase spreading in the system model.

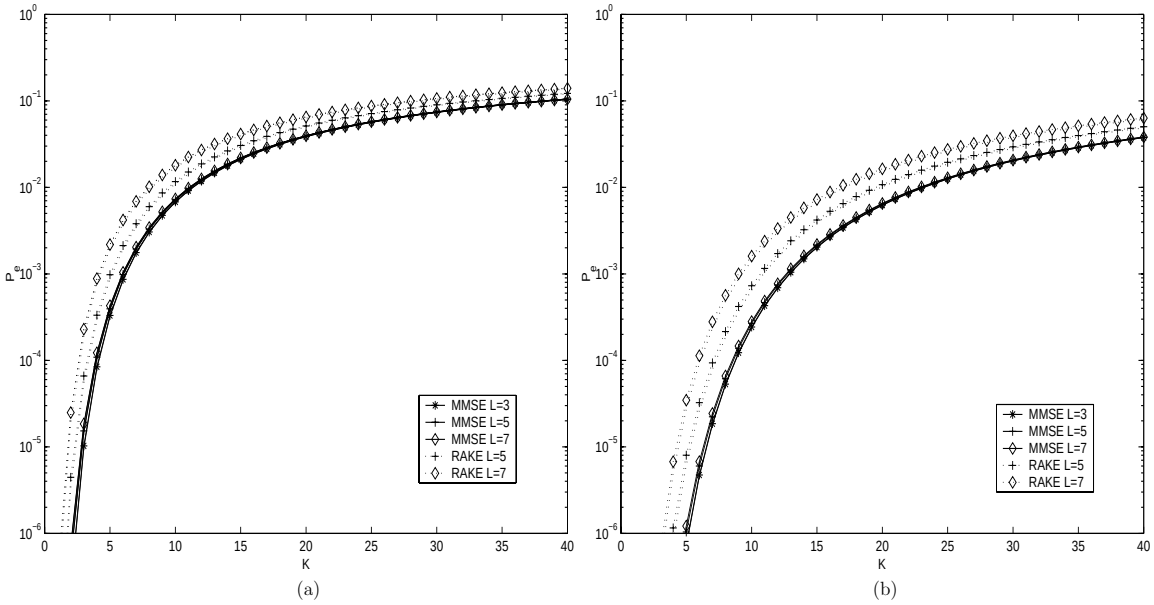

Figure 4.3: P_e vs. K for the LMMSE and coherent Rake receiver when the chip pulse is the Sqrt-RC pulse with $\alpha = 0$, $L = 3$, and $L^{(0)} = \{3, 5, 7\}$. Solid and dotted curves represent, respectively, P_e for the LMMSE and Rake receivers in two cases: (a) $N = 32$, and (b) $N = 64$.

The Effect of Non-Uniform Power Distributions

By a simple example, it will be illustrated here that the near-far resistance of the LMMSE receiver to power imbalance, reported in [18, 30] for AWGN channels, diminishes in multipath channel conditions.

Consider the case where two active users are in the system: the desired user and a strong interferer with a signal power eight times (or 9 dB) higher than the power of the desired user. The pulse excess BW is $\alpha = 22\%$ and $N = \{64, 128\}$. The P_e performance of the desired user is examined for two cases: (a) the AWGN channel where $L^{(0)} = L^{(1)} = L = 1$, and (b) the multipath channel where $L^{(0)} =$

Scenario: $\alpha = 0$, $L = 3$	$K+1$ for SRake	$K+1$ for LMMSE	Capacity Improvement
$N = 32, L^{(0)} = 5$	6	7	17%
$N = 64, L^{(0)} = 5$	12	14	17%
$N = 32, L^{(0)} = 7$	5	7	40%
$N = 64, L^{(0)} = 7$	10	14	40%

Table 4.2: Capacity improvments of the LMMSE receiver over the SRake receiver for the scenarios of Fig. 4.3 with the QoS of $P_e = 10^{-3}$.

$L^{(1)} = L = 3$. In case (a), the correlating CMF returns an average $P_e = 2.0 \times 10^{-5}$ for $N = 64$ and $P_e = 3.7 \times 10^{-9}$ for $N = 128$. The LMMSE receiver, on the other hand, effectively tunes out the high-powered interferer and returns P_e levels that could not be measured with the numerical accuracy of the simulation program. More specifically, $P_e \leq 10^{-14}$ for $N = \{64, 128\}$. In case (b), the ARake receiver returns $P_e = 3.3 \times 10^{-5}$ for $N = 64$ and $P_e = 8.7 \times 10^{-9}$ for $N = 128$. However, the LMMSE receiver no longer shows near-far resistance to the high-power user. For $N = 64$ and $N = 128$, it returns $P_e = 3.4 \times 10^{-6}$ and and $P_e = 3 \times 10^{-10}$, respectively.

Combination of the Results

The last set of numerical results illustrate the combined effect of chip pulse shaping and multipath density on the performance of both receivers. Fig. 4.4 plots the P_e bounds of the LMMSE and Rake receiver vs. K for the Sqrt-RC chip pulse with $\alpha = 22\%$ for $N = \{32, 64\}$. The signal of each user arrives via $L^{(k)} = 7$ paths and the SRake receiver has $L = 3$ fingers. The LMMSE receiver takes advantage of the CS property of the MAI and harnesses the energy of all paths of the desired user.

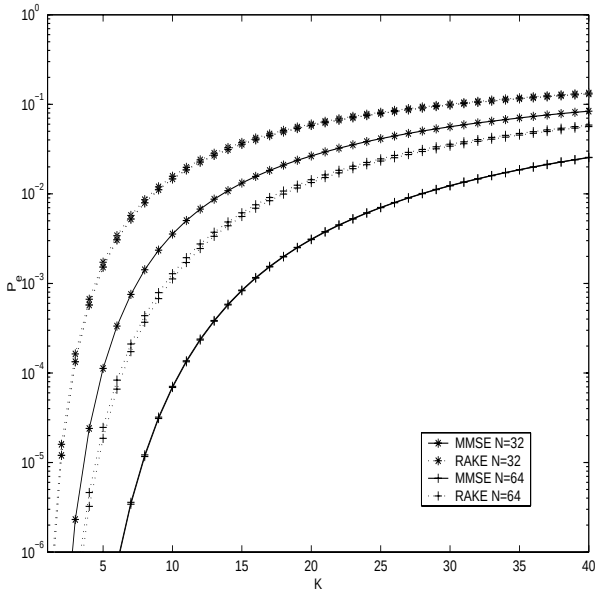

Figure 4.4: P_e vs. K for the LMMSE and coherent Rake receiver when the chip pulse is the Sqrt-RC pulse with $\alpha = 22\%$, $L = 3$, $L^{(0)} = 7$, and $N = \{32, 64\}$. Solid and dotted curves represent, respectively, P_e for the LMMSE and Rake receivers.

In contrast, the SRake receiver treats MAI as AWGN and acquires only the three strongest paths of the desired user. The combined effect of these two distinguishing features of the LMMSE receiver yields a 60% improvement in system capacity if the desired QoS is $P_e = 10^{-3}$. One third of this improvement originates from interference suppression capability of the LMMSE receiver and the rest comes from its ability to process all paths of the desired user. Table 4.3 summarizes the results of Fig. 4.4 for $P_e = 10^{-3}$.

Scenario: $\alpha = 0.22$ $L^{(0)} = 7$, $L = 3$	$K+1$ for Rake	$K+1$ for MMSE	Capacity Improvement
$N = 32$	5	8	60%
$N = 64$	10	16	60%

Table 4.3: Capacity improvments of the LMMSE receiver over the Rake receiver for the scenario of Fig. 4.4 with the QoS of $P_e = 10^{-3}$.

4.8 Concluding Remarks

This chapter studied the P_e performance of the LMMSE receiver and compared it with that of the coherent Rake receiver. The analysis, based on the IGA technique, revealed that the bit-decision statistic approaches the Gaussian distribution when the spreading factor takes moderate to large values (e.g., $N \geq 32$) for any K as long as the chip delays and phase offsets are fixed. Closed form P_e expressions were presented for both receivers. It was also shown that the IGA method reduces to the SGA if two additional conditions are satisfied: quadriphase random spreading and zero (or small) pulse excess BW. The former turns the bit decision statistic into a circularly symmetric random process while the latter makes it a WSS random process. In such case, the SGA is an accurate approximation even for a small number of users in the system.

Simulation results were presented to verify the analytical results. It was shown that the analytical expressions predict the simulated scenarios accurately. Numerical examples were also presented illustrating the performance improvement achieved by the LMMSE receiver. It was shown that the LMMSE receiver yields a 20% gain in system capacity over a coherent ARake receiver if $\alpha = 22\%$ and QoS$= 10^{-3}$. In terms of output SNR, this amounts to $0.5-0.6$ dB improvement in link budget [76].

The same result is also reported in [19] within the context of ICI suppression by the MMSE technique. In [19, 20], more improvements in link performance are reported when the MMSE receiver replaces the CMF and higher signal constellations (e.g., 16-QAM) are adopted in the system model. It is expected that the LMMSE receiver performance improvement also grows under such signal constellations making it a suitable choice for high data rate applications of next generation systems. This issue, however, is the subject of future work.

In dense multipath environments, the LMMSE receiver results in more capacity gains over the SRake receiver. For instance, with $L^{(0)} = 7$, the LMMSE receiver achieves an additional 40% gain in system capacity over a 3-finger Rake receiver. Finally, it was shown that the near-far resistance of the LMMSE receiver, reported in previous works for the AWGN channel, diminishes in multipath channel conditions.

Chapter 5

Adaptive Implementations

Brute-force implementation of the LMMSE receiver as defined by the matrix equations of Appendix C requires the knowledge of many parameters which are enlisted in Section 3.6. Such information is normally not accessible in the receiver side. In this chapter, adaptive implementations of the LMMSE filter are presented that function independently and without the knowledge of a majority of these parameters. This chapter discusses the proposed adaptive architecture and updating algorithms. The contributions of this chapter are as follows:

- An adaptive implementation is proposed that relies on training sequences for convergence to the MMSE solution. The proposed structure is based on the well-known least-mean-square (LMS) and recursive least-squares (RLS) algorithms. Forward link of cellular CDMA systems (e.g., IS-95) can be named as an application of such receivers where a strong known pilot signal, broadcast by the base station to all users in the cell, can be used as a training sequence.

- A blind adaptive implementation is proposed that is no longer dependent on training sequences. The implementation is based on the leaky constant modulus algorithm (LCMA) and the recursive constant modulus algorithm (RCMA). Its applications constitute radio links in which pilot signals are either absent or costly to include. To the best of the author's knowledge, CMA has not been investigated for long-code CDMA systems.

- Pilot-channel-aided (PCA) adaptive implementations are also investigated. In PCA methods, pilot symbols are always present and code-multiplexed with the traffic channel. It is in contrast to pilot-symbol-aided (PSA) schemes where pilot symbols are time-multiplexed with information symbols. Reverse link of cdma2000 standard can be named as an application of PCA methods. It will be shown that the accuracy of channel estimation in the reverse link is strongly dependent on the pilot channel power, which often constitutes a small portion of the mobile user signal power. Higher levels of pilot power improve the performance in channel estimation but compromise the capacity of the traffic channel.

- Inspired by the constant modulus algorithm (CMA), a new set of algorithms is proposed that jointly utilizes the statistics of both the traffic and pilot channels. It is shown that, at the expense of increased computational complexity, the proposed algorithms can reduce the pilot power and still perform equal to, or even better than, the conventional PCA algorithms which utilize only the statistics of the pilot channel. Such savings in pilot power translate into substantial improvements in system and channel capacity on the reverse

link.

- Numerical results are presented that quantitatively investigate the performance of the proposed algorithms from two different perspectives: *i)* the steady-state SNR, and *ii)* the convergence rate. Also, the computational complexity of each algorithm is examined.

The chapter begins with an amendment to the system model to account for pilot channels. The adaptive receiver architecture is presented next. Four sets of updating algorithms are discussed. They are: *i)* training-based algorithms, *ii)* blind algorithms, *iii)* PCA algorithms, and *iv)* hybrid (HYB) algorithms that are combination of the blind and PCA algorithms. The computational complexity of each algorithm is examined. The chapter ends with a new list of required parameters for adaptive implementation of the LMMSE receiver followed by a comprehensive set of numerical results that quantify the SNR performance and convergence rate of these algorithms. The material in this chapter can also be found in [90]-[93].

5.1 Amendment to System Model

The system model of Section 3.1.2 is amended to account for the presence of pilot channels in the forward and reverse links. The baseband representation of the quadriphase DS-CDMA signal of user k was previously expressed as

$$s^{(k)}(t) = \sqrt{\frac{P_k}{2}} \left[x_I^{(k)}(t) - j x_Q^{(k)}(t) \right]. \tag{5.1}$$

The I and Q components are modified to

$$x_{\mathcal{B}}^{(k)}(t) = \sum_{n=-\infty}^{\infty} \left[\sqrt{1-\beta_k}\; b_n^{(k)} c_i^{(k,T)} + \sqrt{\beta_k}\; c_i^{(k,P)} \right] a_n^{(\mathcal{B},k)} (t - nT_b^{(k)}) \qquad (5.2)$$

with $\mathcal{B} \in \{\mathrm{I}, \mathrm{Q}\}$. There are now two code-multiplexed channels associated with user k (traffic and pilot channels). The information symbol on the traffic channel is $b_n^{(k)}$ as before. The pilot channel is unmodulated and successive '+1' symbols, known in the receiver side, are transmitted. The percentage of total signal power, P_k, allocated to the pilot channel of user k is represented by $\beta_k \in [0, 1]$. In the reverse link, the pilot channel power normally constitutes a small portion of the total signal power (e.g., $\beta_k = 12.5\%$). However, in the forward link, a strong pilot channel is broadcast to all users in the cell. With the above model, such a pilot channel can be modelled as a separate user by adjusting its P_k as needed with $\beta_k = 1$. It is also noted that by setting $\beta_k = 0$, the modified model reduces to the original model of Section 3.1.2.

Prior to scrambling with $a_n^{(\mathcal{B},k)}$, the traffic and pilot symbols of user k are spread by orthogonal Walsh codes. The Walsh code for the traffic channel of user k forms the $N^{(k)} \times 1$ vector $\boldsymbol{c}^{(k,T)} = [c_0^{(k,T)}, c_1^{(k,T)}, \ldots, c_{N^{(k)}-1}^{(k,T)}]'$. Similarly in the pilot channel, the Walsh code is $\boldsymbol{c}^{(k,P)} = [c_0^{(k,P)}, c_1^{(k,P)}, \ldots, c_{N^{(k)}-1}^{(k,P)}]'$ where

$$\boldsymbol{c}^{(k,T)'} . \boldsymbol{c}^{(k,P)} = 0. \qquad (5.3)$$

All other symbols and parameters are as before.

5.2 Receiver Architecture

This section describes the block diagram of the proposed receiver and the error signals used by the updating algorithms. In the end, other alternatives to the proposed structure will be discussed.

5.2.1 Block Diagram

The block diagram of the adaptive receiver is depicted in Fig. 5.1. The received signal, $r(t)$ as defined in (3.3), is fed to the CMF and the output, $x(t) = r(t) \otimes q(t)$, is sampled at a rate higher than the chip rate; i.e., $T_{s_1} = T_c/N_s$ where $N_s > 1$. The samples are next input to an FSE whose structure is shown in Fig. 5.2. The FSE has M complex tap weights spaced T_{s_1} apart and supports a time window of $(M-1)T_{s_1}$ seconds. The tap weights form an $M \times 1$ vector of $\boldsymbol{w}(n) = [w_0(n), w_1(n), \ldots, w_{M-1}(n)]'$ where n denotes the discrete bit index; i.e., $\boldsymbol{w}(n)$ contains tap weights for the detection of $b_n^{(0)}$. The FSE input is stacked in an $M \times 1$ vector of $\boldsymbol{x}(n,i)$ defined as

$$\boldsymbol{x}(n,i) = [x(nT_b+iT_c-\mathcal{T}), x(nT_b+iT_c-\mathcal{T}+T_{s_1}), \ldots, x(nT_b+iT_c-\mathcal{T}+MT_{s_1}-T_{s_1})]^T \tag{5.4}$$

where $\mathcal{T}$ introduces a delay to input samples that is dependent on the chip pulse shape. The input vector $\boldsymbol{x}(n,i)$ embeds the information bit $b_n^{(0)}$ and the pilot symbol '+1' scrambled with their corresponding Walsh codes and PN sequences.

The value of M is a design parameter. It can be chosen for the FSE to either spread over a typical multipath channel or just span a time window which contains

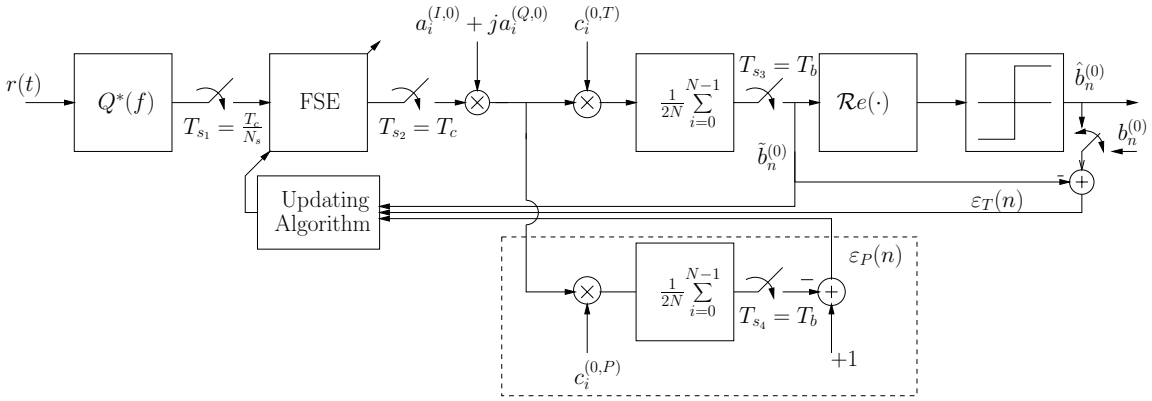

Figure 5.1: Adaptive receiver structure for user 0. The dashed block is only present when the pilot channels are available.

the major portion of the signal energy. For instance, to support a 6-μs channel [12] with a chip rate of 1.2288 MHz, a total of $M = 30$ taps is needed if $N_s = 4$. Some field measurements, however, indicate that the first 3 μs contains more than 90% of the signal energy [60]. To cover this time window, $M = 15$ is sufficient. More than one tap is assigned to a chip interval ($T_{s_1} < T_c$) to improve diversity combining.

The FSE output is sampled at the chip rate and despread with the locally generated PN sequences of the I and Q phases. The PN sequence generators are coarsely synchronized with the earliest path of the desired user. Therefore, a code synchronization and tracking unit is required to acquire $\tau_1^{(0)}$. This block is not shown in Fig. 5.1. Next, on the top branch, the effect of the traffic channel Walsh code, $c_i^{(0,T)}$, is removed to obtain a chip estimate. A total of N chip estimates are normalized, summed, and sampled again at the bit rate to form the bit estimate.

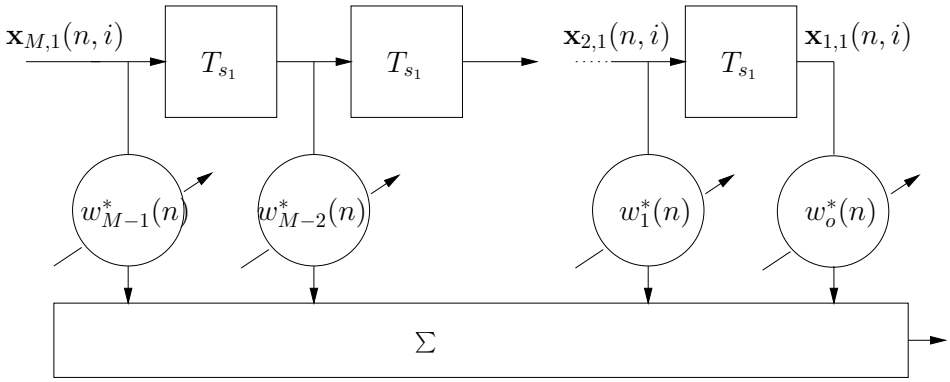

Figure 5.2: The FSE with M complex taps and $M-1$ delay elements of duration T_{s_1}.

More precisely,

$$\tilde{b}_n^{(0)} = \frac{1}{2N} \sum_{i=0}^{N-1} c_i^{(0,T)} (a_{i+nN}^{(I,0)} + j a_{i+nN}^{(Q,0)}) \left[\boldsymbol{w}^H(n) \boldsymbol{x}(n,i) \right] \tag{5.5}$$

where superscript H represents Hermitian transpose.[1]

In the presence of pilot channels ($\beta_0 \neq 0$), the effect of the pilot channel Walsh code is also removed in the bottom branch in a similar fashion. The estimate of the pilot symbol can be expressed as

$$\tilde{d} = \frac{1}{2N} \sum_{i=0}^{N-1} c_i^{(0,P)} (a_{i+nN}^{(I,0)} + j a_{i+nN}^{(Q,0)}) \left[\boldsymbol{w}^H(n) \boldsymbol{x}(n,i) \right] \tag{5.6}$$

where the index in $\tilde{d}$ is removed since it is assumed that the pilot symbol is always '+1'.

[1]The factor of 2 in (5.5) is introduced to correct for the factor of 2 generated by the multiplication of $(a_{i+nN}^{(I,0)} - j a_{i+nN}^{(Q,0)})$ by its conjugate.

5.2.2 Error Signals

Three error signals are input to the updating algorithm block. Depending on the employed adaptive algorithm, one, two, or all of these signals may be used in updating the FSE tap weights (See Table 5.1). The first input is the bit estimate, $\tilde{b}_n^{(0)}$, as formulated in (5.5). Although $\tilde{b}_n^{(0)}$ is not an error signal by itself, it is used, as explained later, to form the error of the signal modulus.

The other two inputs are the error signals from the traffic and pilot channels, $\varepsilon_T(n)$ and $\varepsilon_P(n)$, respectively. They can be expressed as:

$$\varepsilon_T(n) = \begin{cases} b_n^{(0)} - \tilde{b}_n^{(0)} & \text{training mode} \\ \\ \text{sgn}(\mathcal{R}e\{\tilde{b}_n^{(0)}\}) - \tilde{b}_n^{(0)} & \text{decision-directed mode} \end{cases} \tag{5.7}$$

$$\varepsilon_P(n) = 1 - \tilde{d}. \tag{5.8}$$

The error signal, $\varepsilon_T(n)$, has two forms. When the receiver is under training, a replica of $b_n^{(0)}$ is accessible and $\varepsilon_T(n) = b_n^{(0)} - \tilde{b}_n^{(0)}$. When the SNR is high enough to make the outputs of the decision device reliable, training is ceased and $\tilde{b}_n^{(0)}$ is used to form the error $\varepsilon_T(n) = \text{sgn}(\mathcal{R}e\{\tilde{b}_n^{(0)}\}) - \tilde{b}_n^{(0)}$.

Adaptive Algorithm	$\tilde{b}_n^{(0)}$	$\varepsilon_T(n)$	$\varepsilon_P(n)$
LMS/RLS		$\surd$	
PCA-LMS/RLS			$\surd$
LCMA/RCMA	$\surd$	$\surd$	
HYB-LMS/RLS	$\surd$	$\surd$	$\surd$

Table 5.1: Type of algorithm and the error signal(s) used.

5.2.3 Alternative Structures

Alternative structures and methods have been investigated in the literature. In contrast to the structure of Fig. 5.1, [18, 21, 33] consider correlation with the PN sequence prior to equalization. This change of order results in significant additions to hardware complexity. Also, in [18, 21], a second vector of observables containing samples of only noise and interference is exploited at the expense of increased complexity. This is in addition to the single vector used here, $\boldsymbol{x}(n, i)$, which contains samples of the desired signal plus noise and interference. Consequently, the receivers of [18, 21] demonstrate a superior rate of convergence.

Due to the balanced signals of the I and Q phases (BPSK modulation, the presence of identical pilot signals, and multipath profiles in both phases), only one FSE is used for equalization. If such balance is violated for any reason (e.g., the presence of pilot signal in only one phase [63] or *offset* QPSK modulation [7]), a separate FSE is required for equalization of each phase.

With respect to pilot channels, IC schemes have been examined in [64, 65, 94, 95] where, with the aid of the pilot channel, the interference from other users is regenerated and removed from the received signal to detect the desired user. However, a Rake architecture is considered in these works and the process of IC is performed in each finger. In this work, however, interference suppression and multipath diversity combining are simultaneously accomplished by the adaptive FSE.

5.3 Adaptive Algorithms

The adaptive algorithm, responsible for updating the FSE tap weights, plays a pivotal role in the performance of the receiver. In this section, four sets of adaptive algorithms are discussed. The first two sets are based on the well-known LMS and RLS algorithms where the adaptive FSE is trained either by a known training sequence or by an always-present pilot channel (PCA). To avoid the cumbersome reliance on training, a duet of blind algorithms are discussed in the third set on the basis of the CMA. To improve the efficiency of PCA algorithms in the reverse link, the last set presents two hybrid (HYB) algorithms that benefit from the pilot channels and the CM property of the information symbols simultaneously. Each set contains a slow but simple steepest descent form and a fast but complex recursive form.

5.3.1 Training-Based Algorithms

In the absence of pilot channels ($\beta_0 = 0$), training sequences are required to supervise the convergence of the FSE to the desired solution. Naturally, the algorithms considered for updating the tap weights are based on minimizing the MSE $J_{MSE} = \mathrm{E}[|\varepsilon_T(n)|^2]$ where $\varepsilon_T(n)$ is defined as in (5.7). Two well-known iterative algorithms, the LMS and RLS, are briefly discussed next. A comprehensive study of both can be found in [72].

LMS

The LMS algorithm operates by adjusting the tap weights towards the direction of an estimate for negative gradient of MSE. It has a low computational complexity but leaves an excess MSE component above the MMSE and is slow in convergence. The tap weights are updated using the iterative equation

$$\boldsymbol{w}(n+1) = \boldsymbol{w}(n) + \mu\ \varepsilon_T^*(n)\boldsymbol{x}_T(n). \tag{5.9}$$

where $\boldsymbol{x}_T(n)$ is the time-averaged despread input vector of the FSE with respect to the traffic channel expressed as

$$\boldsymbol{x}_T(n) = \frac{1}{2N}\sum_{i=0}^{N-1}\left[(a_{i+nN}^{(I,0)} + ja_{i+nN}^{(Q,0)})c_i^{(0,T)}\right]\boldsymbol{x}(n,i). \tag{5.10}$$

The small step size μ tunes the speed of convergence and excess MSE. It is important to note that the LMS algorithm of (5.9) is different than that suggested in [76] which uses the instantaneous, rather than time-averaged, value of the input vector. The above algorithm demonstrates improvements in the rate of convergence.

RLS

The common form of the RLS algorithm is based on the method of exponentially weighted least-squares which seeks to minimize the cost function

$$J[\boldsymbol{w}(n)] = \sum_{i=1}^{n}\nu^{n-i}|\varepsilon_T(n)|^2 \tag{5.11}$$

where ν is an exponential weighting factor, also referred to as the *forgetting factor*, chosen in the range of $0 \ll \nu \leq 1$. Instead of a single step size for the tap weight vector, the RLS algorithm assigns a step size to every element of $\boldsymbol{w}(n)$ and corrects them accordingly. Hence, its speed of convergence is much faster compared to that of the LMS algorithm at the expense of increased computational complexity. The tap weights are updated using the following algorithm:

$$\boldsymbol{k}_T(n) = \frac{\boldsymbol{P}(n-1)\boldsymbol{x}_T(n)}{\nu + \boldsymbol{x}_T^H(n)\boldsymbol{P}(n-1)\boldsymbol{x}_T(n)} \tag{5.12}$$

$$\boldsymbol{w}(n) = \boldsymbol{w}(n-1) + \boldsymbol{k}_T(n)\varepsilon_T^*(n) \tag{5.13}$$

$$\boldsymbol{P}(n) = \nu^{-1}\boldsymbol{P}(n-1) - \nu^{-1}\boldsymbol{k}(n)\boldsymbol{x}_T^H(n)\boldsymbol{P}(n-1) \tag{5.14}$$

where $\boldsymbol{k}$, and $\boldsymbol{P}$ are, respectively, the $M \times 1$ complex gain vector, and the $M \times M$ inverse correlation matrix that needs a non-zero initialization upon start-up. In [72], the recommended choice for the initial value of $\boldsymbol{P}$ is $\boldsymbol{P}(0) = \delta^{-1}\boldsymbol{I}$ where $\boldsymbol{I}$ is the $M \times M$ identity matrix. The parameter δ is a constant which is small compared to $0.01\sigma_{\boldsymbol{x}}^2$ where $\sigma_{\boldsymbol{x}}^2$ is the variance of a data sample $\boldsymbol{x}(n,i)$. Roundoff noise and high computational complexity limit the use of this algorithm in many applications.

5.3.2 PCA Algorithms

The next generation of CDMA systems will have pilot channels incorporated in the reverse link as well [9, 10, 62]. The presence of pilot channels serves as an always-on training sequence. However, it decreases channel capacity due to the reduction of traffic channel power. In the reverse link, the power of pilot channels is limited and

usually lower than that of traffic channels. The LMS and RLS algorithms of the previous section are slightly modified to minimize $\varepsilon_P(n)$ instead of $\varepsilon_T(n)$.

PCA-LMS

The iterative equations of (5.9) is modified to:

$$\boldsymbol{w}(n+1) = \boldsymbol{w}(n) + \mu\, \varepsilon_P^*(n)\boldsymbol{x}_P(n) \tag{5.15}$$

$$\boldsymbol{x}_P(n) = \frac{1}{2N}\sum_{i=0}^{N-1}\left[(a_{i+nN}^{(I,0)} + ja_{i+nN}^{(Q,0)})c_i^{(0,P)}\right]\boldsymbol{x}(n,i). \tag{5.16}$$

PCA-RLS

Equations (5.12)-(5.14) are modified with respect to the pilot channel to:

$$\boldsymbol{k}_P(n) = \frac{\boldsymbol{P}(n-1)\boldsymbol{x}_P(n)}{\nu + \boldsymbol{x}_P^H(n)\boldsymbol{P}(n-1)\boldsymbol{x}_P(n)} \tag{5.17}$$

$$\boldsymbol{w}(n) = \boldsymbol{w}(n-1) + \boldsymbol{k}_P(n)\varepsilon_P^*(n) \tag{5.18}$$

$$\boldsymbol{P}(n) = \nu^{-1}\boldsymbol{P}(n-1) - \nu^{-1}\boldsymbol{k}(n)\boldsymbol{x}_P^H(n)\boldsymbol{P}(n-1). \tag{5.19}$$

Their interpretations remain the same as those of (5.12)-(5.14).

5.3.3 Blind Algorithms

To rid the receiver from the cumbersome reliance on training, blind adaptive receivers based on CMA are developed here. CMA, a fourth order statistics algorithm, seeks to minimize a cost function defined by the CM criterion. The CM criterion penalizes deviations in the modulus (i.e., magnitude) of the equalized signal away

from a fixed value; the dispersion constant. Remarkably, it can successfully equalize signals characterized by source alphabets not possessing a constant modulus (e.g., 16-QAM), as well as those possessing a constant modulus (e.g., QPSK).

Simulation results show that the conventional CMA [67, 68], by itself, fails to properly detect all paths of the desired user and suppress interference. It converges to local minima with undesirable excess MSE. Here, a special form of CM cost function is employed which does not involve powers of the estimated modulus. A quadratic constraint is also imposed on the FSE tap weights. Consequently, ill-convergence is prevented and the CMA converges to the global minimum.

Leaky CMA

Existing adaptive receivers based on the CMA for short-code CDMA systems have two common features: *i)* they benefit from linear constraints, and *ii)* they employ the conventional CM cost function.

In short-code CDMA, the received signal is a wide sense cyclostationary (WSCS) random process with a period of T_b. The periodic statistical behavior of the received signal is directly related to the short PN sequences assigned to users. Hence, in many adaptive receivers (e.g., [69]-[71]), a linear constraint based on the short PN sequence of the user of interest is developed and exploited. In long-code CDMA, the received signal is still a WSCS random process though the period is reduced to T_c [96]. The linear constraints of short-code CDMA receivers can no longer be applied.

The conventional CM cost function involves powers of the bit estimate and can

be expressed as

$$J_{CM}(\boldsymbol{w}) = E\left[\left(R_p - |\tilde{b}_n^{(0)}|^2\right)^2\right] \tag{5.20}$$

where R_p is the dispersion constant defined as [67, Eq. (25)]:

$$R_p = \frac{E[|b_n^{(0)}|^{2p}]}{E[|b_n^{(0)}|^p]} \tag{5.21}$$

Simulation results show that such cost function fails to detect and combine the multipath components of the desired signal. Depending on the initialization strategy, the FSE either locks on one or two strong paths and suppresses the rest or does not detect any of the desired paths at all.

The proposed cost function employs a special member of the CM class and imposes a quadratic constraint on the FSE tap weights. It can be expressed as

$$J(\boldsymbol{w}) = (1-\lambda)J_{CM}(\boldsymbol{w}) + \lambda J_L(\boldsymbol{w}) \tag{5.22}$$

where

$$J_{CM}(\boldsymbol{w}) = E[|\ R_p - |\tilde{b}_n^{(0)}|\ |] \tag{5.23}$$

is the CM cost function [68] with R_p defined as in (5.21). For $p = 2$ and $b_n^{(0)} \in \{\pm 1\}$, it can be shown that $R_p = 1$. The quadratic constraint, $J_L(\boldsymbol{w})$, is defined as

$$J_L(\boldsymbol{w}) = \|\boldsymbol{w}\|^2 = \sum_{i=0}^{M-1} |w_i|^2. \tag{5.24}$$

The second term, $J_L(\boldsymbol{w})$, is also referred to as the *complexity penalty* term and is discussed in the field of *complexity regularization* [97, pp. 219–220]. Various

methods exist for complexity regularization. However, the simplest technique is the *weight-decay procedure* [97] described by (5.24). It operates by forcing some of the weights in FSE to take values close to zero, while permitting other weights to retain their relatively large values. Therefore, the FSE taps are grouped roughly into two categories: those that take noticeable values (corresponding to a detected path), and those that take insignificant values (corresponding to no path) which are also referred to as excess weights. The *regularization parameter*, λ, represents the relative importance of the complexity-penalty term with respect to the performance-measure term.

Invoking a standard stochastic gradient search on (5.22), the recursive updating algorithm can be expressed as:

$$\boldsymbol{w}(n+1) = (1-\mu\lambda)\boldsymbol{w}(n) + \mu(1-\lambda)\left(\frac{\tilde{b}_n^{(0)}}{|\tilde{b}_n^{(0)}|}.\mathrm{sgn}[1-\tilde{b}_n^{(0)}]\right)^* \boldsymbol{x}_T(n) \qquad (5.25)$$

The iterative equation of (5.25) does not involve powers of bit estimate and results in reduced word requirements and computational complexity. It resembles the LMS algorithm of (5.9) except for a different error signal. Hence, it is capable of opening the channel eye by detecting the multipath components of the desired signal properly. The parameter λ satisfies $0 < \lambda < 1$. As the MAI level rises and the number of interfering users with constant modulus data grows, the value of λ is increased to put more emphasis on $J_L(\mathbf{w})$ rather than $J_{CM}(\boldsymbol{w})$. The scalar $(1-\mu\lambda)$ is referred to as the *leakage factor*. Leakage is another common terminology for the weight-decay procedure. It is used in digital implementation of the LMS algorithm to prevent overflow in finite-precision environments by providing a compromise

between minimizing the MSE and containing the energy of FSE [72].

The complexity penalty term of (5.24) treats all FSE weights equally suggesting a uniform initialization strategy of setting all weights equal to a small non-zero value. This strategy enables the FSE to detect and equalize the desired paths appropriately and is in contrast to the common single- or multiple-spike initialization.

When the channel eye is opened enough to make the outputs of the decision device reliable, the standard DD-LMS algorithm takes over updating the tap weights with the leakage factor set to one to change the cost function back to the standard MSE and allow the adaptive algorithm to approach the theoretical MMSE solution.

Recursive CMA

Similar to the LMS algorithm, the stochastic gradient form of the LCMA results in a slow rate of convergence. Moreover, the CMA is generally known to converge even slower than the LMS algorithm [68]. Hence, its applications are limited to fixed or low-mobility wireless users where the channel conditions change slowly. To address this problem, the rapidly-converging RCMA [98]-[100] is examined.

RCMA is based on the analogy to the RLS algorithm as a fast version of the LMS algorithm. It removes the limitation of LCMA (only one degree of freedom in the steepest descent form) at the expense of increased computational complexity. It also preserves the main advantage of the CMA which is reliance on apriori knowledge of the constant envelope of the signal to avoid the need for training. RCMA is globally stable and significantly faster than LCMA [98].

With the constant modulus approach, the error term in the cost function of

(5.11) can be shown to alter from $\varepsilon_T(n)$ to

$$\varepsilon_{CM}(n) = \frac{\tilde{b}_n^{(0)}}{|\tilde{b}_n^{(0)}|}.\text{sgn}[1 - \tilde{b}_n^{(0)}] \tag{5.26}$$

which is identical to the error term in (5.25). Following the same steps in the derivation of the RLS algorithm, the iterative equations of the RCMA can be expressed as in (5.12)-(5.14) with equation (5.13) modified to [100]:

$$\boldsymbol{w}(n) = \boldsymbol{w}(n-1) + \boldsymbol{k}_T(n)\varepsilon_{CM}^*(n) \tag{5.27}$$

The RCMA, like the RLS algorithm, requires initializing the recursive equations by selecting a starting value for $\boldsymbol{P}(0)$ and $\boldsymbol{w}(0)$. The starting value of $\boldsymbol{P}(0)$ can be the same as that of the RLS algorithm. However, it can be shown that by using such choice for $\boldsymbol{P}(0)$, the recursive equations no longer minimize the cost function defined in (5.11). Instead, they seek to minimize the modified cost function [72]:

$$J[\boldsymbol{w}(n)] = \delta\nu^n\|\boldsymbol{w}(n)\|^2 + \sum_{i=1}^{n}\nu^{n-i}|\varepsilon_{CM}(i)|^2. \tag{5.28}$$

The first term in (5.28) is similar to the *complexity penalty* term in the LCMA cost function of (5.22). Consequently, the same initialization strategy of setting all tap weights equal to a small non-zero value is suitable for $\boldsymbol{w}(0)$.

A Note on Phase-Invariance of CMA

It can be observed that the class of CM cost functions, as expressed in (5.20) and (5.23), are phase-invariant, i.e., they are blind to the phase of the bit estimate

and only equalize its magnitude. Hence, blind adaptive receivers based on CMA equalize the channel up to a phase ambiguity [101]. One of the following two courses of action can be taken to track the phase of the channel: *i)* employing a phase-lock loop circuitry, and *ii)* adopting phase-independent modulation schemes (e.g., differential BPSK). It is noted that the presence of any of the above solutions is only necessary when the CMA is responsible for updating the FSE taps, which is less than few tens of iterations, as shown later in training curves.

5.3.4 Hybrid Algorithms

Pilot channels, which already exist in the forward link, has recently been incorporated in the reverse link of CDMA systems to make coherent reception feasible [9, 10, 62]. However, in contrast to the forward link where a high-powered pilot is broadcast orthogonally to all users, the pilot in the reverse link is only orthogonal to the traffic channel of the associated mobile user and its power constitutes a small portion of the total power of the mobile user. Low-powered pilot signals are often dominated by MAI and can be problematic since they affect the accuracy of channel estimation procedures. High levels of pilot power, on the other hand, improve channel estimation but compromise the capacity of the traffic channel. Such a tradeoff has triggered research on the optimization of pilot channel power (e.g., [65, 102]) which is not the subject of this chapter.

A set of iterative hybrid (HYB) algorithms is proposed here that jointly utilizes the statistics of both the traffic and pilot channels. Inspired by the CM approaches previously studied, the new algorithms rely on the CM property of the information

symbols in addition to the conventional error signals formed from the pilot symbols. More specifically, the updating algorithms initially ignore the polarity of the information symbols and use their equalized magnitude to adjust the tap weights. When the traffic channel eye is opened, the outputs of the decision device is used to form the error. At all times, the pilot symbols on the dedicated channel, known to the receiver, furnish the updating algorithm with a training sequence as they did in PCA schemes. The additional statistics of the traffic channel, normally stronger in power compared to the pilot channel, provide the adaptive algorithm with more reliable estimates of channel parameters and yield performance improvements.

HYB-LMS

The major portion of a mobile user's signal power is allocated to the traffic channel. It will be wasteful not to use the statistics of the stronger traffic channel and rely only on the weak pilot channel. The problem, however, is the closed eye of the traffic channel in the start-up. The CM approaches previously outlined proves to be an efficient technique to open the channel eye in the cold start.

For the proposed algorithm, a hybrid cost function is considered which mixes the CM cost function on the traffic channel with the MSE cost function on the pilot channel. More precisely, the hybrid cost function can be written as

$$J[\boldsymbol{w}(n)] = (1-\lambda)J_{MSE}[\boldsymbol{w}(n)] + \lambda J_{CM}[\boldsymbol{w}(n)] \tag{5.29}$$

where $0 < \lambda < 1$ is the weighting factor indicating the relative importance of the second cost function with respect to the first. Since normally $\beta_k < 0.5$, the

cost function of (5.29) can be adjusted to weight more in favor of J_{CM} by setting $\lambda > 0.5$. Invoking a standard stochastic gradient search on (5.29), the iterative updating algorithm can be expressed as

$$\boldsymbol{w}(n+1) \;=\; \boldsymbol{w}(n) + \mu(1-\lambda)\; \varepsilon_P^*(n)\boldsymbol{x}_P(n) + \;\mu\lambda\; \varepsilon_{CM}^*(n)\boldsymbol{x}_T(n) \qquad (5.30)$$

where $\varepsilon_{CM}(n)$ is defined in (5.26).

It is important to note that in deriving (5.30), $J_{MSE}[\boldsymbol{w}(n)]$ and $J_{CM}[\boldsymbol{w}(n)]$ are independent of $\boldsymbol{x}_T(n)$ and $\boldsymbol{x}_P(n)$, respectively. When the channel eye is open enough to make the outputs of the decision device reliable, the updating algorithm changes to

$$\boldsymbol{w}(n+1) \;=\; \boldsymbol{w}(n) + \mu(1-\lambda)\; \varepsilon_P^*(n)\boldsymbol{x}_P(n) + \;\mu\lambda\; \varepsilon_T^*(n)\boldsymbol{x}_T(n) \qquad (5.31)$$

It is noted that as $\beta \to 0$, the correction term related to the pilot channel, the middle terms in (5.30) and (5.31), fades in significance and the hybrid algorithm converges to the leaky CM algorithm. However, $\varepsilon_P(n)$ is still beneficial in avoiding ill-convergence of the CM algorithm.

HYB-RLS

In a similar fashion, the recursive updating algorithm HYB-RLS can be written as:

$$\boldsymbol{w}(n+1) = \boldsymbol{w}(n) + (1-\lambda)\; \varepsilon_P^*(n)\boldsymbol{k}_P(n) + \lambda\; \varepsilon_T^*(n)\boldsymbol{k}_T(n) \qquad (5.32)$$

where $\boldsymbol{k}_T(n)$ and $\boldsymbol{k}_T(n)$ are gain vectors obtained from the statistics of the traffic and pilot channels, respectively. They are defined in equations of (5.12) and (5.17). Switch to decision-directed mode is again made by changing $\varepsilon_{CM}(n)$ in (5.32) to $\varepsilon_T(n)$ when the output SNR is high enough.

5.4 Discussion

Four sets of algorithms were presented in the previous section with each set containing a slow stochastic-gradient and a fast recursive form. The proper choice of an adaptive algorithm for a specific application depends on three critical figures of merit: i) performance in terms of achievable MSE (or output SNR), ii) rate of convergence to the steady-state solution, and iii) computational complexity. This section comments on the comparison of these adaptive algorithms based on the above three criteria. A more quantitative examination by numerical results will be shortly presented.

5.4.1 MSE Performance

The maximum output SNR, SNR_{max}, of the ideal LMMSE receiver is formulated in (4.34). It serves as an upper bound for the performance of the adaptive algorithms where no pilot channel exists (training-based or blind algorithms). In the presence of pilot channels, the power of the traffic channel for the desired user is reduced to $(1-\beta_0)P_0$. It is straightforward to show that the upper bound for output SNR of the PCA algorithms decreases to $(1-\beta_0)\text{SNR}_{max}$.

The RLS algorithm is known to leave little or no excess MSE above the the-

oretical MMSE [72]. The LMS algorithm, however, always incurs some loss in performance whose value depends on the eigenvalues of the correlation matrix $\boldsymbol{R} = E[\boldsymbol{x}(n)\boldsymbol{x}^H(n)]$ and can be less than 3 dB if the step size is chosen correctly [72]. The CM algorithms also suffer from performance loss in MSE since they operate based on the modulus of bit decision statistics only. Their performance loss is expected to grow by increasing the number of interferers with CM signals [73].

In general, the training-based RLS algorithm, which allocates 100% of the signal power to training, is expected to perform well. The PCA-RLS algorithm, however, is expected to incur some loss in performance (specially if the pilot channel power is low) since channel estimation can not be as accurately accomplished. The HYB-RLS algorithm is designed to improve upon PCA-RLS. The LMS-based algorithms can be compared in a similar way.

5.4.2 Convergence Rate

In [72], it is shown that the ensemble-averaged learning curve of the LMS algorithm is approximated by a single exponential with time constant τ_{avg} where

$$\tau_{avg} \approx \frac{1}{2\mu\lambda_{avg}} \tag{5.33}$$

and λ_{avg} is the average eigenvalue for the correlation matrix $\boldsymbol{R}$ defined as

$$\lambda_{avg} = \frac{1}{M}\sum_{i=1}^{M}\lambda_i. \tag{5.34}$$

The above is determined based on the independence theory which does not hold for the system model and receiver structure of this paper. Thus, the LMS algorithm requires more iterations to converge. However, τ_{avg} can generally be considered as a lower bound for convergence time. The multipath profile of the desired and interfering users obviously play an important role in shaping $\boldsymbol{R}$ and its eigenvalues. Due to its different cost function, the LCMA is typically slower than the LMS algorithm [73].

By invoking the independence theory, the RLS algorithm is proved in [72] to stabilize near the MMSE solution after only $2M$ iterations where M is the number of FSE tap weights. This can again be considered as a lower bound for convergence time of the RLS algorithm although simulation results show that more iterations are required for the RLS to converge. The RCMA is typically slower than the RLS too. However, unlike their steepest descent counterparts, the convergence time of the RLS and RCMA is determined by the number of FSE taps, M.

5.4.3 Computational Complexity

The computational complexity of the stochastic gradient algorithms is on the order of $\mathcal{O}(M)$ whereas that of the recursive algorithms is on the order of $\mathcal{O}(M^2)$. The exact amount of summations, multiplications, divisions, and square root operations for each algorithm are summarized in Table 5.2. It is noted that two facts have been exploited in deriving the values of Table 5.2. First, the time domain impulse response of the optimum MMSE filter is real (Refer to Fig. 3.4) and therefore, the calculations related to imaginary parts are unnecessary. Second, the correla-

tion matrix $\boldsymbol{R}$ is *Hermittian* [72] and, hence, only the upper (or lower) triangle of $\boldsymbol{R}$ needs to be calculated. No further optimization was performed in calculating the algorithms' complexities. However, improving the complexity of the adaptive algorithms has been the subject of many papers (e.g., [103] and many references therein). It has been shown in [103] that by exploiting the *near-Toeplitz* property of $\mathbf{R}$, along with other symmetries, the complexity of the RLS algorithm can be reduced by an order of magnitude to $\mathcal{O}(M)$. Moreover, alternatives such as the conjugate gradient (CG) algorithm exist that converge as fast as the RLS algorithm with lower computational complexity [104].

Algorithm	Summation	Multiplication	Division	Square root
LMS	$2M+1$	$2M+2$	0	0
LCMA	$2M+3$	$3M+5$	2	1
HYB-LMS	$4M+3$	$4M+6$	2	1
RLS	$3M^2+10M-2$	$6M^2+10M$	M^2+2M	0
RCMA	$3M^2+10M$	$6M^2+10M+2$	M^2+2M+2	1
HYB-RLS	$6M^2+20M-2$	$12M^2+20M+2$	$2M^2+4M+2$	1

Table 5.2: Complexity of the adaptive algorithms.

5.5 Summary of the Required Parameters

In Section 3.6, a list of the required parameters for brute-force implementation of the LMMSE receiver was presented. As discussed in this chapter, the knowledge of a majority of these parameters are not necessary for adaptive implementation. The new short list is as follows:

1. *An estimate of the earliest path of the desired user:* $\tau_1^{(0)}$.

2. *Desired user's signature sequences:* $\boldsymbol{a}_n^{(I,0)}$ and $\boldsymbol{a}_n^{(Q,0)}$.

3. *Chip pulse shape:* $Q(f)$.

4. *Chip rate:* $1/T_c$.

Parameter	Rake	LMMSE
$1/T_c$	$\surd$	$\surd$
$Q(f)$	$\surd$	$\surd$
$\boldsymbol{a}_n^{(I,0)}$ and $\boldsymbol{a}_n^{(Q,0)}$	$\surd$	$\surd$
$\tau_1^{(0)}$	$\surd$	$\surd$
$\tau_2^{(0)}$	$\surd$	
$\vdots$	$\surd$	
$\tau_L^{(0)}$	$\surd$	

Table 5.3: Comparison of the required parameters by the Rake and adaptive LMMSE receivers.

Table 5.3 compares the parameters that are required by the Rake and adaptive LMMSE receivers. Table 5.3 shows that the adaptive LMMSE receiver needs fewer parameters compared to the Rake receiver. More precisely, an estimate of the arrival delays of the L strongest paths are needed in the Rake architecture whereas the adaptive LMMSE receiver only requires an estimate of the earliest path. The adaptive LMMSE receiver has a centralized structure and spans the multipath profile of the desired user by means of an FSE. It can still lock on the user of interest if the estimate of $\tau_1^{(0)}$ is a few chip periods off. In contrast, the Rake receiver, due to its decentralized structure, requires estimates of the arrival delays of all the L paths with an accuracy of at least $\pm T_c/2$ or better [3, 7]. This results in significant reductions in hardware complexity of the adaptive LMMSE receiver compared to the Rake receiver as the former requires only one code-tracking unit.

5.6 Numerical Results

Simulation results are presented in three parts. First, a sample training curve for each of the discussed algorithms is illustrated to demonstrate the transient behavior and convergence rate of each algorithm. Next, the steady-state shape of the FSE is examined for a simple channel to compare the FSE impulse response with the ideal $G(f)$ filter. Third, the steady-state SNR performance of the adaptive algorithms are simulated under various levels of MAI to quantify their corresponding performance losses. In the following, the multipath parameters are generated according to the distributions outlined in the numerical results of Chapter 4. Each scenario is simulated for $500-1000$ multipath profiles and $50-100$ sample runs per profile. The results are either averaged, as in training curves, or used to obtain confidence intervals, as in SNR performance results. The FSE is assumed to spread the entire multipath channel in each case. In the recursive algorithms, the *forgetting factor* is $\nu = 1$. Also, $N = 32$, $N_s = 4$, $T_c = 1$, $\mathcal{T} = 2.5T_c$, and $\mathcal{N}_0 = 0$.

5.6.1 Training Curves

LMS vs. LCMA

Fig. 5.3 illustrates the training curves of the LMS algorithm and its blind counterpart, the LCMA. The system has $K = 4$ interferers and the multipath profile of the desired user consists of $L^{(0)} = 5$ paths and spreads $23T_c$ seconds which requires the FSE to have $M = 90$ taps to span the whole profile. The solid horizontal line indicates the average MMSE calculated for each multipath profile based on

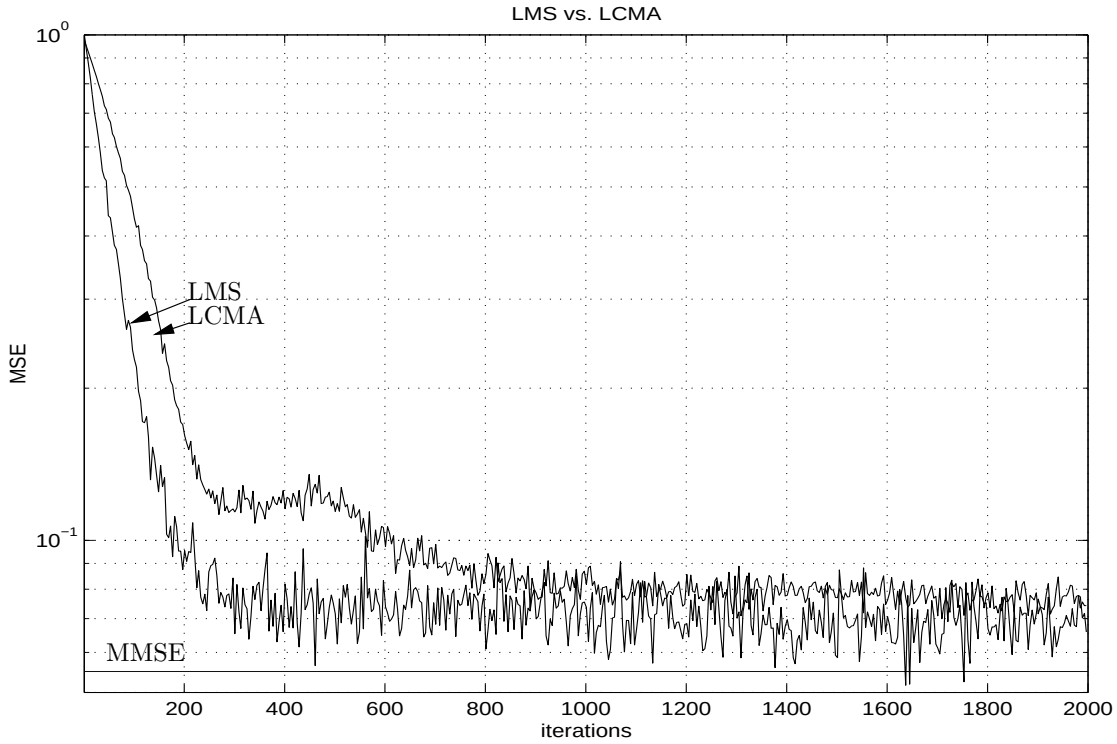

Figure 5.3: Training curves of the LMS and LCMA algorithms for a system with $K+1=5$ equally powered active users in the system and $L^{(0)}=5$, $M=90$, $N=32$, and $N_s=4$. The solid horizontal line represents the MMSE= 0.055.

(4.34). The step size μ is chosen as $\mu = 0.1/\boldsymbol{x}^H(n)\boldsymbol{x}(n)$ in accord with the normalized LMS (NLMS) procedure [72]. The initial value of the FSE tap vector is set to $\boldsymbol{w}(0) = \mathbf{0}_{M\times 1}$. No apriori information on the multipath profiles is known except an estimate of $\tau_1^{(0)}$. The LMS algorithm converges to its steady-state solution after approximately 1500 iterations and leaves about 20% excess MSE. For the blind LCMA, the regularization parameter is set to $\lambda = 0.5$ and all the FSE tap weights are initialized with a small positive constant. The LCMA algorithm is slower and leaves a slightly higher excess MSE compared to the LMS. In both

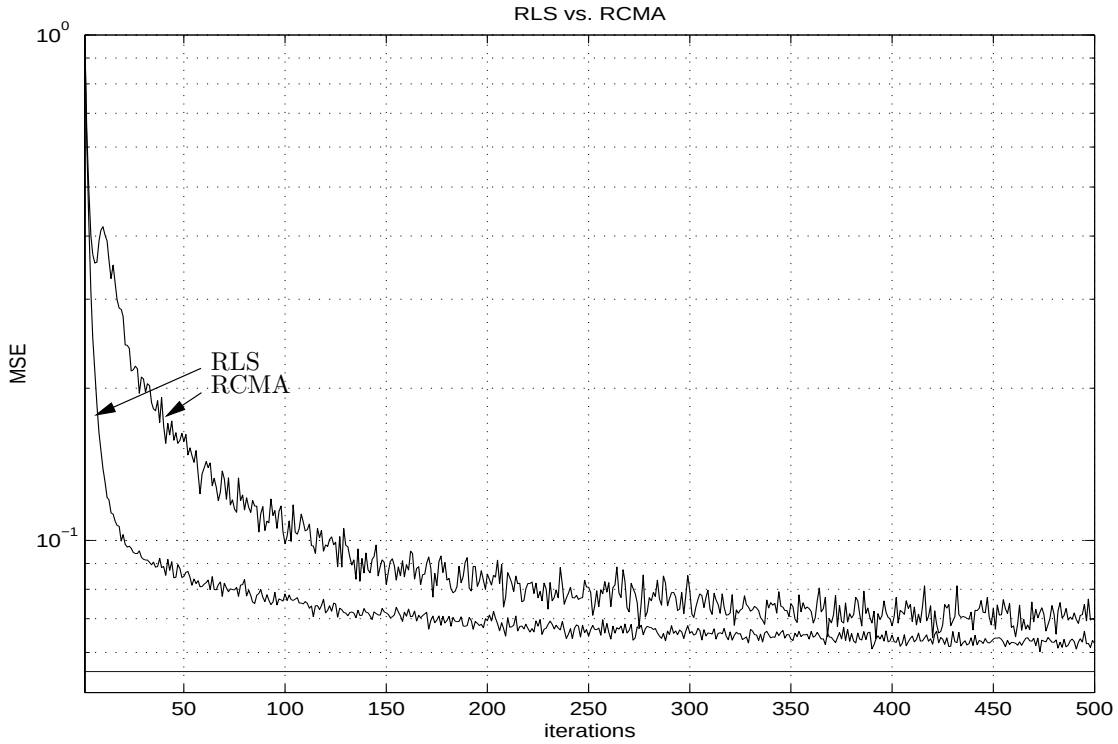

Figure 5.4: Training curves of the RLS and RCMA algorithms for a system with $K+1=5$ equally powered active users in the system and $L^{(0)}=5$, $M=90$, $N=32$, and $N_s=4$. The solid horizontal line represents the MMSE= 0.055.

cases, the algorithms switch to the DD mode after the MSE drops well below 0.15 which is approximately 5 dB larger than the MMSE= 0.055. This happens after approximately 200 iterations for the LMS and 400 iterations for the LCMA.

RLS vs. RCMA

Fig. 5.4 depicts the training curves of the RLS algorithm and its blind counterpart, the RCMA. The parameter settings are identical to those of Fig. 5.3. The inverse correlation matrix $\boldsymbol{P}$ is initialized with $\boldsymbol{P}(0)=\sigma^2\boldsymbol{I}_{M\times M}$ where σ^2 is chosen as

discussed in Section 5.3.1. The recursive algorithms are approximately an order of magnitude faster. The RLS converges to the steady-state solution after approximately 250 iterations. Similar to their stochastic gradient counterparts, the RCMA is slower than the RLS and leaves larger excess MSE in steady state. The switch to the DD mode occurs after 25 iterations for the RLS and 50 iterations for the RCMA.

PCA-LMS vs. HYB-LMS

Fig. 5.5 presents the training curves of the PCA-LMS algorithm for two pilot power levels of $\beta = \{12.5\%, 25.0\%\}$ and compares them with the HYB-LMS algorithm where the pilot power level is at $\beta = 12.5\%$. The weighting factor is $\lambda = 2/3$. The compromise between the pilot power and performance of the PCA algorithm can be visibly noticed in Fig. 5.5. When $\beta = 12.5\%$, the adaptive receiver is shown to be slow in convergence. It also leaves an excess MSE of more than 6 dB above the MMSE= 0.061. By doubling the pilot power to $\beta = 25.0\%$, the performance of the PCA algorithm is significantly improved. The convergence is now faster and the excess MSE is reduced to 3 dB above the MMSE= 0.069. However, such gain in performance is achieved at the expense of reducing the traffic channel capacity. The HYB-LMS algorithm, on the other hand, can perform equal to (or in this case even better than) the PCA-LMS algorithm (with $\beta = 25.0\%$) without increasing the pilot power. In Fig. 5.5, the HYB-LMS algorithm with $\beta = 12.5\%$ converges faster than the PCA-LMS algorithm with $\beta = 25.0\%$ and leaves a smaller excess MSE (about 2.3 dB) at the steady state. The HYB-LMS algorithm initially opens the channel eye by simultaneously minimizing the modulus of information symbols

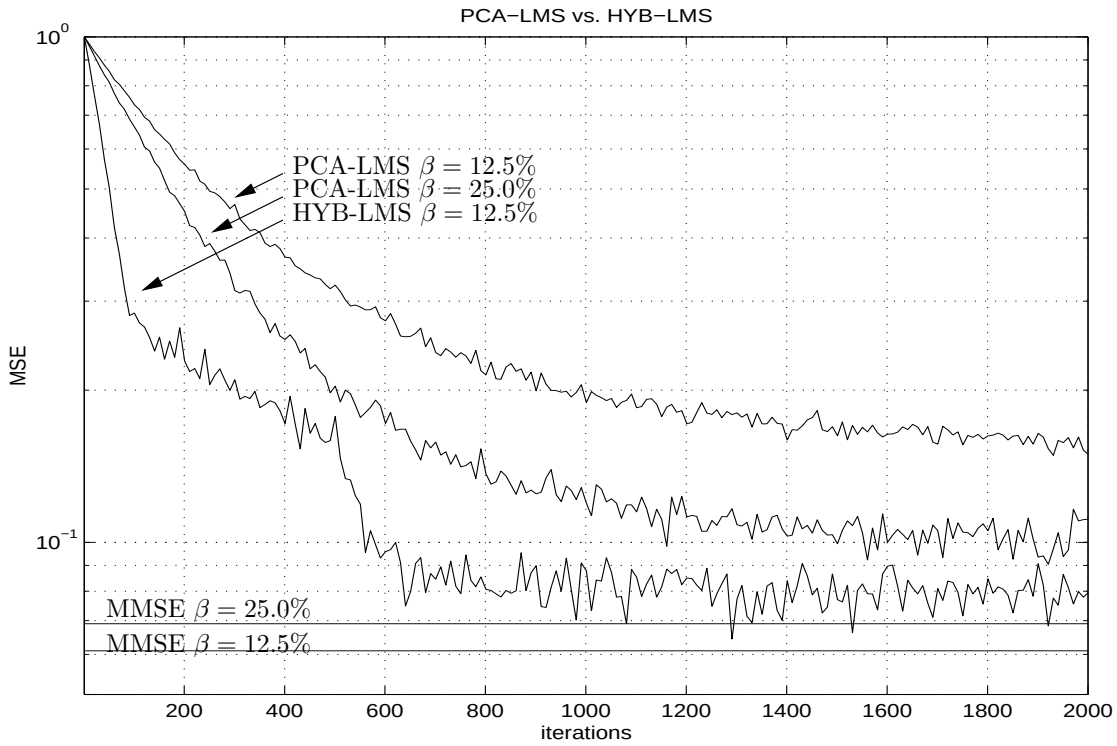

Figure 5.5: Training curves of the PCA-LMS algorithm with $\beta = \{12.5\%, 25.0\%\}$ and HYB-LMS algorithm with $\beta = 12.5\%$. The parameter settings are identical to those of Fig. 5.3. The solid horizontal lines represent the MMSE= 0.061 for $\beta = 12.5\%$ and MMSE= 0.069 for $\beta = 25.0\%$.

and MSE of the pilot symbols. After approximately 500 iterations, the SNR in the traffic channel is high enough to make the switch to DD mode safe. From here on, the algorithm minimizes the MSE in both the traffic and pilot channels.

PCA-RLS vs. HYB-RLS

Fig. 5.6 illustrates the training curves of the PCA-RLS algorithm for two pilot power levels of $\beta = \{12.5\%, 25.0\%\}$ and compares them with the HYB-RLS algorithm

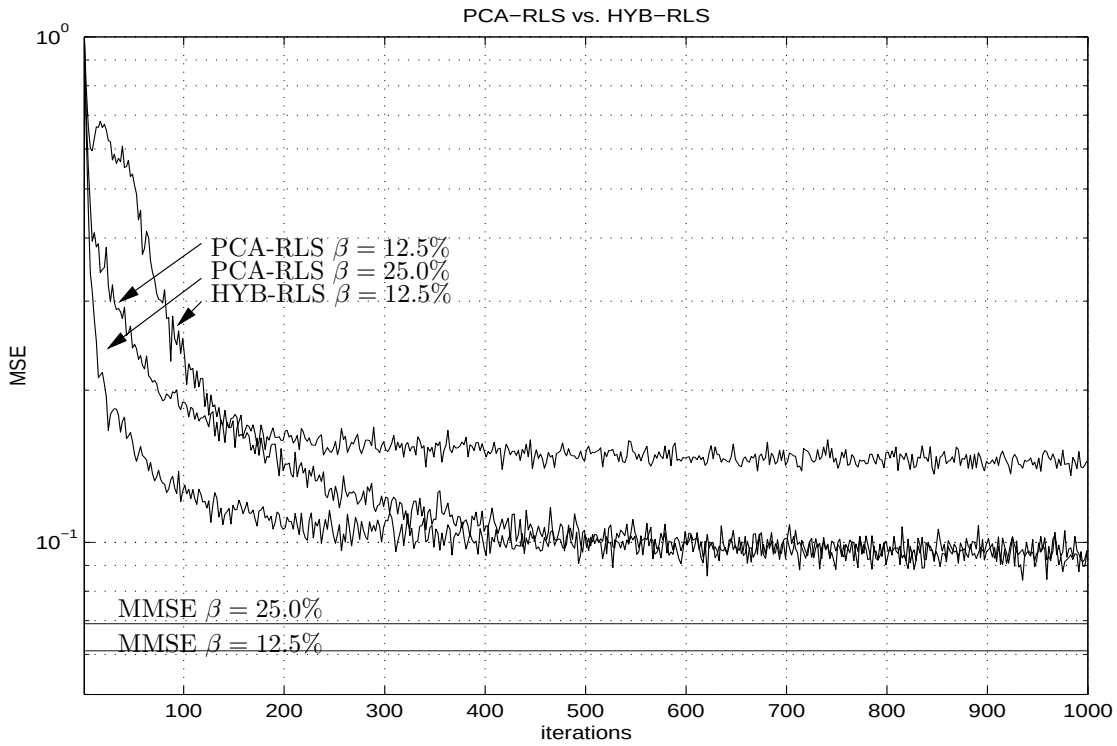

Figure 5.6: Training curves of the PCA-RLS algorithm with $\beta = \{12.5\%, 25.0\%\}$ and HYB-RLS algorithm with $\beta = 12.5\%$. The parameter settings are identical to those of Fig. 5.4. The solid horizontal lines represent the MMSE= 0.061 for $\beta = 12.5\%$ and MMSE= 0.069 for $\beta = 25.0\%$.

where the pilot power level stays at $\beta = 12.5\%$. The weighting factor is $\lambda = 2/3$. The PCA curves demonstrate the same behavior as that in Fig. 5.5. The HYB-RLS algorithm with $\beta = 12.5\%$ performs equally well as the PCA-RLS algorithm with $\beta = 25.0\%$. The switch to DD mode in the traffic channel happens approximately after 20 iterations.

5.6.2 Steady-State Filter Response

Fig. 5.7 demonstrates an example of the steady-state filter response of the adaptive receiver and compares it with the $G(f)$ and $Q(f)$ filters. The intent is to show the steady-state filter response achieved by the adaptive receiver, compare it with that of the ideal filter, and distinguish it from the CMF response. There are $K+1=10$ equally powered users in the system. Each user's signal is received via $L^{(k)}=1$ path so the receiver is focused only on the interference suppression capability. Chip delays and phase offsets are generated as before. The FSE has $M=50$ tap weights covering approximately $12T_c$ which is enough to entail more than 99% of the chip pulse shape energy. The adaptive algorithm is the RLS.

The vertical bars show the normalized values of the FSE tap weights averaged over the last 100 iterations (when the adaptive receiver has converged to its steady-state solution). The solid curve is the normalized ideal $G(f)$ filter obtained from the formulations of Appendix C. The dashed curve is the normalized CMF, $Q(f)$. Fig. 5.7 illustrates how well the FSE impulse response follows that of the ideal $G(f)$ filter. Conformity of the FSE response in the first two lobes and zero-crossings is particularly impressive. The difference between the $G(f)$ and $Q(f)$ can be readily observed as well. It is interesting to note that except for the peak value at $t=0$, the CMF has zero-crossings at times when the $G(f)$ filter hits a minimum or maximum.

5.6.3 Steady-State SNR Performance

The objective of this subsection is to examine the effect of increasing the level of interference on the steady-state performance of the adaptive receiver. Steady-

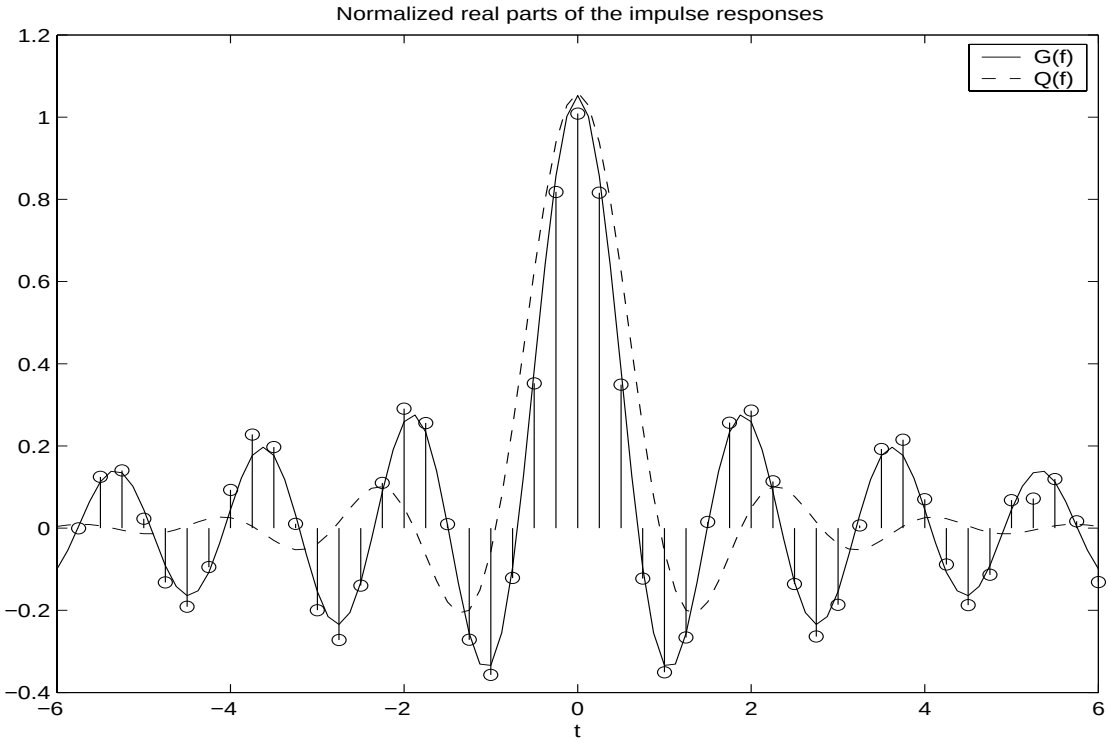

Figure 5.7: Normalized steady-state filter response of the adaptive receiver when the RLS algorithm is used. Vertical bars are the average FSE tap weights in the steady-state. Solid curve is the ideal impulse response of the $G(f)$ filter and the dashed curve is the CMF response $Q(f)$. There are 10 equally powered users in the system with $L^{(k)} = 1$.

state SNR is defined as the output SNR achieved by the adaptive receiver when it converges to the steady-state solution. In the steady-state, the adaptive filter jitters around an MSE solution. For instance, in Fig. 5.3, the adaptive FSE converges to an MSE value which is 20% above the MMSE and randomly moves around it after approximately 1500 iterations (with the LMS algorithm). The average MSE achieved after 1500 iterations results in an average output SNR which is named the steady-state SNR and chosen as the performance criterion.

LMS vs. LCMA

Fig. 5.8 illustrates the steady-state SNR vs. K for the training-based LMS algorithm and its blind counterpart: LCMA. Different number of active users correspond to various levels of signal-to-interference ratios ($E_b/\mathcal{I}_0$). Generally, $E_b/\mathcal{I}_0$ is more dominant than $E_b/\mathcal{N}_0$. Figs. 5.8-5.11 cover a wide range of $E_b/\mathcal{I}_0$ reflecting a range of more than 10 dB in output SNR. For each simulated point, corresponding to a specific K, 500-1000 multipath profiles were generated. For each profile, the steady-state SNR was averaged over 50 sample paths and the result was compared with the maximum achievable SNR. The dashed lines marked by '$\star$' and '$+$' represent the 99% confidence intervals of steady-state SNR for the LMS and LCMA, respectively.

Fig. 5.8 shows that the LMS algorithm incurs a performance loss of about 0.75 dB for small K. The performance loss grows to 1.0 dB when K increases. The performance of the LCMA is slightly inferior compared to that of the LMS as expected from its blind nature. The performance loss of the LCMA grows from 0.85 dB for small K to 1.20 dB for large K.

RLS vs. RCMA

Fig. 5.9 plots the steady-state SNR vs. K for the training-based RLS algorithm and its blind counterpart: RCMA. The curves are similar to those of Fig. 5.8. The RLS incurs a performance loss of about 0.60-0.70 dB for K in the range of 1-30. The RCMA, however, suffers more as K grows. The RCMA loss increases from 0.95 dB for $K = 1$ to 1.20 dB for $K = 30$.

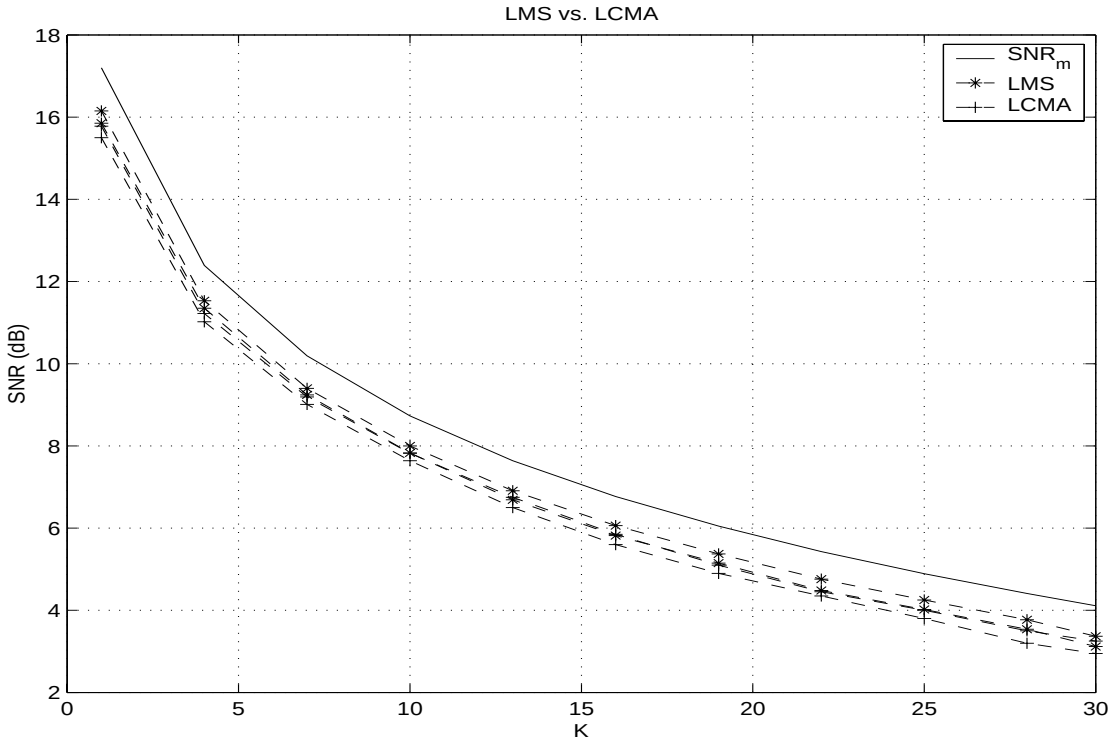

Figure 5.8: Steady-state SNR vs. K for the training-based LMS algorithm and its blind counterpart: LCMA. Solid line represents the maximum achievable SNR. Dashed lines marked by '$\star$' and '$+$' represent, respetively, the 99% confidence interval of the steady-state SNR for the LMS and LCMA. All users are equally powered. Also, $N = 32$, $M = 90$, $N_s = 4$, and $L^{(k)} = 5$.

PCA-LMS vs. HYB-LMS

Fig. 5.10 plots the steady-state SNR performance of the PCA-LMS algorithm for two levels of pilot power $\beta = \{12.5\%, 25.0\%\}$ and compares them with that of the HYB-LMS algorithm with $\beta = 12.5\%$. Solid lines represent the maximum achievable SNR for two pilot power levels of $\beta = 12.5\%$ (the upper line) and $\beta = 25.0\%$. Dashed lines represent the 99% confidence intervals of the steady-state

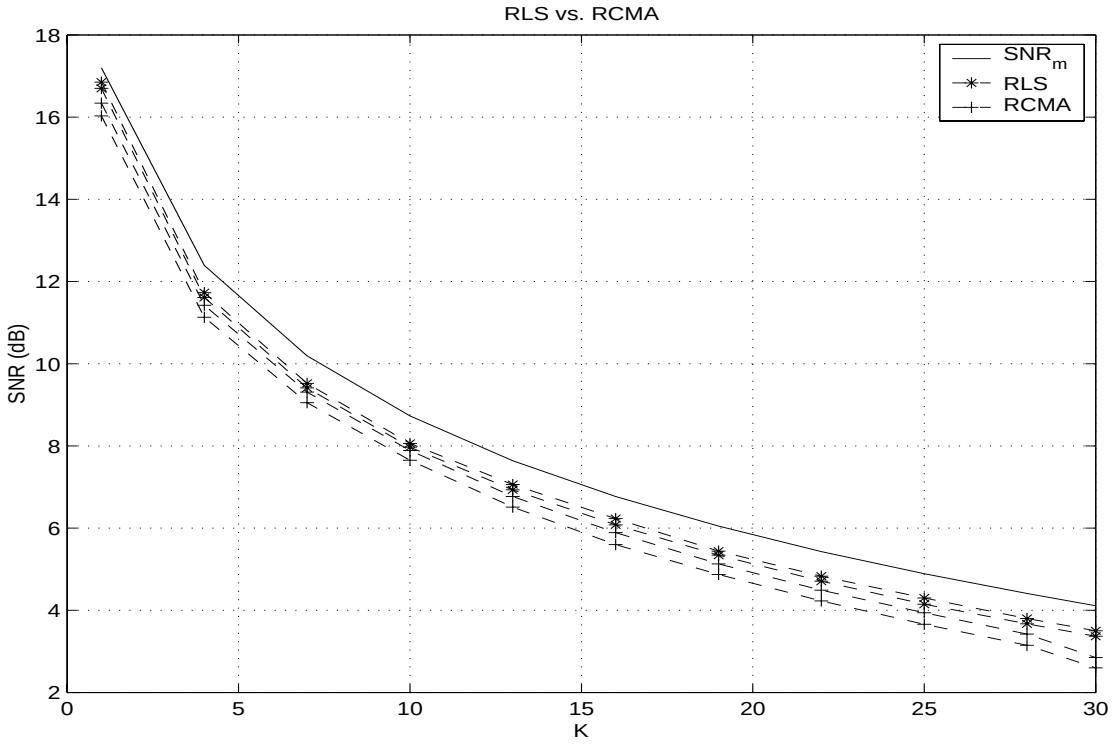

Figure 5.9: Steady-state SNR vs. K for the training-based RLS algorithm and its blind counterpart: RCMA. Solid line represents the maximum achievable SNR. Dashed lines marked by '$\star$' and '$+$' represent, respetively, the 99% confidence interval of the steady-state SNR for the RLS and RCMA. All users are equally powered. Also, $N = 32$, $M = 90$, $N_s = 4$, and $L^{(k)} = 5$.

SNR for the three cases. In the case of $\beta = 12.5\%$, the PCA-LMS causes a loss of 2.0 dB for small K. As K increases and MAI dominates the pilot channel, the performance loss significantly grows to as high as 6.10 dB for $K = 30$. Increasing the pilot power to $\beta = 25.0\%$ leads to a remarkable improvement in performance as the SNR loss is reduced to 0.9 dB for small K and 3.0 dB for $K = 30$. However, such an improvement can also be achieved by employing the HYB-LMS algorithm without increasing the pilot power. The HYB-LMS with $\beta = 12.5\%$ results in

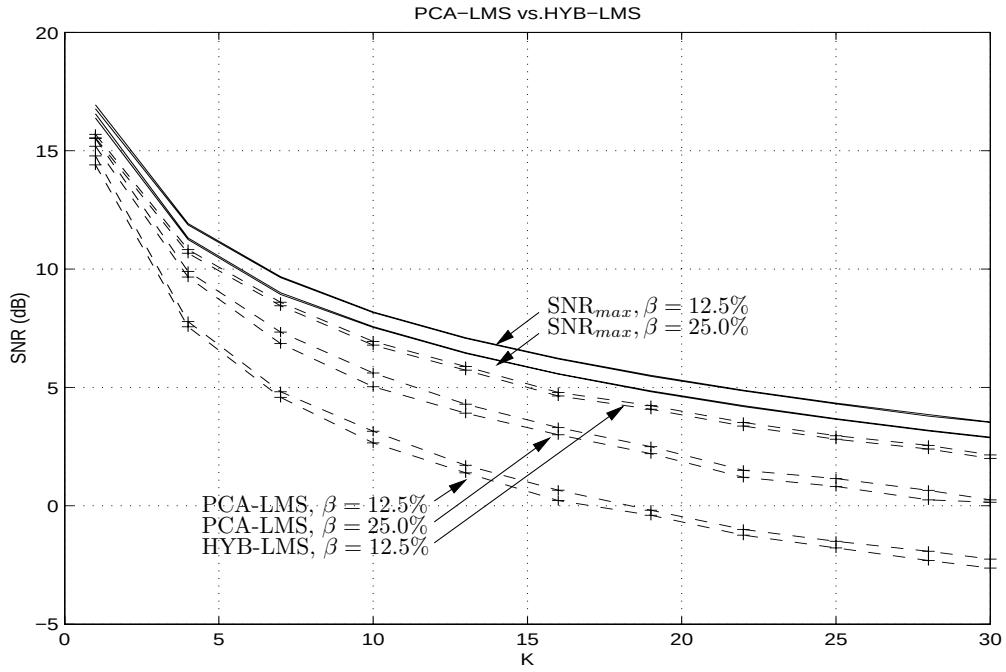

Figure 5.10: Steady-state SNR vs. K for the PCA-LMS and HYB-LMS algorithms. Solid lines represent the maximum achievable SNR for two pilot power levels of $\beta = 12.5\%$ (the upper line) and $\beta = 25.0\%$. Dashed lines represent the 99% confidence interval of the steady-state SNR for the PCA-LMS algorithm with $\beta = \{12.5\%, 25.0\%\}$ and HYB-LMS algorithm with $\beta = 12.5\%$. All users are equally powered. Also, $\lambda = 2/3$, $N = 32$, $M = 90$, $N_s = 4$, and $L^{(k)} = 5$.

1.0–1.6 dB loss in SNR for K =1–30.

PCA-RLS vs. HYB-RLS

Fig. 5.11 plots the steady-state SNR performance of the PCA-RLS algorithm for two levels of pilot power $\beta = \{12.5\%, 25.0\%\}$ and compares them with that of the HYB-RLS algorithm with $\beta = 12.5\%$. The curves are similar to those in Fig. 5.10. For $\beta = 12.5\%$, the HYB-RLS incurs an SNR loss of 2.0–6.0 dB for K =1–30. For

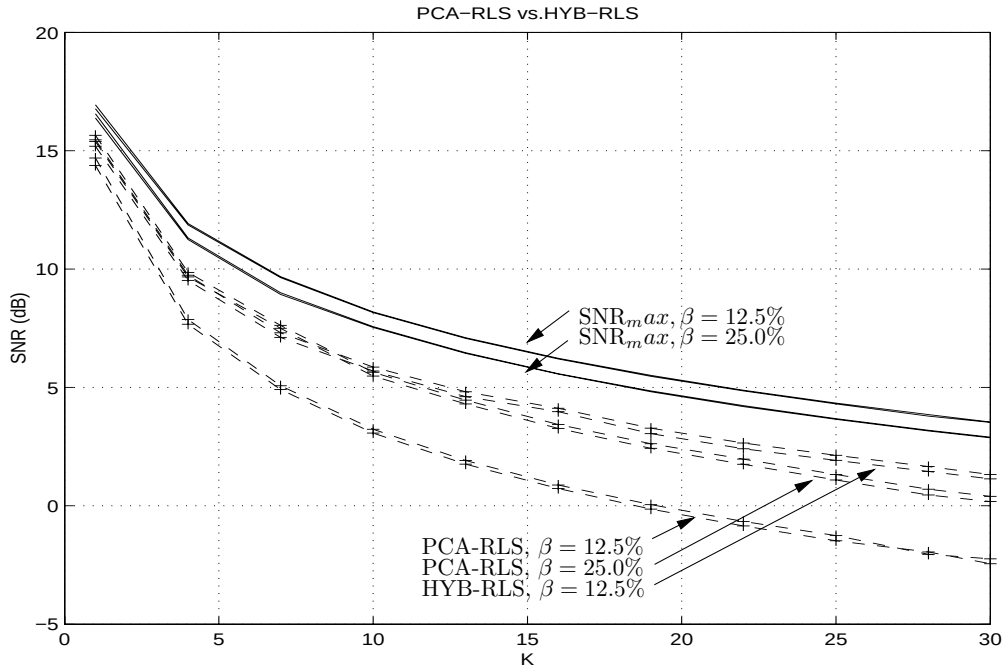

Figure 5.11: Steady-state SNR vs. K for the PCA-RLS and HYB-RLS algorithms. Solid lines represent the maximum achievable SNR for two pilot power levels of $\beta = 12.5\%$ (the upper line) and $\beta = 25.0\%$. Dashed lines represent the 99% confidence interval of the steady-state SNR for the PCA-RLS algorithm with $\beta = \{12.5\%, 25.0\%\}$ and HYB-RLS algorithm with $\beta = 12.5\%$. All users are equally powered. Also, $\lambda = 2/3$, $N = 32$, $M = 90$, $N_s = 4$, and $L^{(k)} = 5$.

$\beta = 25.0\%$, however, this loss decreases to 0.8–2.8. The HYB-RLS with $\beta = 12.5\%$ results in an SNR loss of 1.2-2.6 dB. This signifies the importance of jointly utilizing the statistics of both the traffic and pilot channels.

5.6.4 Summary of the Numerical Results

The proper choice of the adaptive algorithm is largely dependent on the the answers to the following three questions:

- How much performance loss does the algorithm incur?
- How fast does it converge?
- How complex is it?

Table 5.4 summarizes the answers to the above questions for the examined algorithms. The specific application in mind determines the performance requirements which consequently lead to the proper algorithm. For instance, in the presence of a strong pilot channel on the forward link (which can be used as a training sequence), high data rate services to low-mobility users (e.g., fixed wireless applications) can be served with the LMS algorithm. The simplicity of the LMS algorithm enables it to support high data rate services. Low mobility of the target users results in slowly-changing radio channels that can be tracked with the LMS algorithm. High-mobility users, on the other hand, require fast-tracking algorithms such as the RLS. However, the RLS can support lower data rates due to its complexity.

Adaptive Algorithm	Performance Loss (dB)	Convergence	Complexity
LMS	0.75–1.0	Slow	$\mathcal{O}(M)$, Low
RLS	0.6–0.7	Fastest	$\mathcal{O}(M^2)$, Medium
LCMA	0.85–1.2	Slower	$\mathcal{O}(M)$, Medium
RCMA	0.95–1.2	Fast	$\mathcal{O}(M^2)$, Medium
PCA-LMS, $\beta = 12.5\%$	2.0 – 6.1	Slowest	$\mathcal{O}(M)$, Low
PCA-LMS, $\beta = 25.0\%$	0.9 – 3.0	Slower	$\mathcal{O}(M)$, Low
HYB-LMS, $\beta = 12.5\%$	1.0 – 1.6	Slow	$\mathcal{O}(M)$, High
PCA-RLS, $\beta = 12.5\%$	2.0 – 6.0	Fast	$\mathcal{O}(M^2)$, Medium
PCA-RLS, $\beta = 25.0\%$	0.8 – 2.8	Faster	$\mathcal{O}(M^2)$, Medium
HYB-RLS, $\beta = 12.5\%$	1.2 – 2.6	Faster	$\mathcal{O}(M^2)$, High

Table 5.4: Comparison of the adaptive algorithms.

5.7 Concluding Remarks

This chapter examined adaptive implementations of the proposed LMMSE receiver. An adaptive receiver architecture was proposed which was based on an FSE whose tap weights were updated by an adaptive algorithm. In addition to having the capability of perfoming interference suppression, the adaptive receiver was shown to have the ARake feature as well. A direct analogy exists between the proposed adaptive receiver for wireless communication systems and the conventional adaptive FSE-based receivers in wired communication systems. In the latter, the FSE equalizes the wired channel and suppresses ISI. Similarly, in the former, the FSE acts as an ARake receiver, which is nothing but equalizing the wireless channel, along with suppressing interference. Moreover, it was shown that the adaptive receiver requires the knowledge of fewer parameters compared to the coherent Rake receiver. Only an estimate of the arrival delay of the first path of the desired user is needed as all other multipath parameters are estimated by the adaptive FSE.

Four sets of adaptive algorithms were examined. Each set included a slow but simple steepest descent form and a fast but complex recursive form. In the first set, the two well-known LMS and RLS algorithms were examined which relied on training. A typical application of such algorithms is on the forward link where a strong pilot signal is broadcast to all users and can be used as a training sequence. In the second set, PCA algorithms were investigated. Focus was on the reverse link where the pilot channel of each user was orthogonal to its traffic channel and the pilot power constituted a small portion of the total signal power of the desired user. It was shown that the performance of the PCA algorithms was strongly re-

lated to the pilot power. Low levels of pilot power caused the PCA algorithms to degrade in performance. Increasing the pilot power improved the performance but also compromised the traffic channel capacity. To avoid the cumbersome reliance on training, the third set presented blind algorithms based on the CMA that were immune to ill-convergence. Blind algorithms are beneficial in applications where training of the receiver is either not possible or costly. To address the tradeoff between performance and pilot power in PCA algorithms, the fourth set of algorithms was presented which was a hybrid of the blind CM algorithms and the PCA algorithms. The hybrid algorithms jointly utilized the statistics of both the traffic and pilot channels. This was in contrast to the conventional PCA algorithms which relied only on the statistics of the pilot channel. It was shown that the hybrid algorithms could reduce the pilot power by half and still perform equal to, or even better than, the conventional PCA algorithms. A typical application for the second and fourth sets of algorithms is the reverse link of cdma2000 systems.

Simulation results were presented to examine the convergence rate and steady-state SNR performance of the proposed algorithms. Their computational complexities were also addressed. Summary of the results appears in Table 5.4. The proper choice of the adaptive algorithm is determined by the specific application, the required convergence rate and SNR performance, and the affordable complexity.

Chapter 6

Thesis Summary & Future Work

6.1 Thesis Summary

The thesis examined the design and implementation of an LMMSE receiver in asynchronous long-code DS-CDMA systems. Chip pulse shaping and multipath channels were the focus of attention throughout. The receiver was shown to be a single-user detector capable of MAI suppression and multipath diversity combining. It maximized SNR with a new chip pulse filter which benefited from the cyclostationarity of the received signal and harnessed the energy of all paths of the desired user that were within its time support.

The performance of the LMMSE receiver was analyzed and compared with that of the coherent Rake receiver. Performance analysis was based on the IGA technique. Moreover, it was shown that the SGA method, known for its inaccuracy in low regions of bit error rate, turned out to be an accurate approximation as long as the system model satisfied: *i)* moderate to large spreading factors, *ii)*

quadriphase random spreading, and *iii)* small chip pulse excess bandwidth. The performance improvement was shown to be 0.6–1.8 dB in output SNR depending on the density of the multipath environment corresponding to 20–60% increase in system capacity.

An adaptive architecture was examined for practical implementation of the receiver. Several adaptive algorithms, training-based and blind, were explored to make the receiver applicable to both forward and reverse links either in the presence or absence of pilot signals. The centralized structure of the adaptive receiver, based on an FSE, made it possible for the receiver to require the estimates of fewer parameters compared to the Rake receiver. The adaptive receiver was, therefore, capable of combining all paths of the desired user at no additional complexity.

Applications of the proposed receiver will be in future wideband CDMA systems which are to support high data rate services. The wideband nature of the systems will distribute the energy of the desired user into many resolvable paths. To make the high data rate services feasible, the existence of a receiver with ARake feature is essential as the authors in [38] have argued. The LMMSE receiver has also been shown to be very efficient in countering the effects of ISI and ICI which are significant at high data rate applications [19, 20].

6.2 Future Work

Future work can be categorized with respect to the themes of Chapters 3–5. The following highlights some of the topics worthy of further research.

Receiver Design:

- The proposed LMMSE receiver was shown to be a single-user detector which suppressed interference from other users. To make its application more attractive in the base station, centralized multi-user LMMSE detectors can be investigated. The central issue will be the extension of the LMMSE concept for multi-user detection purposes without significantly increasing the computational complexity.

- The proposed LMMSE receiver was examined for binary information symbols and quadriphase spreading. To make it applicable to next-generation CDMA systems, the design can be extended to higher signal constellations (e.g., 16-QAM). In such cases, the effect of ISI and ICI, ignored here in the design of the LMMSE receiver, will not be negligible and should be taken into account. It is expected that the LMMSE receiver yields greater performance improvements over the Rake receiver as the signal constellation grows in density.

Performance Analysis:

- The SGA technique was shown to be an accurate approximation when quadriphase random spreading was used, the spreading factor was moderate to large, and the chip pulse excess BW was small to zero. Next-generation

CDMA systems will offer services with a wide range of data rates and diverse spreading factors. More specifically, the spreading factor can be as small as 4 and as large as 512. Therefore, it is essential to examine the accuracy of the widely-used SGA technique for small spreading factors and quantify the error between the actual P_e and that predicted by the SGA. In doing so, both the CMF and more advanced receiver filters must be considered.

Adaptive Implementations:

- Existing performance analyses of adaptive implementations are either limited to short-code CDMA system models (e.g., [44]) or simplified by the assumption of *independence theory* (e.g., [72]). Performance analysis of adaptive implementations based on the long-code CDMA system model will help in developing a guiding framework for the selection of a proper algorithm. Theoretical performance bounds can obliviate the need for a significant part of simulations.

- Oversampling the received signal and using the FSE in temporal diversity combining is strongly linked to using antenna arrays in spatial diversity combining. The application of the proposed blind and hybrid adaptive algorithms in antenna arrays is also a subject of investigation.

Finally, the actual implementation of the proposed receiver with digital signal processing (DSP) kits is worthy of a project at the masters level. The distribution of complexity to DSP power, devising performance evaluation procedures, and

examining the performance and tracking capability of adaptive algorithms in time-varying channels are specific aspects that require attention.

Appendix A

The Coherent Rake Receiver

The coherent Rake receiver [34] consists of a number of fingers in its structure where a common CMF is used for all fingers. A typical depiction of the structure of the Rake receiver can be found in [7, pp. 90–91]. A simplified version, in line with the structure of LMMSE receiver in Figs. 3.2 and 3.3, can be found in Fig. A.1. Not shown in the figure are the code-tracking unit for each finger responsible for tracking the PN code of the corresponding path and the search mechanism that finds the resolvable paths and assigns them to the available fingers.

Throughout this work, it is assumed that the contributions of multipath components are summed according to the maximal-ratio-combining (MRC) scheme.[1] It is also assumed that perfect code acquisition, tracking, channel estimation, and bit timing synchronization are accomplished in each branch. An L-finger Rake receiver focused on user 0 processes L paths of user 0. The value of L and the strategy of selecting paths can lead to the following three cases:

[1] Other methods have also been proposed in the literature (e.g. [45, 46].)

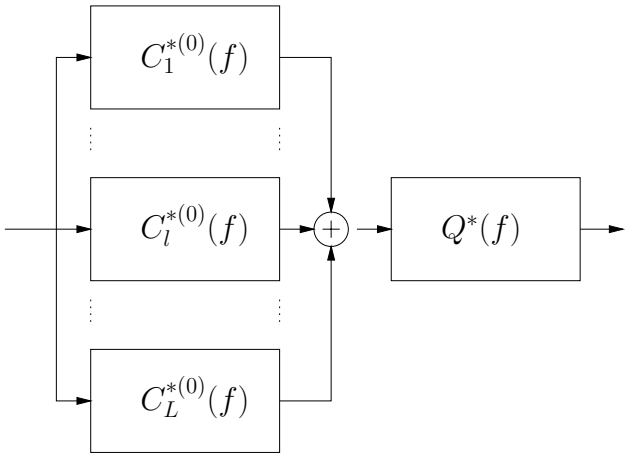

Figure A.1: Simplified structure of the Rake receiver with L fingers. The CMF replaces $G(f)$ in Fig. 3.2.

- $L = L^{(0)}$: All paths of the desired user are processed. The Rake receiver is referred to as *All Rake* (ARake) [36].

- $L < L^{(0)}$: The L strongest paths are processed. The Rake receiver is referred to as *Selective Rake* (SRake) [36]. By ignoring weak paths, SRake becomes less complex than ARake but it also incurs some performance loss. However, in typical narrowband multipath channels, the impact of ignoring the weak paths is usually insignificant.

- $L < L^{(0)}$: The first L paths are processed. The Rake receiver is referred to as *Partial Rake* (PRake) [105]. PRake is less complex than SRake since it does not require a selection mechanism. It eliminates the need to sort the paths by their instantaneous gain which requires fast and accurate channel estimation. This strategy is suitable in multipath environments where the path gains have an exponential distribution.

The output SNR expression of the coherent Rake receiver for the adopted system model can be found in [76, Appendix B]. Similar SNR analysis has also appeared in [36, 58, 60]. The bit error rate expression of the Rake receiver is derived in parallel with that of the LMMSE receiver in Chapter 4.

Appendix B

The Expression for β_n

The scaling factor β_n, introduced in (3.17), can be expressed as

$$\beta_n = \frac{\sqrt{\frac{P_0}{8}}}{(1 + \mathrm{SNR}_{\max,n})} \tag{B.1}$$

where

$$\mathrm{SNR}_{\max,n} = \frac{P_0}{2}\mathcal{R}e\left[\sum_{l=1}^{L^{(0)}} e^{j\theta_l^{(0)}}\alpha_l^{(0)}\int_{-\infty}^{\infty} a_n^{(I,0)}(u-\tau_l^{(0)}-nT_b)h_n(T_b-u) \right.$$
$$\left. -ja_n^{(Q,0)}(u-\tau_l^{(0)}-nT_b)h_n(T_b-u)du\right]. \tag{B.2}$$

An alternative form of $\mathrm{SNR}_{\max,n}$ is given in (4.34).

Appendix C

The $G(f)$ Chip Pulse Filter

The frequency response of the $G(f)$ filter is formulated here. First, the $G(f)$ filter is solved for when interpath interference (IPI) is ignored. Then, the solution is extended to account for IPI. An alternative closed form expression for SNR is also included.

C.1 The $G(f)$ Filter Without IPI

Using the HSR of signals, the new chip filter can be expressed as

$$G(f) = \sum_{m=-M_H}^{M_H} G^{[m]}(f - m/T_c) \tag{C.1}$$

where $M_H = \lceil \alpha/2 \rceil$, $G^{[m]}(f) = V(f)G(f+m/T_c)$ and $V(f) = 1$ if $|f| \leq 1/(2T_c)$ and $V(f) = 0$, otherwise. The functions $G^{[m]}(f)$ are obtained by solving the following

set of $L_H = 2M_H + 1$ equations with L_H unknowns:

$$\boldsymbol{R}(f)\boldsymbol{G}(f) = \boldsymbol{C}^{(0)H}(f)\boldsymbol{Q}^H(f)\boldsymbol{u}^H \tag{C.2}$$

over $f \in [-\frac{1}{2T_c}, \frac{1}{2T_c}]$. The unknowns exist in the $L_H \times 1$ column vector $\boldsymbol{G}(f)$ where $[\boldsymbol{G}(f)]_{m,1} = G^{[m]}(f)$. [1] The diagonal matrix $\boldsymbol{C}^{(0)}(f)$ holding the HSR elements of $C^{(0)}(f)$, the Fourier transform of the desired user's multipath channel defined by (3.24), is given by

$$[\boldsymbol{C}^{(0)}(f)]_{m,n} = C^{[m](0)}(f)\delta_{mn} \tag{C.3}$$

where $C^{[m](0)}(f) = V(f)C^{(0)}(f + m/T_c)$. Similarly, the diagonal matrix $\boldsymbol{Q}(f)$ has the HSR elements of $Q(f)$ and is defined by $[\boldsymbol{Q}(f)]_{m,n} = Q^{[m]}(f)\delta_{mn}$. The row vector $\boldsymbol{u}$ is given by $[\boldsymbol{u}]_{1,m} = 1$. The matrix function $\boldsymbol{R}(f)$ representing the cross spectral density (CSD) matrix of the noise is

$$\boldsymbol{R}(f) = \frac{\mathcal{N}_0}{2}\boldsymbol{I}_{L_H} + \frac{1}{2T_c}\boldsymbol{Q}^H(f)\mathcal{P}\boldsymbol{Q}(f) \tag{C.4}$$

where $\boldsymbol{I}_{L_H}$ is the $L_H \times L_H$ identity matrix. All the information concerning the interferer chip delays and signal powers is contained in the MAI power matrix

$$\mathcal{P} = \sum_{k=1}^{K}\sum_{l=1}^{L^{(k)}} \boldsymbol{P}_{k,l}^{(C)}\boldsymbol{P}_{k,l}^{(C)H} \tag{C.5}$$

[1] For simplicity, matrix indices are allowed to take zero or negative values.

where the column vector $\boldsymbol{P}_{k,l}^{(C)}$ is

$$[\boldsymbol{P}_{k,l}^{(C)}]_{n,1} = \sqrt{P_k}\alpha_l^{(k)} \exp\left(\frac{j2\pi n T_l^{(k)}}{T_c}\right). \tag{C.6}$$

C.2 The $G(f)$ Filter With IPI

Fig. 3.2 illustrates how the $G(f)$ filter can be broken down to $L^{(0)}$ branches. The formulation of previous section ignored the effect of IPI. In real life, however, multipath components of a desired user's signal cause interference on one another. The $G_l(f)$ filter of each branch shapes its impulse response accordingly to counter IPI. Here, the $G(f)$ formulation is extended to account for IPI with focus on the sub filters $G_l(f)$. As mentioned earlier,

$$G(f) = \sum_{l=1}^{L^{(0)}} C_l^{*(0)}(f) G_l(f) \tag{C.7}$$

As before, using the HSR of signals, the $G_l(f)$ filter can be expressed as

$$G_l(f) = \sum_{m=-M_H}^{M_H} G_l^{[m]}(f - m/T_c). \tag{C.8}$$

The functions $G_l^{[m]}(f)$ are obtained by solving the following set of $L_H = 2M_H + 1$ equations with L_H unknowns:

$$\boldsymbol{R}(f)\boldsymbol{G}_l(f) = \boldsymbol{Q}^H(f)\boldsymbol{u}^H \tag{C.9}$$

over $f \in [-\frac{1}{2T_c}, \frac{1}{2T_c}]$ where the elements of the column vector $\boldsymbol{G}_l(f)$ are $[\boldsymbol{G}_l(f)]_{m,1} =$

$G_l^{[m]}(f)$. The remaining parameters are defined as before. The matrix $\boldsymbol{C}^{(0)}(f)$ is absent in (C.9), compared to (C.2), since the desired user's channel impulse response has already been accounted for in (C.7) and Fig. 3.2. To include the effect of IPI, the power matrix is modified to

$$\mathcal{P} = \sum_{k=0}^{K} \sum_{l'=1}^{L^{(k)}} \boldsymbol{P}_{k,l'}^{(C)} \boldsymbol{P}_{k,l'}^{(C)H} \tag{C.10}$$

where $l' \neq l$ for $k = 0$ and the column vector $\boldsymbol{P}_{k,l'}^{(C)}$ is

$$[\boldsymbol{P}_{k,l'}^{(C)}]_{n,1} = \sqrt{P_k}\alpha_{l'}^{(k)} \exp\left[\frac{j2\pi n\left(T_{l'}^{(k)} - T_l^{(0)}\right)}{T_c}\right]. \tag{C.11}$$

Appendix D

Application of CLTs to MAI and IPI Statistics

Three impediments exist that prevent the application of central limit theorems (CLTs) [88] to the sums of RVs in the expressions of (4.9) and (4.11). First, CLTs consider the limiting distribution of $1/\sqrt{N}\sum_{i=0}^{N-1} X_i$ rather than $1/N\sum_{i=0}^{N-1} X_i$ which defines a sample mean [88]. It is clear that as $N \to \infty$, then $\mathcal{M}_{|\boldsymbol{T},\boldsymbol{\Theta}} \to 0$ and $\mathcal{I}_{|\boldsymbol{T}^{(0)},\boldsymbol{\Theta}^{(0)}} \to 0$. To circumvent this impediment, the effect of κ is introduced to the expression in (4.9) where $\kappa = L^{(0)}\sum_{k=1}^{K} L^{(k)}$ is the *virtual* number of users that contribute to MAI. Assume κ is linearly proportional to N such that $\lambda = \kappa/N$ remains constant as N increases. The expression of (4.9) can now be reformulated in the desired form as a sum of κN RVs normalized by $1/\sqrt{\kappa N}$ and scaled by $\sqrt{\lambda}$

$$\mathcal{M}_{|\boldsymbol{T},\boldsymbol{\Theta}} = \sqrt{\lambda}.\frac{1}{\sqrt{\kappa N}}\sum_{i=0}^{N-1}\sum_{l=1}^{L^{(0)}}\sum_{k=1}^{K}\sum_{l'=1}^{L^{(k)}} V_{l,i}^{(k,l')} \tag{D.1}$$

where

$$V_{l,i}^{(k,l')} = a_i^{(I,0)} \left\{ \zeta_k \frac{\alpha_l^{(0)} \alpha_{l'}^{(k)}}{\gamma} \sum_{m=-(M-1)}^{M} \rho_l(mT_c - T_{l'}^{(k)} + T_l^{(0)}) \right. \\ \left. \left[d_{i-m}^{(I,k,l')} \cos(\theta_{l'}^{(k)} - \theta_l^{(0)}) + d_{i-m}^{(Q,k,l')} \sin(\theta_{l'}^{(k)} - \theta_l^{(0)}) \right] \right\} \\ + a_i^{(Q,0)} \left\{ \zeta_k \frac{\alpha_l^{(0)} \alpha_{l'}^{(k)}}{\gamma} \sum_{m=-(M-1)}^{M} \rho_l(mT_c - T_{l'}^{(k)} + T_l^{(0)}) \right. \\ \left. \left[-d_{i-m}^{(I,k,l')} \sin(\theta_{l'}^{(k)} - \theta_l^{(0)}) + d_{i-m}^{(Q,k,l')} \cos(\theta_{l'}^{(k)} - \theta_l^{(0)}) \right] \right\}. \tag{D.2}$$

Similarly, by introducing $\kappa_0 = L^{(0)}(L^{(0)} - 1)$ and defining $\lambda_0 = \kappa_0/N$, the expression in (4.11) can be modified as follows

$$\mathcal{I}_{|\boldsymbol{T}^{(0)}, \boldsymbol{\Theta}^{(0)}} = \sqrt{\lambda_0} . \frac{1}{\sqrt{\kappa_0 N}} \sum_{i=0}^{N-1} \sum_{l=1}^{L^{(0)}} \sum_{\substack{l'=1 \\ l' \neq l}}^{L^{(0)}} V_{l,i}^{(0,l')} \tag{D.3}$$

The second and third impediments concern the distribution of RVs in (D.1) and (D.3). Consider the set of κN RVs in (D.1)

$$S_V = \left\{ \begin{array}{cccc} V_{1,0}^{(1,1)} & V_{1,1}^{(1,1)} & \cdots & V_{1,N-1}^{(1,1)} \\ \vdots & \vdots & \vdots & \vdots \\ V_{1,0}^{(K,L^{(K)})} & V_{1,1}^{(K,L^{(K)})} & \cdots & V_{1,N-1}^{(K,L^{(K)})} \\ \vdots & \vdots & \vdots & \vdots \\ V_{L^{(0)},0}^{(1,1)} & V_{L^{(0)},1}^{(1,1)} & \cdots & V_{L^{(0)},N-1}^{(1,1)} \\ \vdots & \vdots & \vdots & \vdots \\ V_{L^{(0)},0}^{(K,L^{(K)})} & V_{L^{(0)},1}^{(K,L^{(K)})} & \cdots & V_{L^{(0)},N-1}^{(K,L^{(K)})} \end{array} \right\} \tag{D.4}$$

where the first $\sum_{k=1}^{K} L^{(k)}$ rows include the RVs from the first finger of the Rake

contributing to MAI statistics and the next $\sum_{k=1}^{K} L^{(k)}$ rows include the RVs from the second finger of the Rake and so on. The RVs in the S_V collection are neither identically distributed nor mutually independent. Hence, the CLT theorem based on i.i.d. RVs cannot be directly applied. Although the distribution of RVs in the same row are identical, those corresponding to RVs from different rows are not. The dependence are due to the fact that the terms $V_{l,i}^{(k,l')}$ can be functions of common RVs in general.

The problem of nonidentical distributions can be resolved by summing the columns of (D.4) to form a new RV as

$$X_i^{\mathcal{M}} = \frac{1}{\sqrt{\kappa}} \sum_{l=1}^{L^{(0)}} \sum_{k=1}^{K} \sum_{l'=1}^{L^{(k)}} V_{l,i}^{(k,l')}. \tag{D.5}$$

Consequently, the MAI component can be written as

$$\mathcal{M}_{|\boldsymbol{T},\boldsymbol{\Theta}} = \sqrt{\lambda}.\frac{1}{\sqrt{N}} \sum_{i=0}^{N-1} X_i^{\mathcal{M}} \tag{D.6}$$

The sequence $\boldsymbol{X}^{\mathcal{M}} = \{X_0^{\mathcal{M}}, X_1^{\mathcal{M}}, \ldots, X_{N-1}^{\mathcal{M}}\}$ is now identically distributed. It can be shown that

$$E[X_i^{\mathcal{M}}] = 0 \tag{D.7}$$

$$\mathrm{Cov}(X_i^{\mathcal{M}}, X_j^{\mathcal{M}}) = 0 \quad \text{if} \quad i \neq j \tag{D.8}$$

$$E[|X_i^{\mathcal{M}}|^3] < \infty \tag{D.9}$$

The first two equations follow from the mutual independence of $a_i^{(I,0)}$, $a_i^{(Q,0)}$, $d_{i-m}^{(I,k,l')}$,

and $d_{i-m}^{(Q,k,l')}$ as also expressed in (E.1). The last equation can be verified by the same approach used for deriving the second moment of $X_i^{\mathcal{M}}$ in Appendix E and noting (E.1) again. As κ takes a finite value, the third power of $|X_i^{\mathcal{M}}|$ will only consist of terms that are products of $a_i^{(I,0)}$, $a_i^{(Q,0)}$, $d_{i-m}^{(I,k,l')}$, and $d_{i-m}^{(Q,k,l')}$ to their third power. Due to their mutual independence and their equi-probable binary format, their expected values are zero.[1]

The same approach can be applied to the IPI component of (D.3) to form the identically distributed sequence $\boldsymbol{X}^{\mathcal{I}} = \{X_0^{\mathcal{I}}, X_1^{\mathcal{I}}, \ldots, X_{N-1}^{\mathcal{I}}\}$.

The problem of lack of independence can be resolved by observing the following property in $\boldsymbol{X}^{\mathcal{M}}$. The RVs $X_i^{\mathcal{M}}$ and $X_j^{\mathcal{M}}$ are independent as long as

$$|i-j| > m = 2M - 1 + \lfloor \frac{\tau_{max}}{T_c} \rfloor \tag{D.10}$$

where τ_{max} is the maximum value of $\tau_l^{(k)}$ across all l and k. Sequences with such property are referred to as *m-dependent* (or *weakly dependent*) sequences. The formal definition is [106][107, pp. 215]:

Definition: Let $\boldsymbol{Y} = \{Y_1, Y_2, \ldots\}$ be a sequence of RVs. The sequence $\boldsymbol{Y}$ is *m-dependent* if $\{Y_1, \ldots, Y_r\}$ is independent of $\{Y_s, Y_{s+1}, \ldots\}$ provided $s - r > m$.

The *m-dependent* nature of $\boldsymbol{X}^{\mathcal{M}}$ and $\boldsymbol{X}^{\mathcal{I}}$ originates from the fact that, in the receiver side, each chip in each finger is correlated with m chips from interfering paths. If the channel is reduced to the AWGN channel, $\tau_{max} = 0$ and $m = 2M - 1$. This result is consistent with that reported in [87]. A special form of the CLT for *m-dependent* sequences [106][107, pp. 219] can now be applied to approximate the

[1]By the same argument, it can be shown that all odd moments of $X_i^{\mathcal{M}}$ are zero.

distribution of MAI component in (D.6) and its IPI counterpart.

Theorem: If $\boldsymbol{Y}$ is a stationary *m-dependent* sequence of RVs with $E[Y_1] = 0$, $E[|Y_1|^3] < \infty$, then, as $n \to \infty$, the limiting distribution of $1/\sqrt{n}\sum_{i=1}^{n} Y_i$ is normal with a mean of zero and a variance of

$$A = \mathrm{Var}(Y_1) + 2\left[\mathrm{Cov}(Y_1, Y_2) + \ldots + \mathrm{Cov}(Y_1, Y_{m+1})\right]. \tag{D.11}$$

The above theorem yields the IGA for general pulses and receiver filters.

Appendix E

Derivation of $\mathrm{Var}(X_0^{\mathcal{M}})$ and $\mathrm{Var}(X_0^{\mathcal{I}})$

In deriving the expression for $\mathrm{Var}(X_0^{\mathcal{M}})$, the reformulation of the received signals given in (3.8) is recalled. More precisely, it can be concluded that

$$E[d_i^{(\mathcal{B}_1,k,l)} d_j^{(\mathcal{B}_2,k',l')}] = \delta_{\mathcal{B}_1\mathcal{B}_2}\delta_{kk'}\delta_{ll'}\delta_{ij}. \tag{E.1}$$

This means that the expectation operation involved in determining $\mathrm{Var}(X_0^{\mathcal{M}})$ results in a non-zero value only when $\mathcal{B}_1 = \mathcal{B}_2$, $k = k'$, $l = l'$, and $i = j$, all at the same time. With this observation, $\mathrm{Var}(X_0^{\mathcal{M}})$ can be written as

$$\begin{aligned}\mathrm{Var}(X_0^{\mathcal{M}}) = \frac{2}{\kappa}\sum_{l=1}^{L^{(0)}}\sum_{l'=1}^{L^{(0)}}\frac{\alpha_l^{(0)}\alpha_{l'}^{(0)}}{\gamma^2}\sum_{k=1}^{K}\sum_{l''=1}^{L^{(k)}}\zeta_k^2|\alpha_{l''}^{(k)}|^2\Omega_{l,l'}^{(k,l'')} \\ \Big[\cos(\theta_{l''}^{(k)}-\theta_l^{(0)})\cos(\theta_{l''}^{(k)}-\theta_{l'}^{(0)})+\sin(\theta_{l''}^{(k)}-\theta_l^{(0)})\sin(\theta_{l''}^{(k)}-\theta_{l'}^{(0)})\Big]\end{aligned} \tag{E.2}$$

where $\Omega_{l,l'}^{(k,l'')}$ is defined as

$$\Omega_{l,l'}^{(k,l'')} = \sum_{m=-(M-1)}^{M} \rho_l(mT_c - T_{l''}^{(k)} + T_l^{(0)})\rho_{l'}(mT_c - T_{l''}^{(k)} + T_{l'}^{(0)}). \tag{E.3}$$

Re-writing the expression in (E.2) with the help of

$$\cos A \cos B = \frac{1}{2}[\cos(A-B) + \cos(A+B)]$$
$$\sin A \sin B = \frac{1}{2}[\cos(A-B) - \cos(A+B)]$$

yields

$$\mathrm{Var}(X_0^{\mathcal{M}}) = \frac{2}{\kappa}\sum_{l=1}^{L^{(0)}}\sum_{l'=1}^{L^{(0)}} \frac{\alpha_l^{(0)}\alpha_{l'}^{(0)}}{\gamma^2}\cos(\theta_{l'}^{(0)} - \theta_l^{(0)}) \sum_{k=1}^{K}\sum_{l''=1}^{L^{(k)}} \zeta_k^2 |\alpha_{l''}^{(k)}|^2 \Omega_{l,l'}^{(k,l'')} \tag{E.4}$$

The expression in (E.4) reveals that a consequence of DS-QPSK modulation is the disappearance of the effect of interfering phase offsets, $\Theta^{(k)}$ for $1 \leq k \leq K$. Also, it can be readily shown that $E[\cos(\theta_{l'}^{(0)} - \theta_l^{(0)})] = 0$ if phase offsets are modeled as independent uniformly distributed RVs over $[0, 2\pi)$. Hence, by averaging out the effect of $\theta_l^{(0)}$, the expression in (E.4) can be further simplified to

$$\mathrm{Var}(X_0^{\mathcal{M}}) = \frac{2}{\kappa}\sum_{l=1}^{L^{(0)}} \frac{|\alpha_l^{(0)}|^2}{\gamma^2} \sum_{k=1}^{K}\sum_{l'=1}^{L^{(k)}} \zeta_k^2 |\alpha_{l''}^{(k)}|^2 \Omega_{l,l}^{(k,l')}. \tag{E.5}$$

Similarly, $\mathrm{Var}(X_0^{\mathcal{I}})$ can be shown to be

$$\mathrm{Var}(X_0^{\mathcal{I}}) = \frac{2}{\kappa_0}\sum_{l=1}^{L^{(0)}} \frac{|\alpha_l^{(0)}|^2}{\gamma^2} \sum_{\substack{l'=1 \\ l' \neq l}}^{L^{(0)}} \zeta_0^2 |\alpha_{l'}^{(0)}|^2 \Omega_{l,l}^{(0,l')}. \tag{E.6}$$

Appendix F

Alternative Expression for $\Omega_{l,l}^{(k,l')}$

The function $B_l(f)$ can also be expressed as

$$B_l(f) = \frac{1}{T_c^3}\left[Q(f)G_l(f)\right] \otimes \left[Q(f)G_l(f)\right]. \tag{F.1}$$

Using the inverse Fourier representation of $\rho_l^2(t)$, $\Omega_{l,l}^{(k,l')}$ can be written as

$$\begin{aligned} \Omega_{l,l}^{(k,l')} &= \sum_{m=-(M-1)}^{M} \rho_l^2(mT_c - T_{l'}^{(k)} + T_l^{(0)}) && \text{(F.2)} \\ &= \sum_{m=-\infty}^{\infty} \int_{-\infty}^{\infty} B_l(f) \exp\left[j2\pi f(mT_c - T_{l'}^{(k)} + T_l^{(0)})\right] df && \text{(F.3)} \end{aligned}$$

Applying the *Poisson's Formula* [108, p. 148] to the above and noting that $B_l(f) = 0$ for $f \geq 2/T_c$ yields

$$\Omega_{l,l}^{(k,l')} = \int_{-\infty}^{\infty} B_l(f) e^{j2\pi f(-T_{l'}^{(k)} + T_l^{(0)})} \frac{1}{T_c} \sum_{m=-\infty}^{\infty} \delta(f + \frac{m}{T_c}).df \tag{F.4}$$

$$= \sum_{m=-\infty}^{\infty} \exp\left[j\frac{2\pi m(T_{l'}^{(k)} - T_l^{(0)})}{T_c}\right] B_l(-\frac{m}{T_c}) \quad \text{(F.5)}$$

$$= B_l(0) + \sum_{\substack{m=-1-\lfloor\alpha\rfloor \\ m\neq 0}}^{1+\lfloor\alpha\rfloor} \exp\left[j\frac{2\pi m(T_{l'}^{(k)} - T_l^{(0)})}{T_c}\right] B_l(-\frac{m}{T_c}) \quad \text{(F.6)}$$

which is identical to (4.20). It is noted that the pulse excess BW is assumed to be $\alpha \leq 100\%$.

Appendix G

$R_{nn^*}(t,u)$ as $\alpha \to 0$

The autocorrelation function of the noise, as expressed in (3.20), can be written as

$$R_{nn^*}(t,u) == \sum_{k=1}^{K} \sum_{l=1}^{L^{(k)}} P_k |\alpha_l^{(k)}|^2 R'_{nn^*}(t,u) + \mathcal{N}_0 \tag{G.1}$$

where

$$R'_{nn^*}(t,u) = \sum_{n=-\infty}^{\infty} q(t - T_l^{(k)} - nT_c) q(u - T_l^{(k)} - nT_c). \tag{G.2}$$

Using the inverse Fourier representation of the two terms on the right hand side of (G.2), $R'_{nn^*}(t,u)$ can be expressed as

$$R'_{nn^*}(t,u) = \int_{-\infty}^{\infty} \int_{-\infty}^{\infty} Q(f)Q(f')\exp[j2\pi(ft + f'u - fT_l^{(k)} - f'T_l^{(k)})]\Delta(f,f')dfdf' \tag{G.3}$$

where

$$\Delta(f,f') = \sum_{n=-\infty}^{\infty} \exp[-j2\pi n T_c(f+f')] = \frac{1}{T_c}\sum_{n=-\infty}^{\infty} \delta(f+f'+\frac{n}{T_c}) \tag{G.4}$$

by applying the *Poission's formula* [108, p. 148]. The right hand side of (G.3) will have nonzero values only for $f' = -f - n/T_c$. Therefore, the double integral in (G.3) reduces to a single integral. Moreover, as $\alpha \to 0$, the product $Q(f)Q(f')$ can have a significant nonzero value only when $n = 0$. This is so since $Q(f)$ is bandlimited to $|f| < (1+\alpha)/(2T_c)$. In the limit when $\alpha = 0$, only $n = 0$ results in nonzero values. Replacing $f' = -f$ yields

$$\Delta(f,-f) = \int_{-\infty}^{\infty} \frac{|Q(f)|^2}{T_c} \exp[j2\pi f(t-u)]df. \tag{G.5}$$

Therefore, $R'_{nn^*}(t,u)$ can be expressed as $R'_{nn^*}(t-u)$. Consequently, $R_{nn^*}(t,u)$ can be expressed as $R_{nn^*}(t-u)$. As a result, MAI becomes a WSS process for $\alpha = 0$. Similar argument can be used for IPI.

Refereed Publications

[1] A. Mirbagheri and Y. C. Yoon, "Adaptive Implementations of a Linear MMSE Receiver for Interference Suppression and Multipath Diversity Combining in Long-Code DS-CDMA Systems," *Submitted to IEEE Transactions on Vehicular Technology, Under Review.*

[2] A. Mirbagheri and Y. C. Yoon, "Performance Analysis of a Linear MMSE Receiver for Bandlimited Random-CDMA Using Quadriphase Spreading over Multipath Channels," *Accepted and queued for publication in IEEE Transactions on Wireless Communications.*

[3] A. Mirbagheri and Y. C. Yoon, "A Linear MMSE Receiver for Multipath Asynchronous Random-CDMA with Chip Pulse Shaping," *IEEE Transactions on Vehicular Technology*, vol. 51, no. 5, pp.1072-1086, Sep. 2002.

[4] A. Mirbagheri and Y. C. Yoon, "Pilot-Assisted Adaptive Receivers for Interference Suppression and Multipath Reception in Long-Code DS-CDMA," *in the Proc. IASTED Intl. Conf. Wireless and Optical Communications*, (Banff, Alberta), Jul. 2003.

[5] A. Mirbagheri and Y. C. Yoon, "A Constant Modulus Approach to Blind Adaptive Implementation of a LMMSE Receiver for Long-code DS-CDMA," *in the Proc. of the 3G Wireless Conference*, (San Francisco, U.S.A.), pp. 451-456, May 2002.

[6] A. Mirbagheri and Y. C. Yoon, "A Blind Adaptive Receiver for Interference Suppression and Multipath Reception in Long-code DS-CDMA," *in the Proc. of the Intl. Conf. on Communications*, (New York, U.S.A.), pp. 242-246, Apr.-May 2002.

[7] A. Mirbagheri and Y. C. Yoon, "A Linear MMSE Receiver for Bandlimited Random-CDMA Using Quadriphase Spreading over Multipath Channels," *in the Proc. of the Intl. Conf. on Wireless Communications*, (Calgary, Alberta), pp. 536-543, Jul. 2001.

[8] A. Mirbagheri and Y. C. Yoon, "Performance Comparison of Linear MMSE and Coherent RAKE Receivers in Multipath Asynchronous Random CDMA," *in the Proc. of the Intl. Symp. on Spread Spectrum Techniques and Applications*, (Parsippany, U.S.A.), pp. 520-524, Sept. 2000.

Bibliography

[1] A. Lightman and W. Rojas, *Brave New Unwired World, The Digital Big Bang and the Infinite Internet*, John Wiley, 2002.

[2] TIA/EIA/IS-95, "Mobile station - base station compatibility standard for dual-mode wideband spread spectrum cellular systems," *tech. rep., TIA/EIA*, July 1993.

[3] R. L. Peterson, R. E. Ziemer, and D. E. Borth, *Introduction to Spread Spectrum Communications*, Prentice Hall, 1995.

[4] R. L. Pickholtz, D. L. Schilling, and L.B. Milstein, "Theory of spread-spectrum communications – A tutorial," *IEEE Trans. Communications*, vol. 30, no. 5, pp. 129–158, May 1982.

[5] T. S. Rappaport, *Wireless Communications*, IEEE Press, 1996.

[6] K. S. Gilhousen, I. M. Jacobs, R. Padovani, A. J. Viterbi, Jr. L. A. Weaver, and C. E. Wheatley III, "On the capacity of a cellular CDMA system," *IEEE Trans. Vehicular Tech.*, vol. 40, no. 2, pp. 303–312, May 1991.

[7] A. J. Viterbi, *CDMA: Principles of Spread Spectrum Communication*, Addison-Wesley Publishing Co., 1995.

[8] R. Meidan, "To spread or not to spread, this is the question," in *Proc. IEEE Vehicular Technology Conf.*, June 1994, pp. 56–59.

[9] "Physical layer standard for cdma2000 spread spectrum systems," in *http://www.3gpp2.org, Technical Steering Group C (TSG-C) Specifications*. Feb. 2002.

[10] E. Dahlman, P. Beming, J. Knutsson, F. Ovesjo, M. Persson, and C. Robool, "WCDMA– The radio interface for future mobile multimedia communications," *IEEE Trans. Vehicular Tech.*, vol. 47, no. 4, pp. 1105–1118, Oct. 1998.

[11] "cdma2000 high rate packet air interface specification (IS-856)," in *http://www.3gpp2.org, Technical Steering Group C (TSG-C) Specifications*. Sept. 2000.

[12] H. Hashemi, "Simulation of the urban radio propagation channel," *IEEE Trans. Vehicular Tech.*, vol. VT-28, no. 3, pp. 213–225, Aug. 1979.

[13] S. U. H. Qureshi, "Adaptive equalization," *Proc. of IEEE*, vol. 73, no. 9, pp. 1349–1387, Sept. 1985.

[14] S. Verdu, "Minimum probability of error for asynchronous Gaussian multiple access channels," *IEEE Trans. Inform. Theory*, vol. 32, no. 1, pp. 85–96, Jan. 1986.

[15] S. Verdu, *Multiuser detection*, New York: Cambridge Press, 1998.

[16] U. Madhow and M. L. Honig, "MMSE interference suppression for direct-sequence spread-spectrum CDMA," *IEEE Trans. Communications*, vol. 42, no. 12, pp. 3178–3188, Dec. 1994.

[17] P. B. Rapajic and B. S. Vucetic, "Adaptive receiver structures for asynchronous CDMA systems," *IEEE J. Select. Areas Communications*, vol. 12, no. 4, pp. 685–697, May 1994.

[18] T. F. Wong, T. M. Lok, and J. S. Lehnert, "Asynchronous multiple-access interference suppression and chip waveform selection with aperiodic random sequences," *IEEE Trans. Communications*, vol. 47, no. 1, pp. 103–114, Jan. 1999.

[19] F. Wang, J. Chen, and G. Agami, "Optimal receiver filter design with applications in IS-2000 CDMA systems," in *Proc. IEEE Wireless Communications and Networking Conf.*, 2003, vol. 1, pp. 496–501.

[20] S. W. Heo, S. W. Ahn, and J. H. Lim, "Performance analysis of SNR degradation by IS-95 filter in CDMA 1xEV-DV system," in *Proc. IEEE Wireless Communications and Networking Conf.*, 2003, vol. 1, pp. 491–495.

[21] T. F. Wong, T. M. Lok, J. S. Lehnert, and M. D. Zoltowski, "A linear receiver for direct-sequence multiple-access systems with antenna arrays and blind adaptation," *IEEE Trans. Inform. Theory*, vol. 44, no. 2, pp. 659–676, Mar. 1998.

[22] X. Wang and H. V. Poor, "Multiuser diversity receivers for frequency-selective Rayleigh fading CDMA channels," in *Proc. IEEE Vehicular Technology Conf.*, 1997, vol. 1, pp. 198–202.

[23] T. Ojanpera and R. Prasad, "An overview of air interface multiple access for IMT-2000/UMTS," *IEEE Communications Magazine*, vol. 36, pp. 82–95, Sept. 1998.

[24] V. K. Garg, *IS-95 CDMA and cdma2000: Cellular/PCS Systems Implementation*, Prentice Hall, 1999.

[25] S. Vembu and A. J. Viterbi, "Two different philosophies in CDMA – A comparison," in *Proc. IEEE Vehicular Technology Conf.*, Apr. 18 to May 1, 1996, pp. 869–873.

[26] L. B. Milstein, "Wideband code division multiple access," *IEEE J. Select. Areas Communications*, vol. 18, no. 8, pp. 1344–1354, Aug. 2000.

[27] S. Parkvall, "Variability of user performance in cellular DS-CDMA-long versus short spreading sequences," *IEEE Trans. Communications*, vol. 48, no. 7, pp. 1178–1187, July 2000.

[28] S. L. Miller, "An adaptive direct-sequence code-division multiple-access receiver for multiuser interference rejection," *IEEE Trans. Communications*, vol. 43, no. 2/3/4, pp. 1746–1755, Feb/Mar/Apr 1995.

[29] M. Honig, U. Madhow, and S. Verdu, "Blind adaptive multiuser detection," *IEEE Trans. Inform. Theory*, vol. 41, no. 4, pp. 944–960, July 1995.

[30] Y. C. Yoon, *SNR Maximizing Linear Filters with Interference Suppression Capabilities for DS-CDMA*, Ph.D. thesis, McGill University, 1998.

[31] Y. C. Yoon, "Linear MMSE interference suppression in asynchronous Random-CDMA," in *Proc. IEEE Vehicular Technology Conf.*, Tokyo, Japan, May 2000, vol. 2, pp. 1465–1469.

[32] Y. C. Yoon and H. Leib, "Chip-delay locked matched filter for DS-CDMA systems using long sequence spreading," *IEEE Trans. Communications*, vol. 49, no. 8, pp. 1468–1478, Aug. 2001.

[33] Y. C. Yoon, "An adaptive linear receiver for interference suppression in asynchronous Random-CDMA," in *Proc. Intl. Conf. on Telecommunications*, Cheju, S. Korea, June 1999, pp. 370–374.

[34] R. Price and P. E. Green Jr., "A communication technique for multipath channels," *Proc. of IEEE*, vol. 46, pp. 550–570, Mar. 1958.

[35] J. G. Proakis, *Digital Communications*, McGraw-Hill, 3rd edition, 1995.

[36] M. Z. Win and Z. A. Kostic, "Impact of spreading bandwidth on RAKE reception in dense multipath channels," *IEEE J. Select. Areas Communications*, vol. 17, no. 10, pp. 1794–1806, Oct. 1999.

[37] J. Kato, T. Tanaka, and T. Fujii, "A study on arrival paths in wide-band mobile communication systems," in *Proc. Intl. Symposium on Antennas and Propagation*, Tokyo, Japan, 1996, pp. 205–208.

[38] J. Aldis and S. K. Barton, "On the feasibility of a 2-Mb/s bearer service in a future cellular radio system using code-division multiple access," *IEEE Trans. Vehicular Tech.*, vol. 48, no. 5, pp. 1392–1403, Sept. 1999.

[39] I. Ghauri and D. T. M. Slock, "Linear receivers for the DS-CDMA downlink exploiting orthogonality of spreading sequences," in *Proc. Asilomar Conf. on Signals, Systems and Computers*, Pacific Grove, California, 1998, pp. 650–654.

[40] T. P. Krauss, M. D. Zoltowski, and G. Leus, "Simple MMSE equalizers for CDMA downlink to restore chip sequence: comparison to zero-forcing and Rake," in *Proc. Intl. Conf. Acoustics, Speech and Signal Processing*, 2000, vol. 5, pp. 2865–2868.

[41] S. Chowdhury, M. D. Zoltowski, and J. S. Goldstein, "Structured MMSE equalization for synchronous CDMA with sparse multipath channels," in *Proc. Intl. Conf. Acoustics, Speech and Signal Processing*, 2001, vol. 4, pp. 2113–2116.

[42] C. D. Frank, E. Visotsky, and U. Madhow, "Adaptive interference suppresion for the downlink of a direct sequence CDMA system with long spreading sequences," *J. of VLSI Signal Processing*, vol. 30, no. 1–3, pp. 273–291, Mar. 2002.

[43] S. Buzzi and H. V. Poor, "Channel estimation and multiuser detection in long-code DS-CDMA systems," *IEEE J. Select. Areas Communications*, vol. 19, no. 8, pp. 1476–1487, Aug. 2001.

[44] Y. Ma and T. J. Lim, "Linear and non-linear chip-rate minimum mean-squared-error multiuser CDMA detection," *IEEE Trans. Communications*, vol. 49, no. 3, pp. 530–542, Mar. 2001.

[45] G. E. Bottomley, "Optimizing the rake receiver for the CDMA downlink," in *Proc. IEEE Vehicular Technology Conf.*, 1993, pp. 742–745.

[46] G. E. Bottomley, T. Ottosson, and Y. E. Wang, "A generalized RAKE receiver for interference suppression," *IEEE J. Select. Areas Communications*, vol. 18, no. 8, pp. 1536–1545, Aug. 2000.

[47] A. M. Monk, M. Davis, L. B. Milstein, and C. W. Helstrom, "A noise-whitening approach to multiple access noise rejection – part I: Theory and background," *IEEE J. Select. Areas Communications*, vol. 12, no. 5, pp. 817–827, June 1994.

[48] E. A. Geraniotis and B. Ghaffari, "Performance of binary and quaternary direct-sequence spread-spectrum multiple-access systems with random signature sequences," *IEEE Trans. Communications*, vol. 39, pp. 713–724, May 1991.

[49] D. J. Torrieri, "Performance of direct-sequence systems with long pseudonoise sequences," *IEEE J. Select. Areas Communications*, vol. 10, no. 4, pp. 770–781, May 1992.

[50] M. O. Sunay and P. J. McLane, "Calculating error probabilities for DS-

CDMA systems: When not to use the Gaussian approximation," in *Proc. IEEE Globecomm Conf.*, London, UK, Nov. 1996, pp. 1744–1749.

[51] R. K. Morrow Jr., "Accurate CDMA BER calculations with low computational complexity," *IEEE Trans. Communications*, vol. 46, pp. 1413–1417, Nov. 1998.

[52] K. Cheun, "Performance of direct-sequence spread-spectrum RAKE receivers with random spreading sequences," *IEEE Trans. Communications*, vol. 45, no. 2, pp. 1130–1143, Sept. 1997.

[53] Y. C. Yoon, "An improved gaussian approximation for probability of bit-error analysis of asynchronous bandlimited DS-CDMA systems with BPSK spreading," *IEEE Trans. Wireless Communications*, vol. 1, no. 3, pp. 373–382, July 2002.

[54] Y. C. Yoon, "Quadriphase DS-CDMA with pulse shaping and the accuracy of the Gaussian approximation for matched filter receiver performance analysis," *IEEE Trans. Wireless Communications*, vol. 1, no. 4, pp. 761–768, Oct. 2002.

[55] J. H. Cho, Y. K. Jeong, and J. S. Lehnert, "Average BER performance of band-limited DS/SSMA communications," *IEEE Trans. Communications*, vol. 50, no. 7, pp. 1150–1159, July 2002.

[56] K. Hooli, M. Latva-aho, and M. Juntti, "Performance evaluation of adaptive chip-level channel equalizers in WCDMA downlink," in *Proc. IEEE Intl. Conf. Communications*, 2001, pp. 1974–1979.

[57] S. Yoon and Y. Bar-Ness, "Performance analysis of linear multiuser detectors for randomly spread CDMA using Gaussian approximation," *IEEE J. Select. Areas Communications*, vol. 20, no. 2, pp. 409–418, Feb. 2002.

[58] V. M. DaSilva, E. S. Sousa, and V. Jovanovic, "Performance of the forward link of a CDMA cellular network," in *Proc. Intl. Symposium on Spread Spectrum Techniques and Applications*, Oulu, Finland, July 4–6 1994, pp. 213–217.

[59] W. Hai and N. Wiberg, "Analysis of a cdma downlink in multi-path fading channels," in *Proc. IEEE Wireless Communications and Networking Conf.*, 2002, vol. 2, pp. 517–521.

[60] N. L. B. Chan, "Multipath propagation effects on a CDMA cellular system," *IEEE Trans. Vehicular Tech.*, vol. 43, no. 4, pp. 848–855, Nov. 1994.

[61] E. A. Geraniotis and M. B. Pursley, "Error probability for direct-sequence spread-spectrum multi-access communications – part ii: Approximations," *IEEE Trans. Communications*, vol. 30, no. 5, pp. 985–995, May 1982.

[62] F. Ling, "Optimal reception, performance bound, and cutoff rate analysis of references-assisted coherent CDMA communications with applications," *IEEE Trans. Communications*, vol. 47, no. 10, pp. 1583–1592, Oct. 1999.

[63] J. Choi, "Multipath CDMA channel estimation by jointly utilising pilot and traffic channels," *IEE Proc. Communications*, vol. 146, no. 5, pp. 312–318, Oct. 1999.

[64] C. Tang, W. Chang, and C. Wei, "Pilot channel aided adaptable interference cancellation scheme for uplink DS/CDMA mobile radio systems," in *Proc. IEEE Globecomm Conf.*, 2001, pp. 3163–3167.

[65] D. Hong, T. Kim, and C. Kong, "Pilot to data channel power allocation for PCA-DC/CDMA with interference canceller," *IEEE Communication Letters*, vol. 5, no. 8, pp. 331–333, Aug. 2001.

[66] G. Chen, X. Yu, and J. Wang, "Adaptive channel estimation and dedicated pilot power adjustment based on the fading-rate measurements for a pilot-aided CDMA system," *IEEE J. Select. Areas Communications*, vol. 19, no. 1, pp. 132–140, Jan. 2001.

[67] D. N. Godard, "Self-recovering equalization and carrier tracking in two-dimensional data communication systems," *IEEE Trans. Communications*, vol. COM-28, no. 11, pp. 1867–1875, Nov. 1980.

[68] J. R. Treichler and B. G. Agee, "A new approach to multipath correction of constant modulus signals," *IEEE Trans. Acoustics, Speech and Signal Processing*, , no. 2, pp. 459–471, Apr. 1983.

[69] N. Zecevic and J. H. Reed, "Blind adaptation algorithms for direct-sequence spread-spectrum CDMA single-user detection," in *Proc. IEEE Vehicular Technology Conf.*, 1997, vol. 3, pp. 2133–2137.

[70] J. Miguez and L. Castedo, "A linearly constrained constant modulus approach

to blind adaptive multiuser interference suppression," *IEEE Communication Letters*, vol. 2, no. 8, pp. 217–219, Aug. 1998.

[71] N. Mangalvedhe and J. H. Reed, "Blind CDMA interference rejection in multipath channels," in *Proc. IEEE Vehicular Technology Conf.*, 1997, vol. 1, pp. 21–25.

[72] S. Haykin, *Adaptive Filter Theory*, Prentice-Hall, 3rd edition, 1996.

[73] C. R. Johnson Jr., P. Schniter, T. J. Endres, J. D. Behm, D. R. Brown, and R. A. Casas, "Blind equalization using the constant modulus criterion: A review," *Proc. of IEEE*, vol. 86, no. 10, pp. 1927–1950, Oct. 1998.

[74] T. J. Lim, Y. Gong, and B. Farhang-Boroujeny, "Convergence analysis of chip- and fractionally-spaced LMS adaptive multiuser CDMA detectors," *IEEE Trans. Signal Processing*, vol. 48, no. 8, pp. 2219–2228, Aug. 2000.

[75] A. Mirbagheri and Y. C. Yoon, "Performance comparison of linear MMSE and coherent RAKE receivers in multipath asynchronous Random-CDMA," in *Proc. Intl. Symposium on Spread Spectrum Techniques and Applications*, Sept. 2000, vol. 2, pp. 520–524.

[76] A. Mirbagheri and Y. C. Yoon, "A linear MMSE receiver for multipath asynchronous Random-CDMA with chip pulse shaping," *IEEE Trans. Vehicular Tech.*, vol. 51, no. 5, pp. 1072–1086, Sept. 2002.

[77] G. L. Turin, "Introduction to spread-spectrum antimultipath techniques and

their application to urban digital radio," *Proc. of IEEE*, vol. 68, no. 3, pp. 328–353, Mar. 1980.

[78] L. E. Miller and J. S. Lee, *CDMA Systems Engineering Handbook*, Artech House Publishers, 1998.

[79] E. A. Lee and D. G. Messerschmitt, *Digital Communication*, Kluwer Academic Publishers, 2nd edition, 1994.

[80] L. Debnath and P. Mikusinski, *Introduction to Hilbert Spaces with Applications*, Academic Press, 2nd edition, 1999.

[81] W. A. Gardner and W. A. Brown, "Frequency-shift filtering theory for adaptive co-channel interference removal," in *Proc. Asilomar Conf. on Signals, Systems and Computers*, Pacific Grove, California, Oct 30 – Nov 1, 1989, pp. 562–567.

[82] W. A. Gardner, "Cyclic wiener filtering: Theory and method," *IEEE Trans. Communications*, vol. 41, no. 1, pp. 151–163, Jan. 1993.

[83] L. E. Franks, "Polyperiodic linear filtering," in *Cyclostationarity in Communications and Signal Processing*, W. A. Gardner, Ed., pp. 240–266. IEEE Press, 1994.

[84] L. Franks, *Signal Theory*, Prentice-Hall, 1969.

[85] A. Mirbagheri and Y. C. Yoon, "A linear MMSE receiver for bandlimited Random-CDMA using quadriphase spreading over multipath channels,"

in *the Proc. of 13th International Conference on Wireless Communications (Wireless 2001)*, July 2001, pp. 536–543.

[86] A. Mirbagheri and Y. C. Yoon, "Performance analysis of a linear MMSE receiver for bandlimited random-CDMA using quadriphase spreading over multipath channels," *To Appear in IEEE Trans. Wireless Communications.*

[87] Y. C. Yoon, "A simple and accurate method of probability of bit error analysis for asynchronous band-limited DS-CDMA systems," *IEEE Trans. Communications*, vol. 50, no. 4, pp. 656–663, Apr. 2002.

[88] A. Papoulis, *Probability, Random Variables, and Stochastic Processes*, McGraw-Hill, 3rd edition, 1991.

[89] R. K. Morrow Jr. and J. S. Lehnert, "Bit-to-bit error dependence in slotted DS/SSMA packet systems with random signature sequences," *IEEE Trans. Communications*, vol. 37, no. 10, pp. 1052–1061, Oct. 1989.

[90] A. Mirbagheri and Y. C. Yoon, "A blind adaptive receiver for interference suppression and multipath reception in long-code DS-CDMA," in *the Proc. of Intl. Conf. Communications (ICC 2002)*, Apr. 2002, vol. 1, pp. 242–246.

[91] A. Mirbagheri and Y. C. Yoon, "A constant modulus approach to blind adaptive implementation of a LMMSE receiver for long-code DS-CDMA," in *Proc. of 3G Wireless Conf. (3GWireless'2002)*, May 2002, pp. 451–456.

[92] A. Mirbagheri and Y. C. Yoon, "Pilot-assisted adaptive receivers fir interference suppression and multipath reception in long-code DS-CDMA," *To*

appear in Proc. of IASTED Conf. Wireless and Optical Communications, 2003.

[93] A. Mirbagheri and Y. C. Yoon, "Adaptive implementations of a linear MMSE receiver for interference suppression and multipath diversity combining in long-code DS-CDMA," *Submitted to IEEE Trans. Vehicular Technology.*

[94] S. Park, H. Suk Oh, W. Yong Lee, and C. Gu Kang, "Performance of pilot/data-combined channel estimation and power allocations for dual-rate DS/CDMA system over mobile radio channels," in *Proc. IEEE Vehicular Technology Conf.*, 2000, pp. 1945–1949.

[95] Z. Kan, W. WanBo, and Y. DaCheng, "Analysis and optimization of pilot-channel-aided QPSK for DS-CDMA systems," in *TENCON'2000*, 2000, pp. 311–316.

[96] Y. C. Yoon and Harry Leib, "Matched filters with interference suppression capabilities for DS-CDMA," *IEEE J. Select. Areas Communications*, vol. 14, no. 8, pp. 1510–1521, Oct. 1996.

[97] S. Haykin, *Neural Networks: A Comprehensive Foundation*, Prentice Hall, 2nd edition, 1999.

[98] B. G. Agee, "The least-squares CMA: A new technique for rapid correction of constant modulus signals," in *Proc. Intl. Conf. Acoustics, Speech and Signal Processing*, 1986, pp. 953–956.

[99] K. Hilal and P. Duhamel, "A general form for recursive adaptive algorithms leading to an exact recursive CMA," in *Proc. Intl. Conf. Acoustics, Speech and Signal Processing*, 1992, pp. 17–20.

[100] R. Pickholtz and K. Elbarbary, "The recursive constant modulus algorithm: A new approach for real-time array processing," in *Proc. Asilomar Conf. on Signals, Systems and Computers*, Nov. 1993, pp. 627–632.

[101] J. R. Treichler, M. G. Larimore, and J. C. Harp, "Practical blind demodulators for high-order QAM signals," *Proc. of IEEE*, vol. 86, no. 10, pp. 1907–1926, Oct. 1998.

[102] P. Schramm, "Analysis and optimization of pilot-channel-assisted BPSK for DS-CDMA systems," *IEEE Trans. Communications*, vol. 46, no. 9, pp. 1122–1124, Sept. 1998.

[103] J. M. Cioffi and T. Kailath, "Fast, recursive-least-squares transversal filters for adaptive filtering," *IEEE Trans. Acoustics, Speech and Signal Processing*, vol. ASSP-32, no. 2, pp. 304–337, Apr. 1984.

[104] S. Chowdhury and M. D. Zoltowski, "Application of conjugate gradient methods in MMSE equalization for the forward link of DS-CDMA," in *Proc. IEEE Vehicular Technology Conf.*, Fall 2001, pp. 2434–2439.

[105] D. Cassioli, M. Z. Win, F. Vatalaro, and A. F. Molisch, "Performance of low-complexity RAKE reception in a realistic UWB channel," in *Proc. IEEE Intl. Conf. Communications*, 2002, vol. 2, pp. 763–767.

[106] W. Hoeffding and H. Robbins, "The central limit theorem for dependent random variables," in *The collected works of Wassily Hoeffding*, N. I. Fisher and P. K. Sen, Eds., pp. 205–213. Springer-Verlag, 1994.

[107] D. A. Fraser, *Nonparametric Methods in Statistics*, John Wiley & Sons, 1957.

[108] S. Haykin, *Digital Communications*, John Wiley & Sons, 1988.